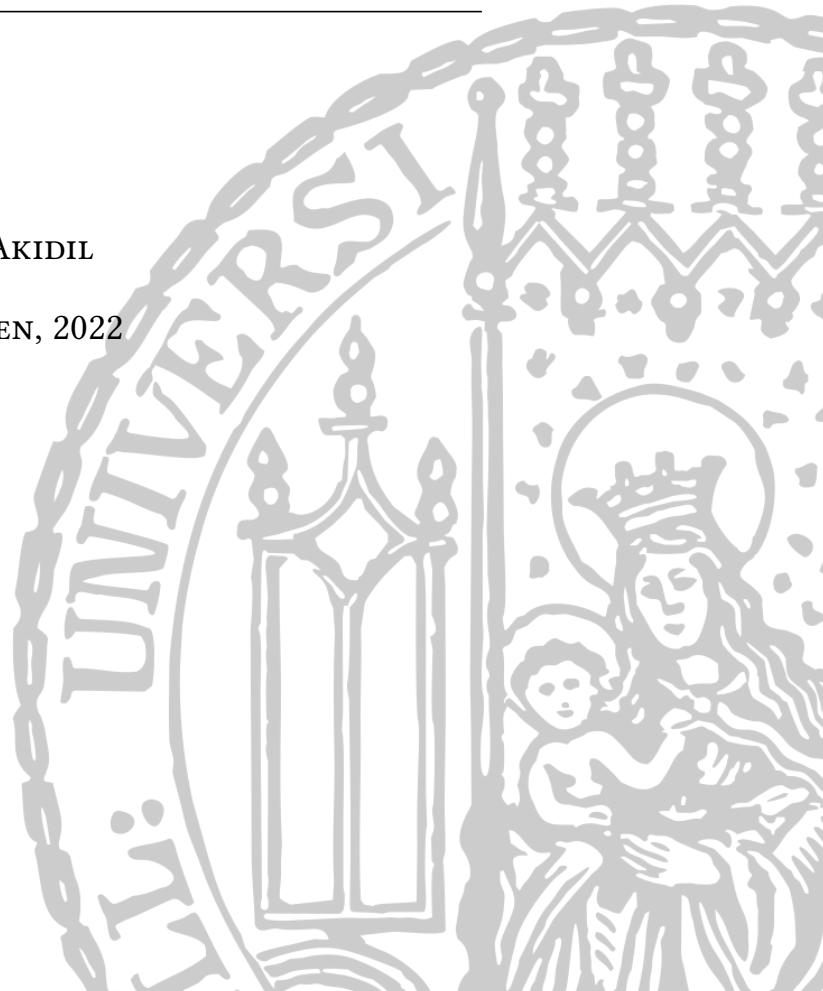


DISSERTATION ZUR ERLANGUNG DES DOKTORGRADES DER FAKULTÄT
FÜR BIOLOGIE DER LUDWIG-MAXIMILIANS-UNIVERSITÄT MÜNCHEN

**CRISPR-Cas9-mediated gene
editing in primary human B cells
identifies critical cellular factors
for Epstein-Barr virus infection**

EZGI AKIDIL

MÜNCHEN, 2022



Erstgutachterin: Prof. Dr. Bettina Kempkes

Zweitgutachter: Prof. Dr. Heinrich Jung

Tag der Abgabe: 27.06.2022

Tag der mündlichen Prüfung: 01.02.2023

Parts of this thesis have been published in:

"Highly efficient CRISPR-Cas9-mediated gene knockout in primary human B cells for functional genetic studies of Epstein-Barr virus infection", Akidil, E, Albanese, M, Buschle, A, Ruhle, A, Pich, D, Keppler, O, Hammerschmidt, W; PLoS Pathogens (2021); 10.1371/journal.ppat.1009117

Eidesstattliche Erklärung

Hiermit erkläre ich an Eides statt, dass die vorliegende Arbeit mit dem Titel

„CRISPR-Cas9-mediated gene editing in primary human B cells identifies critical cellular factors for Epstein-Barr virus infection ”

von mir selbständig und ohne unerlaubte Hilfsmittel angefertigt wurde, und ich mich dabei nur der ausdrücklich bezeichneten Quellen und Hilfsmittel bedient habe. Die Arbeit wurde weder in der jetzigen noch in einer abgewandelten Form einer anderen Prüfungskommission vorgelegt.

München, den 27.06.2022

Ezgi Akidil

Abstract

In humans, Epstein-Barr virus (EBV) infection can cause Infectious Mononucleosis and is associated with various malignancies, e.g. Burkitt's lymphoma, Hodgkin's lymphoma, and several lymphoproliferative diseases. Upon infection *in vitro*, EBV activates resting human B cells and transforms them into indefinitely proliferating lymphoblastoid B cell lines (LCL), in which the virus establishes a stable latent infection. While EBV genetics is feasible with EBV mutant viruses, studies into genetic variants of human B cells have not been possible. In my PhD thesis, I succeeded in performing very efficient genetic engineering in primary resting human B cells using Cas9 ribonucleoprotein complexes, followed by EBV infection or culturing the cells on CD40 ligand feeder cells supplemented with IL-4 to drive their cell survival. I demonstrated gene editing of the *CD46* locus with very high efficiencies and provided studies into the kinetics of double-strand breaks by Cas9 within hours after nucleofection. Next generation sequencing of CD46 mRNAs metabolically labeled with 4-thiouridine (4sU) documented locus repair and active transcription of the edited gene locus within 24 hours. For a functional proof-of-principle, I targeted an EBV relevant cellular gene, *CDKN2A*, encoding the cell cycle regulator p16^{INK4a}. Infection of *CDKN2A* knockout B cells with wild-type EBV or an EBNA3 oncoprotein mutant strain of EBV allowed me to conclude that p16^{INK4a} is the only cellular barrier to EBV-induced B cell proliferation. The efficient targeting of a specific gene loci in primary human B cells is a major achievement in the B cell field.

EBV DNA is epigenetically naïve when it is delivered upon infection but is maintained as fully chromatinized extrachromosomal plasmid DNA with mostly repressive marks in latently infected B cells. In my PhD work, I studied the role of replication-dependent and -independent histone chaperones which supposedly can load cellular histones onto the incoming viral DNA. Using novel CRISPR technology, I investigated the consequences of single or multiple knockouts of histone chaperone genes in primary human B cells. EBV infected CHAF1B depleted B cells were severely compromised and did not survive infection. My results indicated that CHAF1B is a critical factor that regulates replication of EBV DNA and prevents the genotoxic stress in the first days of infection with EBV while other histone chaperones such as HIRA, DAXX or ATRX seemed to be less critical during early viral infection.

Contents

Abstract	v
1 Introduction	1
1.1 Epstein-Barr Virus	1
1.1.1 EBV's life cycle in B cells	1
1.1.2 EBV reprograms infected B cells	2
1.2 Epigenetics	5
1.2.1 DNA methylation	5
1.2.2 Nucleosome assembly	6
1.2.2.1 Histone chaperones	6
1.2.3 Nucleosome dynamics	11
1.2.4 Post translational modifications of histones	12
1.3 Epigenetic changes during EBV infection	13
1.4 Gene editing with the CRISPR-Cas9 technology	15
1.5 Scope of my thesis	17
2 Results	19
2.1 Model of genome editing in primary human B cells - the experimental design	19
2.1.1 How to design gRNAs for efficient CRISPR-Cas9 genome editing	20
2.2 Highly efficient CRISPR-Cas9-mediated gene knockout in primary human B cells	21
2.2.1 Targeting the locus of cell surface protein CD46 in primary human B cells	21
2.2.2 Knock-out efficiency is independent of the source of B cells	23
2.2.3 Kinetics of induced DNA breaks and their repair in genome edited B cells	23
2.3 Transcriptome analysis in RNP complex treated primary human B cells	26
2.3.1 Metabolic labeling of newly transcribed RNAs with 4sU and their analysis	27
2.3.2 Detailed analysis of 4sU labeled transcripts	29
2.3.3 Studying the effect of CRISPR-Cas9 on the transcriptome of B cells	31
2.4 Functional knockout of the cell cycle inhibitor <i>CDKN2A</i> encoding p16 ^{INK4a} and its role during EBV infection of primary human B cells	32

2.4.1	p16 ^{INK4a} is a functional barrier to EBV driven proliferation of lymphoblastoid cells.	33
2.4.2	p16 ^{INK4a} negative B cells infected with Δ EBNA3A/C EBV do not differentiate into plasma cells.	35
2.5	Histone chaperones and their role in the early phase of EBV infected B cells.	37
2.5.1	Does the survival of EBV infected B cells depend on certain histone chaperones?	37
2.5.2	Regulation of the cellular metabolism in <i>CHAF1B</i> knockout B cells	43
2.5.3	EBV infected, <i>CHAF1B</i> knockout B cells arrest in the early S phase.	45
2.5.4	<i>CHAF1B</i> knockout results in high γ -H2A.X levels, DDR and DRS in EBV infected but not in CD40L/IL-4 stimulated B cells.	47
2.5.5	Control of immediate early EBV genes in the absence of <i>CHAF1B</i>	49
2.5.6	Viral DNA accumulates in <i>CHAF1B</i> knockout cells and leads to cell death of EBV infected B cells	51
3	Discussion	55
3.1	Scope and aims of my thesis	55
3.2	Genome editing in primary human B cells with the CRISPR-Cas9 technology	56
3.3	Kinetics of double stranded break repair and transcription at the site of gene editing	58
3.4	CRISPR-Cas9 genome editing identifies functions of cellular genes relevant for EBV	60
3.5	The role of histone chaperones in the biology of EBV infected B cells	61
3.6	Outlook	66
3.6.1	Possible improvements for genome editing of primary human B cells for future immunotherapeutic strategies.	66
3.6.2	How does the CAF-1 complex control EBV's DNA replication in the pre-latent phase?	66
3.6.3	Where and when do histone marks on viral DNA occur during the early phase of infection?	67
4	Materials	69
4.1	Plasmids	69
4.2	Virus supernatants	69
4.3	Antibodies	70
4.4	Eukaryotic cell lines	70
4.5	Oligonucleotides	71
4.6	Cell culture media	72

4.7	Enzymes and other chemicals	73
4.8	Commercial Kits	73
4.9	Material and devices	74
4.10	Software packages and web tools	74
5	Methods	75
5.1	Working with eukaryotic cells	75
5.1.1	Cultivation of suspension and adherent cells	75
5.1.2	Long-term storage of cells	75
5.1.3	Cell number calculation	76
5.1.4	Irradiation of CD40L expressing LL8 stimulator cells	76
5.1.5	Isolation of B cells from adenoid biopsies	76
5.1.6	Isolation of B cells from PBMCs	77
5.1.7	Virus supernatant production from HEK293 6008 and B95-8 cell lines	77
5.1.8	Determination of the virus titer	77
5.1.9	EBV infection of primary human B cells and generation of LCL	78
5.1.10	B cell activation using CD40 ligand feeder cells together with IL-4	78
5.1.11	IFN- α release assay and quantitation by ELISA	78
5.2	Flow cytometry measurements	79
5.2.1	Staining of B cell surface markers for flow cytometry	79
5.2.2	Cell cycle analysis	79
5.2.3	Staining with 2-NBDG, TMRE and Annexin V following their analysis	80
5.2.4	Intracellular staining of γ -H2A.X for flow cytometry	80
5.3	Nucleic acid related techniques	81
5.3.1	Genomic DNA purification from eukaryotic cells	81
5.3.2	Nuclear-associated compartment fractionation by NP-40	81
5.3.3	Polymerase chain reaction (PCR)	81
5.3.4	Quantitative real time PCR (qPCR)	82
5.4	CRISPR/Cas9 mediated genome editing	82
5.4.1	sgRNA design for CRISPR/Cas9 mediated genome editing	82
5.4.2	Assembly of ribonucleoprotein (RNP) complexes	83
5.4.3	Nucleofection of primary human B cells with RNP complexes	83
5.4.4	Next generation sequencing and knockout quantification	83
5.5	Protein Biochemistry	84
5.5.1	Whole cell protein lysate preparation	84

5.5.2	Protein concentration measurement	84
5.5.3	WES platform western blotting	84
5.6	4sU-RNA Seq experiment	85
5.6.1	Metabolic labeling of newly transcribed RNA with 4sU	85
5.6.2	RNA isolation	85
5.6.3	Library preparation and sequencing	86
5.7	Bioinformatic analysis	86
5.7.1	Quality control and data normalization	86
5.7.2	Gene set enrichment analysis (GSEA)	87
5.7.3	Accession number and Data availability	87
5.8	Statistical Analysis	87
6	Appendix	89
	Bibliography	97
	Acknowledgements	119
	Curriculum Vitae	121

List of Figures

1.1	The life cycle and latency programs of Epstein-Barr Virus (EBV).	3
1.2	Schematic overview of parts of the histone chaperone network.	7
1.3	EBV's tripartite life cycle.	13
2.1	Principle steps of the knockout (KO) of a cellular gene in primary human B cells using the CRISPR-Cas9 technology.	19
2.2	Highly efficient inactivation of the locus encoding the CD46 cell surface protein in primary human B cells.	22
2.3	Comparison of human B cell subsets purified from adenoid tissue or PBMCs and their susceptibility to CRISPR-Cas9 mediated genetic alteration of the CD46 locus.	24
2.4	Kinetics of DNA strand break repair in the second exon of <i>CD46</i> in non-infected and EBV-infected primary human B cells.	25
2.5	Transcriptional activity in the second exon of <i>CD46</i> in non-infected and EBV-infected primary human B cells.	28
2.6	Plots with the read coverage of 4sU labeled transcripts show a reduced transcription of only exon 1 and 2 of <i>CD46</i> in cells 24 hours after CD46-Cas9 RNP complex nucleofection.	30
2.7	Nucleofection of the CD46-Cas9 RNP complexes has no major impact on the transcriptome of human B cells.	31
2.8	Next generation sequencing of the <i>CDKN2A</i> locus in p16 KO and WT cells.	33
2.9	p16 ^{INK4a} is a functional barrier to EBV driven proliferation of lymphoblastoid cells.	34
2.10	p16 ^{INK4a} negative B cells infected with Δ EBNA3A/C do not differentiate into plasma cells.	36
2.11	Functional analysis of four different histone chaperones in primary B cells after CRISPR-Cas9 knockout and infection with EBV.	38
2.12	Transcripts of the histone chaperones CHAF1B, HIRA, DAXX and ATRX in primary human B cells infected with wild-type (WT) EBV.	39

2.13	CRISPR-Cas9 knockout of the replication independent histone chaperones <i>HIRA</i> , <i>DAXX</i> and <i>ATRX</i> in primary B cells and their functional analysis.	41
2.14	Reduced metabolic activity and fitness of B cells after <i>CHAF1B</i> KO when infected with EBV.	43
2.15	<i>CHAF1B</i> depleted and EBV infected B cells arrest in early S phase.	46
2.16	EBV infected, <i>CHAF1B</i> depleted primary B cells show high γ -H2AX levels indicative of DDR and DRS.	48
2.17	In <i>CHAF1B</i> knockout cells EBV infection leads to marginally higher expression of the early EBV gene BMRF1, but neither the induction of EBV's lytic phase nor BZLF1 have a critical role in the survival of <i>CHAF1B</i> knockout cells.	50
2.18	Viral DNA accumulates in <i>CHAF1B</i> knockout and EBV infected B cells.	52
6.1	Target sites of gRNAs for four different cellular targets (<i>CHAF1B</i> , <i>HIRA</i> , <i>DAXX</i> and <i>ATRX</i>) with their corresponding knockout efficiencies	93
6.2	Tracking of pro-apoptotic B cells during the first days after CD46- and <i>CHAF1B</i> -RNP complexes nucleofection.	94
6.3	Tracking of mitochondrial activity in B cells nucleofected with CD46- and <i>CHAF1B</i> -RNP complexes and activated by CD40L/IL-4 or EBV during the first days.	95
6.4	Uptake of the glucose analogue 2-NBDG (coupled with FITC-A) during the first days after CD46- and <i>CHAF1B</i> -RNP complexes nucleofection and activation by CD40L/IL-4 or EBV.	96

List of Tables

4.1	Virus Supernatants	69
4.2	Monoclonal antibodies	70
4.3	Common cell lines	70
4.4	PCR and sequencing primers	71
4.5	qPCR primer	71
4.6	crRNAs for genome editing	72
4.7	Media and media supplements for cultivating eukaryotic cell lines.	72
4.8	The list of enzymes and other chemicals used in this thesis	73
4.9	Commercial Kits	73
4.10	Material and devices	74
4.11	Software packages and web tools	74
5.1	LightCycler 480 cycling conditions	82
6.1	Differential gene expression (DGE) analysis comparing the transcriptomes of CD46-Cas9 and WT B cell samples.	89

List of Abbreviations

°C	degree Celcius	IM	Infectious mononucleosis
%	Percent	IGV	Integrated Genome Viewer
2-NBDG	2-[N-(7-nitrobenz-2-oxa-1,3-diazol-4-yl)amino]-2-deoxy-D-glucose	kb	kilo base
aa	amino acids	kDa	kilo Dalton
A	Adenine	KSHV	Kaposi Sarcoma associated Herpesvirus
ASF1	Anti Silencing Factor 1	l	liters
AIDS	Acquired immunodeficiency syndrome	LCLs	Lymphoblastoid B cell lines
ATRX	Alpha thalassemia/mental retardation X-linked syndrome protein	LMP	Latent Membrane Protein
ATP	Adenosine-5'-Triphosphate	mRNA	messenger RNA
M	Molar	m	milli or meter
BL	Burkitt's Lymphoma	MA	Mean Average
BCR	B Cell Receptor	MACS	Magnetic Activated Cell Sorting
BbD	Barr body Deficient	MHC	Major Histocompatibility Complex
C	Cytosine	min	minute
CAF-1	Chromatin assembly factor-1	miRNA	micro RNA
CARs	Chimeric antigen receptors	mM	milli Molar
Cas9	CRISPR-associated protein 9	MNase	Micrococcal Nuclease
cDNA	complementary DNA	MS	Multiple Sclerosis
CENPA	Centromer protein A	MOI	Multiplicity of Infection
CpG	Cytosine-phosphatidyl-guanosine	ncRNA	non-coding RNA
ChIP	Chromatin immuno precipitation	NAP-1	Nucleosome Assembly Protein-1
crRNA	CRISPR RNA	NK	Natural Killer
CRISPR	Clustered Regularly Interspaced Short Palindromic Repeats	NPC	Nasopharyngeal Carcinoma
CDKN2A	Cyclin dependent kinase inhibitor 2A	NFR	Nucleosome free regions
DA	Dalton(g/mol)	NHEJ	non-homologous end joining
		ORC	Origin Recognition Complex
		p.i.	post infection

DAXX	Death domain-associated protein 6	PAGE	Polyacrylamide gel electrophoresis
DDR	DNA Damage Response	PAM	Protospacer Adjacent Motif
DSBs	Double Stranded Breaks	PCR	Polymerase Chain Reaction
DNMT	DNA methyltrans	PCNA	Proliferating Cell Nuclear Antigen
DNA	Deoxyribonucleic acid	PTMs	Post-Translational Modifications
DNase	Deoxyribonuclease	PBMCs	Peripheral Blood Mononuclear Cells
DGE	Differential Gene Expression	PTLD	Post-Transplant Lymphoproliferative Disease
DRS	DNA Replication Stress	PML	Promyelotic leukemia
DS	Dyad Symmetry	RNA	Ribonucleic acid
EBV	Epstein Barr Virus	RNA pol II	RNA polymerase II
EBER	EBV-encoded RNA	RNA-seq	Ribonucleic acid sequencing
EBNA	EBV-encoded nuclear antigen	RNP	Ribonucleoprotein
i.e.	id est	RT	Room Temperature
IgG	Immunoglobulin G	sgRNA	single guide RNA
et al.	et alii	siRNA	small interfering RNA
etc.	et cetera	ssDNA	single stranded DNA
EtOH	ethanol	sec	second
FACS	Fluorescence-activated cell sorting	TFs	Transcription factors
FCS-A	Forward scatter area	TCRs	T cell receptors
qPCR	quantitative PCR	TMRE	Tetramethylrhodamine ethyl ester
g	gram	T	Thymine
G	Guanine	TFs	Transcription factors
GFP	Green Fluorescent Protein	tracrRNA	trans-activating CRISPR RNA
GO	Gene Ontology	TSSs	Transcription Start Sites
GSEA	Gene Set Enrichment Analysis	o/n	overnight
GC	Gastric Carcinoma	U	Unit(s)
H3	Histone H3	uH2A	ubiquitinated H2A
HL	Hodgkin's Lymphoma	UV	Ultra Violet
HP1	Heterochromatin Protein 1	WT	Wild Type
HDAC	Histone DeAcetylases		
HSV	Herpes Simplex Virus		
HIV	Herpes Immunodeficiency Virus		
h	hour(s)		
HHV-4	Humanes Herpesvirus-4		

HIRA	Histone Regulator A
H3K4	Histone H3 at lysine 4
H3K9me3	trimethylated Histone H3 at lysine 9
H3K27me3	trimethylated Histone H3 at lysine 9
H3K36me3	trimethylated Histone H3 at lysine 36
H3K9ac	acetylated Histone H3 at lysine 9
IFN	Interferon
IL	Interleukin

Chapter 1

Introduction

1.1 Epstein-Barr Virus

Epstein-Barr Virus (EBV), a human herpes virus 4 and also called HHV-4 was discovered in medical samples from patients suffering from Burkitt's lymphoma in sub-Saharan Africa by Epstein, Barr and Achong in 1964 (Epstein et al., 1964). With the help of electron microscopy, the structure of the virus was identified (Epstein et al., 1964; Hummeler et al., 1966) and its ability to infect and transform B cells was discovered a bit later (Henle et al., 1967; Pope et al., 1968). EBV was the first human tumor virus identified. *In vitro*, EBV transforms quiescent human B lymphocytes into continuously proliferating and latently infected lymphoblastoid B cell lines (LCLs). EBV escapes from the host immune system as the infected cells express a minimal number of viral genes, only, but the virus uses additional viral strategies to tweak immune recognition.

More than 90% of the world population is infected with the virus for a lifetime. If the first infection does not take place early during childhood, EBV can cause acute Infectious Mononucleosis (IM) in adolescents and adults, which is characterized by high fever, enlarged lymph nodes and tiredness (Rickinson et al., 2014). IM poses a risk to develop malignant, EBV-associated diseases (Crawford, 2001) and Multiple Sclerosis (MS) later in life (Robinson and Steinman, 2022). EBV is also associated with several malignancies beyond Burkitt's lymphoma (BL) such as nasopharyngeal carcinoma (NPC), Hodgkin's Lymphoma (HL), gastric cancer and certain T/NK cell lymphomas besides post-transplant lymphoproliferative disease (PTLD), a non-Hodgkin lymphoma, in immunocompromised patients (Taylor et al., 2015; Gottschalk et al., 2005).

1.1.1 EBV's life cycle in B cells

The journey of EBV towards resting B cells in the lymphoid tissue begins with the spread of EBV between individuals via saliva and entry of EBV through the epithelial layer of the Waldeyer's ring in the pharynx. How EBV crosses the epithelium in the oropharynx is unknown. On EBV's target

B cells the virus binds via its gp350 glycoprotein to the cellular surface molecule CD21 (Nemerow et al., 1987; Tanner et al., 1987), makes contact via a trimeric glycoprotein complex consisting of gH/gL/gp42 with MHC class II molecules, is internalized by receptor-mediated endocytosis and fuses with the endosomal membrane via its fusogenic gB glycoprotein. The viral capsid contains the viral genome, which is composed of a single double-stranded DNA molecule of approximately 170 kbp in length and codes for about 80 proteins (Speck et al., 2000; Young and Rickinson, 2004). Viral genomic DNA enters the nucleus of the infected cell when the viral capsid makes contact with a nuclear pore, but the exact mechanism of how EBV DNA is delivered is evasive.

EBV has a smart strategy to persist as an asymptomatic, lifelong infection in mostly resting quiescent memory B cells. During the early phase of infection, EBV activates the infected resting B cell by the expression of its latency III program which includes the viral genes EBNA1, 2, 3A/B/C, -LP as well as LMP1, 2A/B, the non-coding small RNAs EBER 1/2 and up to 44 miRNAs (Thorley-Lawson, 2015). *In vitro*, EBV infection reprograms resting B cells turning them into B blasts leading to their continuous proliferation as lymphoblastoid cell lines (LCLs). In contrast to *in vivo* infection, the differentiation of the reprogrammed B cells is blocked at this stage *in vitro*. The latency III program of EBV leads to massive proliferation of the infected B cells which results in an antiviral immune response by the host organism and clearance of the majority of infected B cells by cytotoxic T cells (CTLs, Figure 1.1). Some infected B cells manage to escape from eradication and establish a life-long latency in the memory B cells compartment. During this process, the viral gene expression is shut off resulting in latency II program characterized by the expression of EBNA1, LMP1, 2A/B and EBERs (Thorley-Lawson, 2015). *In vivo*, EBV infected cells evolve to become long-lived memory B cells in which the virus adopts its latency 0/I program as shown schematically in Figure 1.1. From this stage of stable latency, the virus can escape, when the memory B cells differentiates into plasma cells and concomitantly express BZLF1, the viral lytic switch gene, which induces virus *de novo* synthesis and release of infectious virions (Figure 1.1).

1.1.2 EBV reprograms infected B cells

The role of viral latent genes in B cell transformation

The expression of certain viral latent genes is essential for the establishment and maintenance of latency in EBV infected B cells. During the early phase of infection, the pre-latent phase, the EBV nuclear antigen 2 (EBNA2) and EBNA-LP are the earliest viral proteins that contribute to cellular transformation (Kempkes et al., 1995; Sinclair et al., 1994). EBNA2 acts as a viral transcription factor and together with its co-activator EBNA-LP, they control the expression of all viral latent genes during latency (Harada and Kieff, 1997; Kempkes and Ling, 2015). Viral EBNA2 also induces

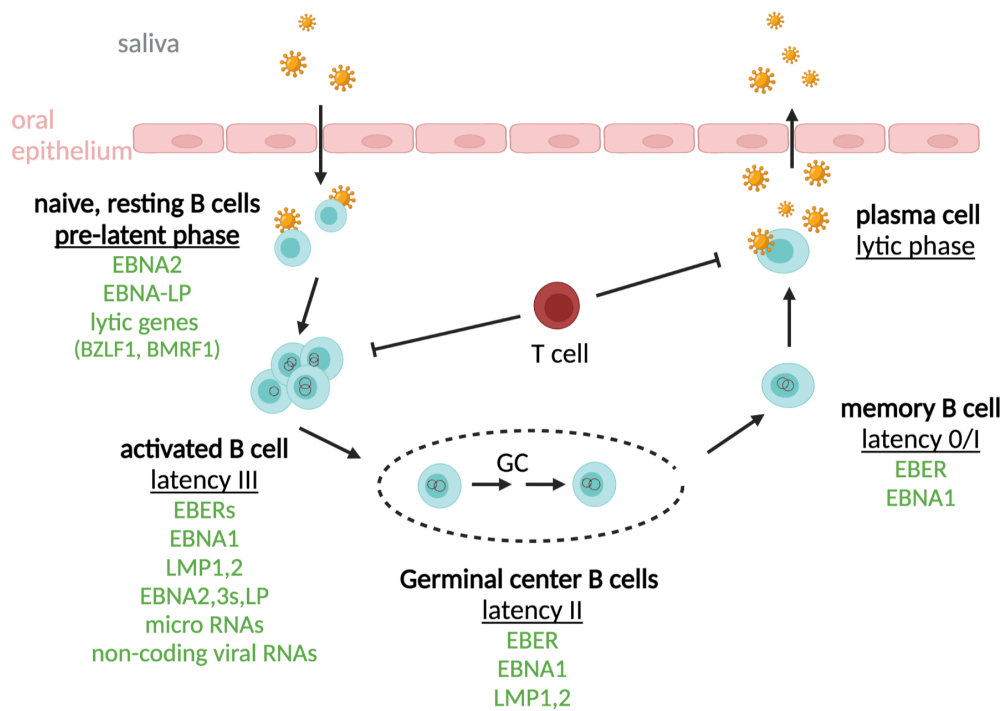


FIGURE 1.1: The life cycle and the latency programs of Epstein-Barr Virus (EBV). EBV's life cycle consists of 5 different phases; pre-latency, latency III, II, 0/I, and the lytic phase. EBV infects naive, resting B cells in the lymphoid tissue of the Waldeyer's ring. Upon infection a set of viral genes is transcribed immediately, which consists of the two viral EBNA2 and EBNA-LP genes together with certain early lytic viral genes including BZLF1, BMRF1, among others. The exact list of early lytic genes expressed during pre-latency is currently unknown. Upon epigenetic repression of lytic viral genes within a few days post infection, only latent viral genes of the latency III program are still expressed. The latency III program comprises 6 EBNA2s, 3 LMPs, 2 EBERS, several micro RNAs and other non-coding viral RNAs. The infected and activated B cells proliferate rapidly and are targets of cytotoxic T cells (CTLs) that recognize EBV derived antigenic epitopes in already EBV infected and immune competent individuals. B cells that escape the CTL response migrate to germinal centers where the cells express the reduced latency II program (EBNA1, LMPs, EBERS) and mature to memory B cells. Certain EBV infected B cells leave the germinal center and express the latency 0/I program (EBERS, EBNA1, but no other latent, protein-coding viral genes) to escape from T cell immune surveillance long-term. Upon antigen encounter and activation of the cells' cognate B cell receptor EBV infected memory B cells can undergo lytic reactivation as they differentiate to plasma cells. Concomitantly, the cells induce the lytic phase of EBV's life cycle and release newly assembled virions into the oropharynx where EBV can be found in the saliva. How EBV crosses the layer of oral epithelium is unknown (adopted from Taylor et al., 2015; Thorley-Lawson, 2015; Kalla et al., 2010).

the expression of cellular proto-oncogene *c-MYC* to support cell growth and cell cycle progression of the infected B cells (Kaiser et al., 1999). Additionally, binding of EBNA2 to enhancer sites of its cellular targets induces alterations in the chromatin architecture (Kempkes and Ling, 2015). Lastly, EBNA2 induces the expression of EBV's latent membrane proteins, the LMPs, and the three members of the EBNA3 family. LMP1 mimics the functions of the activated, i.e., ligand-bound cellular CD40 receptor (Dent et al., 1997), which stimulates and activates B cells for their continuous proliferation, independent from signals provided by T cells (Gires et al., 1997). Additionally, LMP1 also has functions in different processes such as immune modulation or gene regulation, cytokine and chemokine release (Mancao and Hammerschmidt, 2007). In addition to LMP1, LMP2A mimics tonic

cellular BCR signaling by recruiting B cell receptor (BCR) associated signal mediators, which subsequently support proliferation of B cells (Mancao and Hammerschmidt, 2007). EBNA3 family proteins consist of EBNA3A, EBNA3B and EBNA3C. Even though the EBNA3B protein is dispensable for B cell transformation, it has a role as a tumor suppressor (White et al., 2012). EBNA3A and EBNA3C function as oncoproteins and regulate cellular proliferation by targeting important tumor suppressor pathways such as pro-apoptotic BIM or the cyclin-dependent kinase inhibitor p16^{INK4a}, which *CDKN2A* encodes (Paschos et al., 2012). EBNA3A and EBNA3C are also involved in the modulation of cell cycle progression (Allday et al., 2015) and regulate epigenetic gene expression (Harth-Hertle et al., 2013; Styles et al., 2017). The EBNA1 protein is a viral factor that acts on promoters of certain viral latent genes (Kennedy and Sugden, 2003) and maintains the plasmid-like EBV genome copies ensuring their proper DNA replication by the host replication machinery in latently infected, proliferating cells (Frappier, 2015).

B cell metabolism after EBV infection

Many viruses depend on the metabolic machinery of their host cells and, consequently, viruses induce metabolic processes such as glycolysis, fatty acid synthesis and glutaminolysis to promote their successful infection and their *de novo* synthesis (Sanchez and Lagunoff, 2015). Although EBV does not turn the infected cell into a virus factory, it also needs to remodel host metabolic pathways to supply the energy required for EBV-induced growth and proliferation of EBV infected B cells. Cells infected with EBV show increased glycolytic activity as well as an increased uptake of glucose together with the expression of early viral genes (McFadden et al., 2016; Mrozek-Gorska et al., 2019). In EBV-infected nasopharyngeal carcinoma (NPC) cell lines, high levels of glycolysis were reported to result from LMP1 expression (Xiao et al., 2014). Similar to EBV infection, B cell activation mediated by IL-4 led to rapid increase in glucose uptake, aerobic glycolysis, and upregulation of specific glycolytic enzymes (Dufort et al., 2007).

Recent reports showed that EBV also induces one-carbon (1C) metabolic pathways when EBNA2 targets and activates *MYC* to efficiently drive the transformation process of B cells *in vitro* (Liang Wei Wang et al., 2019). 1C metabolism supported by a distinct mitochondria population is a group of pathways responsible for nucleotide synthesis, amino acid homeostasis and redox regulation (Ducker and Rabinowitz, 2017). This mechanism is also actively involved in cell growth and proliferation during T cell activation.

The mevalonate pathway produces compounds for cholesterol synthesis and also intermediate compounds necessary for subsequent post-translational modifications of proteins. A current study showed that upregulation of the mevalonate pathway by EBNA2 induces post-translational activation of target proteins involved likely in the trafficking of the EBV proteins LMP1 and LMP2A (Liang

Wei Wang et al., 2019).

Taken together, EBV induced activation and reprogramming of primary B cells *in vitro* depends on a plethora of cellular factors and pathways supporting EBV's success in establishing latency in its target cells.

1.2 Epigenetics

In multicellular organisms, all cells originate from the same totipotent stem cell carrying the identical genetic information. However, the gene expression profiles change dramatically in individual cells depending on cellular identity, environmental influences, growth phase, cell type and cellular functions. The term 'epigenetics' describes these phenotypic changes that do not result from changes at the level of genetic information (Weinhold, 2006). The molecular actors participating in epigenetic regulation are covalent modifications of single nucleotides and histone tails, transcription factors, noncoding RNAs (ncRNAs) and DNA binding proteins. The sum of these modifications defines active (euchromatin) or silent (heterochromatin) segments of the genome (Allis and Jenuwein, 2016). Euchromatin mainly consists of coding sequences in open configuration, thus accessible for transcription factors or other DNA binding proteins. Major parts of the mammalian genome consist of heterochromatin segments with noncoding and repetitive sequences. In contrast to euchromatin, heterochromatin is tightly packed and condensed, thus inaccessible for enzymes such as RNA polymerase II or transcriptional activators.

Epigenetic modifications generally appear as DNA methylation of CpG dinucleotides, variations of the local density of nucleosomes and activating or repressing histone modifications (and combinations thereof). These different aspects will be discussed in detail in the following sections.

1.2.1 DNA methylation

Methylation of DNA is an important epigenetic mark found in several eukaryotic lineages and is essential for mammalian development and disease. The methylation of the fifth carbon of cytosines (5-methylcytosine (5mC)) at cytosine-guanine (CpG) dinucleotides in the major groove of the DNA does not disturb the Watson/Crick base pairing capacity of nucleotides (Jeltsch, 2002) but maintains parental imprinting and controls gene expression by interfering with the DNA binding of transcription factors. Mammalian genomes show especially high CpG methylation levels as 70 to 80% of all CpGs contain 5-methylcytosines (Li and Zhang, 2014). DNA methylation patterns can be deregulated in certain cancers. A prominent example is EBV-associated gastric carcinoma (GC), which is known to have a high level of genome CpG methylation compared with most other gastric cancers

(Lizasa et al., 2012). DNA methylation might interfere with the expression of tumor suppressors supporting oncogenesis (Baylin and A.Jones, 2016).

1.2.2 Nucleosome assembly

Packaging of DNA into higher order structures to achieve high compaction of DNA in the nucleus could inhibit the binding of proteins such as transcription factors and RNA polymerase complexes that are required to synthesize mRNA in the cell. Therefore, nucleosomes are essential to regulate gene expression indirectly in addition to providing the DNA with structural stability and compactness.

Nucleosomes consist of a core of histone proteins with two copies each of the canonical histones H2A, H2B, H3 and H4, forming the so-called histone octamer (Kornberg, 1977). A single nucleosome is wrapped twice with 147 bp of DNA. Individual nucleosomes are separated by a linker region to which H1 linker histones bind forming a bead-like structure (Luger et al., 1997). The nucleosome is a highly dynamic entity which is regulated by additional protein complexes and which occupies important regulatory regions in the DNA competing with other transcription factors. Nucleosomes undergo extensive posttranslational modifications at their N-terminal side chains and, additionally, they also exist as many histone variants. Histone chaperones place histones onto DNA. Thus histone chaperones regulate nucleosome occupancy, which has an essential role in regulating chromatin structure and gene expression.

1.2.2.1 Histone chaperones

The process of nucleosome acquisition is controlled by histone chaperones. Nucleosome acquisition is essential for DNA replication, transcription, cellular differentiation and genomic stability of the cell. Histone chaperones transfer H3-H4 histone proteins onto DNA forming a tetrasome. In the following, two dimers of H2A-H2B histones are loaded onto the tetrasome to complete the nucleosome octamer and allow wrapping of the remaining DNA (Burgess and Zhang, 2013; Richmond and Davey, 2003). Specific histone chaperones adopt different roles in depositing specific histone dimers and variants. Two classes of histone chaperones are operationally defined. One class consists of chaperones that act on newly replicated DNA whereas the second class comprises chaperones that deposit histones replication-independently onto DNA (Figure 1.2).

Replication-dependent assembly of histones

'Anti-Silencing Factor 1' (ASF1) acts as a sink of non-nucleosomal H3/H4 histones and delivers them to 'Chromatin assembly factor 1' (CAF-1), which deposits H3/H4 onto newly replicated DNA (Sharp et al., 2001). CAF-1 also interacts with 'proliferating cell nuclear antigen' (PCNA) directly

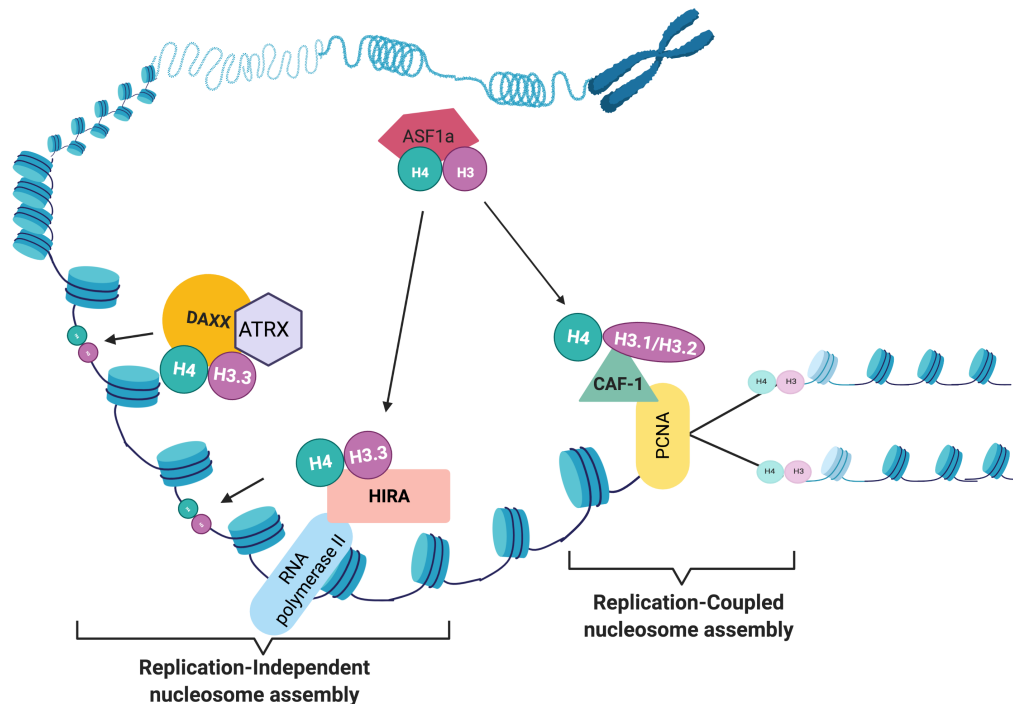


FIGURE 1.2: **Schematic overview of parts of the histone chaperone network.** ASF1 as the central histone chaperone delivers newly synthesized H3.1/H3.2-H4 dimers to CAF-1 and H3.3-H4 dimers to HIRA complexes for replication-coupled and replication-independent deposition on DNA, respectively. Replication-independent histone deposition is also supported by DAXX-ARTX chaperones and independent of ASF1's co-chaperoning function. The H2A-H2B supply is handled by NAP1 and FACT (not shown in the diagram).

behind the replication forks, where tetrasomes are formed (Burgess and Zhang, 2013; Shibahara and Stillman, 1999). In addition, nucleosome assembly protein' (NAP-1), another S phase chaperone is involved in the transport and deposition of H2A-H2B dimers on DNA during replication. Beside NAP-1, the 'facilitating chromatin transcription' (FACT) complex also acts as an H2A-H2B chaperone during transcription, DNA replication and repair (Wang et al., 2018). Incorporation of new H2A-H2B is not necessarily coupled to DNA replication as the majority of H2A-H2B exchanges also occurs replication independently (Kimura and Cook, 2001).

In terms of histone variants, the CAF-1 complex has a specific preference for the replication-dependent H3.1 variant, which is produced specifically during S phase. Although the replication dependent H3.2 variant differs from H3.1 by only one amino acid, CAF-1 does not interact with it. Lastly, the variant H3.3 is synthesized continuously and can be assembled into chromatin at any point of cell cycle (Ahmad and Henikoff, 2002). 'Histone Regulator A' (HIRA) but not CAF-1 is the preferred histone chaperone for H3.3 (Tagami et al., 2004).

CAF-1 is a trimeric heterocomplex composed of a large (CAF1-p150, CHAF1A), a small (RbAp48, P48) and a medium (CAF-1-p60, CHAF1B) subunit. CHAF1A is a multi-domain protein with roles

in replication-dependent nucleosome assembly and replication-independent stabilization of heterochromatic regions. The N-terminal region of CHAF1A contains a motif responsible for the interaction with PCNA whereas its CHAF1B interacting region resides at the C-terminus (Shibahara and Stillman, 1999). RbAp48 is a 7x WD repeat protein with two alpha-helical domains at both ends that facilitate H4 binding (Qian et al., 1993; Zhang et al., 2013). CHAF1B has also a 7x WD repeat domain that is responsible for mediating the interaction between ASF1/H3/H4 and CHAF1A within the CAF-1 complex (Smith and Stillman, 1989; Tyler et al., 2001). Therefore, CHAF1B is the central player of S phased linked CAF-1 functions. The knockdown of either CHAF1A or CHAF1B was reported to lead to the immediate halt of nucleosome acquisition and rapid degradation of the other subunits (Kaufman et al., 1995).

As CHAF1B plays an important role in DNA replication and chromatin assembly in proliferating tissues, it is linked with the pathogenesis of certain malignant cancers, including high-grade gliomas, prostate, tongue and breast cancer, salivary gland tumors and melanoma (Tayrac et al., 2013; Mascolo et al., 2010; Polo et al., 2010; Staibano et al., 2007). Therefore, CHAF1B could be a promising molecular target to counter tumor progression and may serve as a prognostic marker and predictor of metastasis. In cancer cells, a CHAF1B knockdown disturbed cell cycle progression and promoted apoptosis (Duan et al., 2019; Volk et al., 2018). Along this line, depletion of CAF-1 in HeLa cells, a cervix cancer derived epithelial cell line was shown to arrest cells in G0/G1 phase and reduced the number of cells passing through S phase. In response to CAF-1 depletion, the checkpoint kinase Chk1 is activated which is consistent with a DNA replication defect (Hoek and Stillman, 2003). Depletion of CAF-1 in yeast is not lethal but results in significantly longer Okazaki fragments due to misplacement of nucleosomes indicating DNA replication stress (Duncan J. Smith and Whitehouse., 2012). Additionally, depletion of the CAF-1 complex in yeast interferes with an activation of mitotic checkpoints due to defects in chromosomal centromere and kinetochore formation especially in combination with additional mutations in the HIRA protein (Sharp et al., 2002). CHAF1B is located on chromosome 21 and the Down syndrome is characterized by the trisomy of the entire chromosome or its distal part. In fact, CHAF1B was found to be associated with Down syndrome related pathologies (Blouin et al., 1996; Katsanis and Fisher, 1996).

Besides its role in the S phase of the cell cycle, CHAF1B has been shown to be essential for nucleotide exchange repair (NER) after DNA damage as CHAF1B brings H3.1 to nucleosomes (De Koning et al., 2007) and it is also important for recruiting ubiquitinated H2A (uH2A) to UV-damaged DNA (Zhu et al., 2009). CHAF1B is also the primary chaperone of a group of histone-like proteins called protamines, which are small linker proteins with homology to histone linker protein H1 and known to protect sperm DNA from physical damage and mutagenesis (Volk et al., 2018).

Previous reports also indicated a role of CAF-1 in nucleosome assembly and in regulating transcription. Several examples support this view. Knockdown of CHAF1A or CHAF1B led to open chromatin at certain enhancer regions of embryonic stem cell genes supporting transcription factor binding to their target loci (Cheloufi et al., 2016). Another study demonstrated the role of CAF-1 in transcriptional silencing of proviruses (Yang et al., 2015) and a knockdown study of CHAF1A in HeLa cells resulted in the loss of repressive histone marks, increase in activation marks and recruitment of RNA pol II (Poleshko et al., 2010).

Replication-independent assembly of histones

When the transcriptional machinery passes through chromatin its structure needs to be cleared to remove the nucleosomal barrier but chromatin also needs to be restored after transcription has passed. These processes are executed by a class of replication-independent histone chaperones (Steven Henikoff and Smith, 2015). This class of chaperones acts on variants of histone proteins such as H3.3, the centromeric histone H3 variant CenH3CENP-A, H2A.Z, H2A.X, H2A.Bbd (Barr body deficient histone), or MacroH2A. The HIRA complex controls the turnover of H3.3 in transcribed regions and promoters (Goldberg et al., 2010) but it is governed by interactions with RNA polymerase II and transcriptional regulators (Ray-Gallet et al., 2011). Additionally, HIRA-dependent histone deposition also facilitates transcriptional recovery after genotoxic stress (Adam et al., 2013).

HIRA forms a multiprotein complex with two proteins, Calcineurin-binding protein 1 (CABIN1) and Ubinuclein 1 (UBN1), which mediate the deposition of H3.3/H4 preferentially together with ASF1A (Pchelintsev et al., 2013; Tagami et al., 2004). Knockdown studies showed the close physical interaction between HIRA, CABIN1 and UBN1 and removal of one of these proteins destabilized the others (Taranjit Singh et al., 2011). Specific deletion of HIRA in developing mouse oocytes resulted in altered chromatin homeostasis including decreased DNA methylation, increased DNase I sensitivity and accumulation of DNA damage, along with a severe fertility phenotype (Nashun et al., 2015). Another set of experiments performed in *Xenopus* egg extracts showed that depletion of HIRA makes chromatin readily accessible to MNase cleavage, which is consistent with an impaired histone deposition (Ray-Gallet et al., 2002).

Besides HIRA, additional H3.3 chaperones, namely a complex comprised of the 'death domain-associated' (DAXX) protein and the 'alpha-thalassemia/mental retardation X-linked syndrome' (ATRX) protein is known to act on the deposition of H3.3. While HIRA is mostly active in euchromatin, DAXX mediates H3.3 deposition at pericentric heterochromatin and telomeres together with ATRX (Goldberg et al., 2010; Lewis et al., 2010). The role of DAXX is distinct from ATRX since DAXX recruits H3.3 to promyelotic leukemia (PML) nuclear bodies prior to depositing H3.3 onto DNA (Delbarre et al., 2013). Interestingly, in DAXX-depleted mouse embryonic fibroblasts a fraction of

H3.3 can be loaded by replication-dependent histone chaperones suggesting that H3.3 deposition is critical because cells can compensate a deficiency of DAXX by using alternate chaperones (Drané et al., 2010).

DAXX has been shown to interact with diverse proteins. DAXX is involved in regulating gene expression as it interacts with several DNA-binding transcription factors (TFs), epigenetic regulators, core histones and chromatin-associated proteins. The structure of DAXX defines its many functions. For example, its N-terminal helical bundle provides a docking site for many DAXX interactors (including, e.g., p53 and ATRX) (Escobar-Cabrera et al., 2010), whereas its central region mediates the core function of H3.3-specific chaperoning (Elsässer et al., 2012). Prior to its defined role as a histone H3.3 chaperone, DAXX was identified as a transcriptional co-repressor that interacts with histone deacetylases (HDAC) and DNA methyltransferases (Hollenbach et al., 2002; Puto and C.Reed, 2008).

The ATRX gene was first discovered in a study with patients suffering from the X-linked mental retardation (MR) syndrome (Gibbons et al., 1995). The N-terminus of the ATRX protein harbors the ATRX-DNMT3-DNMT3L (ADD) domain, which supports a role of ATRX during DNA methylation (Gibbons et al., 2000) and also interacts with the N-terminal tail of H3.3. On the other hand, its C-terminus contains a helicase/ATPase domain classifying ATRX as part of the chromatin remodeling factors of the SWI/SNF2 superfamily (Argentaro et al., 2007). ATRX plays a role in controlling embryonic stem cells proliferation and differentiation, besides its role in sister chromatid cohesion and chromosome congression during mitosis (Ritchie et al., 2008).

Mutations inactivating the function of DAXX and ATRX are commonly found in pancreatic neuroendocrine tumors, relapsed acute myeloid leukemia, neuroblastoma and glioblastoma (Cheung and So, 2011; Liu et al., 2012). Since these tumors have an alternative lengthening of telomeres (Lovejoy et al., 2012), ATRX and DAXX also contribute to the maintenance of telomeric chromatin structures (Wong et al., 2010). On the contrary, several cancer types including prostate, ovarian and gastric cancer show increased DAXX expression levels (Pan et al., 2013; Tsourlakis et al., 2013) suggesting that DAXX is also involved in controlling cell death, cell survival and DNA repair (Chang et al., 1998).

The H3 histone variants (H3.1/2 and H3.3) represent the bulk of nucleosome-associated histones, but multiple histone variants contribute to the diversity of chromatin structure and function (Probst et al., 2009). The replication-independent histone variant CenH3^{CENP-A} defines the centromere where it serves as an essential platform for the assembly of the kinetochore (Allshire and Karpen, 2008). Holliday junction recognition protein (HJURP) is a CenH3 specific chaperone that promotes the maintenance of CenH3 at centromeres (Foltz et al., 2009).

Among core histones, the H2A family exhibits highest sequence divergence with largest number

of variants. H2A.Z is enriched at the flanks of nucleosome-depleted regions surrounding active promoters to regulate gene activation (Raisner and Madhani, 2006). H2A.X is closely related to other H2A variants but carries an additional serine (Kinner et al., 2008), which is phosphorylated in response to DNA damage. As a consequence, phospho-H2A.X (γ -H2AX) accumulates in the nucleus at sites of DNA stress and repair. MacroH2A is another histone variant with a large carboxy-terminal ligand-binding domain (Pehrson and Fried, 1992). MaroH2A is enriched at the inactive X chromosome (Carl Costanzi & John R. Pehrson, 1998). On the contrary, H2A.BbD (Barr body deficient) is a variant that is excluded from the inactive X chromosome but colocalizes with acetylated histone H4 demonstrating its role in maintaining euchromatic functions (Chadwick and Willard, 2001).

1.2.3 Nucleosome dynamics

Two processes contribute to nucleosome dynamics. ‘Nucleosome occupancy’ refers to the probability of a nucleosome being present at a defined location whereas ‘nucleosome positioning’ describes the probability of a nucleosome at a fixed genomic coordinate. Both processes determine the accessibility of DNA regions including cellular functions from transcription to DNA replication and repair. Transcriptionally active promoters and enhancers are characterized by constitutively nucleosome free regions (NFR), which ensure that DNA is accessible to proteins, including chromatin remodelers, transcription and replication machineries. Nucleosomes are also regulated via post-translational modifications (PTMs) and the assembly of histones and histone variants into canonical or non-canonical (alternative) structures. Additionally, numerous regulatory factors, including DNA sequence preferences, PTMs, chromatin remodelers, histone chaperones and histone variant readers influence the organization of chromatin.

The flexibility of DNA depends on particular dinucleotides such as AA, TT and TA. The arrangement of these dinucleotides influences the rotation of the DNA molecule and can increase the size of the major groove of double-stranded DNA. On the contrary, a high local density of GC dinucleotides contracts the major groove, makes the DNA stiffer and prevents the wrapping of DNA around the histone octamer (Jiang and Pugh, 2009). In higher eukaryotes, cytosine methylation at CpG dinucleotides decreases the ability of DNA to bend into the major groove and CpG rich sequences can therefore influence nucleosome positioning (Nathan and Crothers, 2002; Pennings et al., 2005). In addition to the nucleotide composition of DNA, histone proteins carrying post-translational modifications have an essential role in the state of chromatin and regulate transcription, replication, and DNA damage response (DDR) (detailed in Section 1.2.3). The main regulators of nucleosome occupancy are chromatin remodelers, which use energy from ATP hydrolysis for the repositioning, reconfiguration or eviction of nucleosomes (Tyagi et al., 2016). As a consequence, remodelers can regulate the binding of transcription factors to their target sites. The replacement of DNA synthesis-coupled

histones with DNA synthesis-independent variants can also alter the composition and distribution of nucleosomes and DNA binding proteins along with the chromatin landscape.

The position and composition of nucleosomes are tightly regulated and have an essential role in regulating transcription and replication (MacAlpine and Almouzni, 2013; Radman-Livaja et al., 2010). Immediately upstream of active transcription start sites (TSSs), the nucleosomal occupancy is low but several well-positioned nucleosomes are found downstream of the TSS and into the gene body and detected across different eukaryotic organisms (Valouev et al., 2008). Not only transcription but also DNA replication are affected by local chromatin. Earlier study showed that euchromatic regions replicate early in S, whereas condensed and gene-poor heterochromatin is copied at the end of S phase (Goldman et al., 1984).

1.2.4 Post translational modifications of histones

Histone proteins carry a variety of post translational modifications at their highly basic N-terminal tails. Operationally, these modifications form the 'histone code' which plays a role in all chromatin processes including transcription, replication, repair, recombination and chromatin condensation (Jenuwein and Allis, 2001). Among the many post translational modifications methylation, acetylation, SUMOylation, ubiquitination and ribosylation of lysine residues and phosphorylation on serine and threonine residues are frequent (Kouzarides, 2007). Histone methyltransferases (HMTs) catalyze the addition of mono-, di- or tri- methyl groups at lysine or arginine residues (Greer and Shi, 2012). Methylation of histone tails is the most complex epigenetic mark which can result in different combinatorial states of individual histones with activating and repressive consequences. For instance, di- or trimethylation (me₂ or me₃) of H3K4 is associated with active transcription whereas modifications such as H3K9me and H3K27me are associated with transcriptional repression. These methylation marks at the N-terminus of histones increase the affinity of proteins with HP1 chromo domains that bind to CHAF1B for their redistribution during replication (Quivy et al., 2004). Yet another activation mark, H3K36me₃ has a role in DNA mismatch repair and DDR. Acetylation at the lysine residues by histone acetyltransferases (HATs) was found to weaken DNA-nucleosome interactions and increase chromatin accessibility for different cellular factors involved in transcription and replication (Görisch et al., 2005). Similar to histone acetylation, histone phosphorylation also reduces the interaction between DNA and nucleosomes and regulates DDR and chromatin remodeling (Rossetto et al., 2012). In sum, PTMs of histones are crucial for shaping, controlling and sustaining the epigenetic state of chromatin (Kouzarides, 2007).

1.3 Epigenetic changes during EBV infection

Epigenetics plays an essential role also in the interaction between the host cell and its pathogens during different phases of infection (Allis and Jenuwein, 2016). Pathogens, especially viruses, regulate cellular processes at the epigenetic level to promote the infection process. Viruses were shown to control epigenetic mechanisms of the infected cell at every step of the virus life cycle including histone modifications, DNA methylation and chromatin structure (Balakrishnan and Milavetz, 2017).

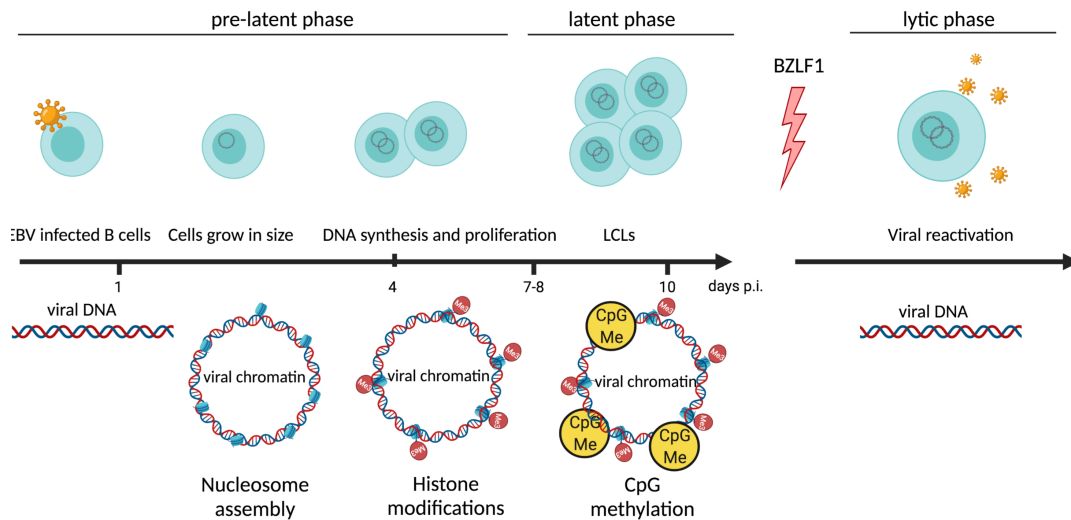


FIGURE 1.3: EBV's tripartite life cycle. The scheme depicts the three main phases of *in vitro* EBV infected human primary B cells. Initially, the infected B cells enter the pre-latent phase of EBV's life cycle during which they become activated and grow in size. Around day 3 post infection, cellular DNA synthesis starts followed by a phase of rapidly cycling and proliferating cells leading to the establishment of lymphoblastoid cell lines, which carry EBV in its latent phase about 2 weeks p.i.. Upon antigen encounter and activation of the B cell receptor the viral transactivator BZLF1 is expressed in the latently infected cells, which concomitantly enter EBV's lytic phase. In this phase, the viral DNA genome replicates asynchronously and independently of the cell cycle, newly synthesized viral DNA is packaged into viral capsids and released to infect neighboring cells. The lower part of the figure illustrates the epigenetic changes of viral DNA during the three different phases. Upon infection, EBV releases its epigenetically naive, linear DNA into the nucleus of its host cell where the viral DNA circularizes rapidly. Certain lytic viral genes are transcribed temporarily but silenced by the ensuing epigenetic modifications including nucleosome assembly, repressive histone modifications and CpG methylation of viral DNA. These measures are believed to be prerequisites for establishing EBV's stable latent phase. With the entry into EBV's lytic phase, the viral DNA loses all its epigenetic modifications and linear, unmethylated viral DNA free of histones is packaged into viral capsids to be released from the cells in a complex membranous envelope of cellular origin.

During early infection of B cells, the genome of EBV is regulated by the cellular epigenetic machinery similar to the host cell DNA (Dyson and Farrell, 1985; Shaw et al., 1979). Epigenetic regulation governs all three different phase of EBV's life cycles, i.e., the pre-latent, latent and lytic phases. Upon infection, EBV's epigenetically naive, linear and naked DNA is free of CpG methylations and lack of histones when it enters its host cell (Figure 1.3). The viral genome rapidly circularizes in the nucleus of the cell, which is presumably an important step to prevent an antiviral DDR response.

During the initial pre-latent phase, early viral gene expression starts at the multicopy W promoters, which nevertheless become epigenetically repressed a few days after infection (Altmann and Hammerschmidt, 2005; Tierney et al., 2000).

To escape from host immune responses, the naked and histone free viral DNA acquires nucleosomes to downregulate transcription of EBV and establish latency (Woellmer et al., 2012; Woellmer and Hammerschmidt, 2013). The acquisition of nucleosomes on EBV's genomic DNA seems to be completed two days after infection based on our very recent experiments (Mrozek-Górska et al., unpublished data). This observation points to the potential role of replication-independent histone chaperones (HIRA, DAXX together with ATRX) because nucleosome acquisition is complete prior to the onset of EBV's first round of DNA replication, which starts three days post infection at the earliest. The acquisition of a nucleosomal structure in EBV DNA might depend on HIRA which also governs nucleosome acquisition during fertilization when the male pronucleus forms (Lin et al., 2014). Conversely, two publications point to DAXX as an important histone chaperone early after EBV infection. Interestingly, BNRF1 is contained in virions and is immediately delivered to the infected B cells to counteract DAXX and to impair the loading of H3.3 onto viral DNA (Huang et al., 2016; Tsai et al., 2014). This impaired function might favor transcription of early latent genes, which are instrumental for reprogramming of the EBV infected resting B cells. A recent study also identified the histone chaperones CHAF1B and HIRA as latency maintenance factors which load H3 variants onto the EBV genome in Burkitt lymphoma cells to repress their entry into EBV's lytic phase (Zhang et al., 2020).

Most EBV genes are under strong epigenetic repression in EBV infected cells to support a stable viral latency. EBV chromatin is characterized by high-density packaging of nucleosomes, repressive histone modifications and prevalent CpG methylation. In latently Kaposi's sarcoma-associated herpesvirus (KSHV) infected cells, promoters of actively transcribed viral genes have activating histone marks such as H3K9ac or H3K4me4 whereas repressed late lytic genes are associated with H3K9me3 and H3K27me3 (Toth et al., 2013). Similar to KSHV, the EBV genome is densely occupied by nucleosomes with the dominating repressive histone marks H3K27me3. This histone mark is removed upon reactivation of the lytic phase in contrast to H3K9me3, a histone mark that remains unaffected (Woellmer et al., 2012). CpG methylation of EBV DNA is another layer of EBV's epigenetic regulation that takes weeks to completion (Kalla et al., 2010). Given the slow dynamics of CpG methylation, it is probably only important to repress lytic genes long-term.

With the establishment of EBV's latent phase, several copies of the viral genome are maintained in the cell as plasmid-like mini-chromosomes, also called episomes. During cell proliferation, viral DNA synthesis initiates at the viral origin of plasmid DNA replication, *oriP*, that contains a dyad symmetry (DS) and another repetitive array termed family of repeats (FR). Two nucleosome-free

regions within *oriP* allow DNA binding of the viral maintenance factor EBNA1 and the recruitment of the origin recognition complex (ORC) (Gahn and Schildkraut, 1989; Schepers et al., 2001). Although, *oriP* functions as a bidirectional replication origin (Little and Schildkraut, 1995), replication can also initiate outside of *oriP* (Norio et al., 2000). It remains elusive, how EBV derived plasmid are maintained and partitioned in proliferating cells. EBNA1 was proposed to regulate the interaction between viral DNA and cellular perichromatin (Sears et al., 2003) and to mediate the partitioning of viral genome copies during cell division (Chiu and Sugden, 2018).

Induction of the viral lytic phase initiates with the expression of BZLF1, a viral transcription factor and a member of the AP-1 family. Upon DNA binding it recruits chromatin remodelers that open repressed chromatin locally at and in vicinity of BZLF1 binding site to allow lytic gene expression (Schaeffner et al., 2019) and, eventually, packaging of the newly replicated EBV DNA into viral capsids for their release (Mckenzie and El-Guindy, 2015).

1.4 Gene editing with the CRISPR-Cas9 technology

The discovery of the Clustered Regularly Interspaced Palindromic repeats (CRISPR) (Mojica et al., 2000) surrounded by CRISPR-associated (Cas) genes (Jansen et al., 2002) in archaeal and bacterial genomes is an efficient defense mechanism against viral invasion in prokaryotes. Only recently, its biological significance and the wide range of applications in the field of biology and biomedical research have become obvious (Barrangou et al., 2007; Jinek et al., 2012). Alexander Bolotin discovered the Cas9 protein in *Streptococcus thermophilus*, which unlike other known Cas9 proteins cleaves DNA site specifically. This finding identified a common sequence in the targeted DNA, known as the protospacer adjacent motif (PAM) that allows Cas9 to recognize and bind its target DNA sequence prior to cleavage (Bolotin et al., 2005). Subsequent studies showed that Cas9 is guided to its target site by CRISPR RNAs (crRNAs) which form duplexes with trans-activating CRISPR RNAs (tracrRNA) (Brouns et al., 2008; Deltcheva et al., 2011). The application of the CRISPR technology was simplified by introducing a synthetic, combined crRNA and tracrRNA construct as a single-strand guide RNA (sgRNA) (Jinek et al., 2012). Later studies demonstrated the successful genome editing using this CRISPR-Cas9 technology in mammalian cells paving the route to a now emerging era of CRISPR-based gene therapies (Cong et al., 2013).

This rapidly evolving technology might be a promising option for treating genetic diseases, metabolic disorders and cancer. For instance, the CRISPR-Cas9 system has been widely used in the correction of human monogenic diseases such as Duchenne muscular dystrophy (DMD) (Min et al., 2019), alpha-1 antitrypsin deficiency (AATD) (Bjursell et al., 2018) and blood disorders, such as beta-thalassemia and sickle cell diseases (SCD) (Khosravi et al., 2019). To fight cancer, the CRISPR

technology allows a targeted immunotherapy with immune cells, such as T cells to express chimeric antigen receptors (CARs) on the cell surface to redirect the T effector cells (Eyquem et al., 2017). The CRISPR-Cas system might also be a promising tool to fight latent or persistent viral infections caused by human immunodeficiency virus (HIV), herpes simplex virus (HSV) or Epstein-Barr Virus. For example, the successful CAR-T cells therapy on post-transplant lymphoproliferative disorder (PTLD) patients is encouraging and EBV specific CAR-T and TCR engineered T cell therapies targeting EBV latent protein LMP1, LMP2 and/or EBNA1 have been developed aiming to kill EBV-positive cancer cells. Although CRISPR-engineered T cells in cancer patients have gained much attention, B cell therapies have a similar potential but the obstacle to engineer primary human B cells has prevented translational progress with autologous B cells in patients.

In the T cell field the *in vitro* assembly of purified bacterial Cas9 nuclease with synthetic crRNA and tracrRNA followed by nucleofection of the ribonucleoprotein (RNP) complex directly into cells was a major breakthrough (Hendel et al., 2015; Schumann et al., 2015). The highly efficient knockout of target genes in primary human T cells proved that the RNP-based CRISPR-Cas9 technology can be applied to other primary cell types (Seki and Rutz, 2018). In contrast to T cells, primary human B cells thus far have received little attention to apply the new technology even though B cells are involved in numerous biological processes as well as autoimmunity and infectious diseases. Thus far, several studies using the CRISPR-Cas9 technology have focused on mouse B cells or immortalized human B cell lines latently infected with Epstein-Barr Virus (EBV) (Cheong et al., 2016). Even though high-efficiency gene knockouts in B cells have been achieved in these cellular models, there clearly remains the need to edit the genome of primary human B cells. Along these lines, three independent groups introduced RNP complexes into human B cells that had been pre-activated with a cocktail of cytokines (Hung et al., 2018; Johnson et al., 2018; Wu et al., 2018). Results from these studies suggested that the efficiency of gene editing correlated with the level of B cell activation prior to nucleofection of the RNP complexes.

It is widely accepted that resting primary human B cells are refractory to genetic manipulation. Transfection of DNA is extremely inefficient (Kempkes et al., 1995) and gene vectors based on retroviruses, lentiviruses or adenoviruses reach transduction rates of <1% in these cells even when my group followed and tested published protocols (Funke et al., 2008; Funke et al., 2009). This refractory state is probably due to the cells' very reduced transcriptional activity, unknown restrictions that prevent efficient viral transduction, and the cells' rapid apoptosis within a couple of hours upon e.g. *in vitro* DNA electroporation (Kempkes et al., 1995). In addition, guide RNA (gRNA) directed Cas9 endonuclease induces double stranded breaks (DSBs) at the target sites that may cause a potentially fatal DNA damage response (DDR) in B cells. DSBs might be yet another problem, because it is uncertain whether endogenous DNA repair mechanisms are active in resting B cells to mend DSBs

adequately. To my knowledge, cellular repair functions of damaged DNA have not been studied in primary human B cells.

1.5 Scope of my thesis

Epstein-Barr Virus is very proficient and reaches high infection rates in resting primary B cells (Hellebrand et al., 2006). Genetic variants of EBV can be easily engineered and tested *in vitro* in this B cell model for their phenotypes, but the lack of an efficient method to modify EBV's target B cells genetically has been a major obstacle in the field. Therefore, molecular studies into human B cell biology and EBV related basic research have not been possible. In particular, the identification of cellular factors on which EBV depends to reprogram the infected B cells is lacking.

Until now and using the CRISPR-Cas technology, efficient gene knockouts in B cells have been achieved in established B cell lines (Cheong et al., 2016) or pre-activated human B cells (Wu et al., 2018), but resting primary human B cells have barely been tackled. Potential genome editing in EBV's target B cells would allow to study the role of cellular factors that, e.g., control the incoming EBV's DNA or govern its subsequent epigenetic modifications.

A recent finding from Paulina Mrozek-Gorska of my lab demonstrated the rapid acquisition of nucleosomes on the incoming EBV DNA in primary B cells within 48 hours post infection. It is very likely that molecular players such as histone chaperones are involved in this process. It seemed rewarding to identify these players as this viral model provides a unique opportunity to study *de novo* chromatin acquisition and nucleosome assembly and their regulation in mammalian cells. It was the aim of my PhD thesis to establish the CRISPR-Cas9 technology in primary human B cells and to characterize the role of histone chaperones in the early phase of EBV infection in these cells.

Firstly, I focused on establishing a protocol to manipulate primary resting human B cells genetically using *in vitro* assembled ribonucleoprotein complexes followed by EBV infection or culturing the B cells on CD40 ligand feeder cells in the presence of IL-4. I also wanted to study the kinetics of double stranded breaks (DSBs) by the Cas9 endonuclease and subsequent DNA repair in primary human B cells. I investigated the possible adverse effects of genome editing and studied the active transcription of the edited gene locus by next generation sequencing of mRNAs metabolically labeled with 4-thiouridine (4sU). Secondly, I applied the new technology in a proof-of-principle approach and targeted a cellular gene which controls B cell proliferation of EBV infected B cells and – supposedly – terminal differentiation of B cells to plasmablast and plasma cells. Thirdly, I wanted to define the role of histone chaperones in the early phase of EBV infected primary human B cells. I screened for gRNA combinations to reach high knockout efficiencies of the cellular chaperones *HIRA*, *DAXX*, *ATRX* and *CHAF1B* and analyzed the EBV infected or CD40L/IL-4 activated B cells for their ensuing

phenotypes. I discovered that CHAF1B is the major histone chaperone that EBV employs to prevent the early genotoxic death of EBV infected B cells in the S phase of the first cell cycle.

Chapter 2

Results

2.1 Model of genome editing in primary human B cells - the experimental design

Considering the central role of B cells in the immune system, I aimed at functional knockouts of selected cellular genes. Towards this aim I developed and optimized a CRISPR genome editing protocol in primary human B cells as depicted in Figure 2.1 and designed Cas9-gRNA ribonucleoprotein (RNP) complexes to target primarily the upstream coding exons of different genes. The parameters and considerations of the design of efficient gRNAs are discussed further in Section 2.1.1.

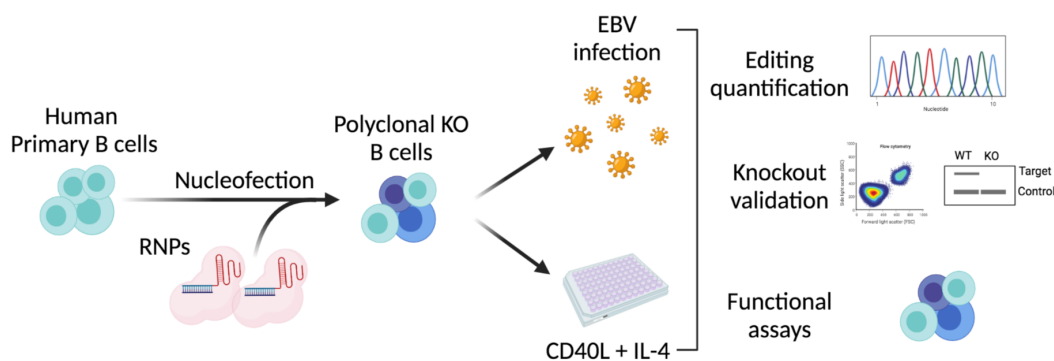


FIGURE 2.1: Principle steps of the knockout (KO) of a cellular gene in primary human B cells using the CRISPR-Cas9 technology. The schematic overview starts with the nucleofection of CRISPR-Cas9 based RNP complexes into primary human B cells isolated from adenoid tissue or PBMCs. 1 h after nucleofection the cells were infected with wild-type (WT) EBV or activated using irradiated CD40 ligand (CD40L) feeder cells together with IL-4. The efficiency of gene editing was determined at the level of nucleotide sequences and protein expression (via FACS analysis or western blot immunodetection). The functional consequences of the inactivated gene were analyzed in different assays using appropriate read-outs.

In short, the recombinant *Streptococcus pyogenes* Cas9 nuclease was assembled *in vitro* using a two-component gRNA protocol with tracrRNA and crRNA (supplied from IDT) or, alternatively, with an artificial single gRNAs (supplied from Synthego). RNP complexes assembled with two different gRNAs (gRNA1, gRNA2) were used individually or in combination. Primary human B cells

purified from human adenoid biopsies or peripheral blood mononuclear cells (PBMCs) (as described in Section 5.1.5 and 5.1.6) were mixed with RNP complexes prior to nucleofection using a Lonza electroporator and its built-in EH100 program. Primary human B cells rapidly undergo apoptosis when cultured *ex vivo* in the absence of stimulatory factors, but EBV infection rescues the B cells from cell death and reprograms them to emerge as proliferating lymphoblastoid cell lines (Mrozek-Gorska et al., 2019). Therefore, I infected the cells with wild-type (WT) EBV at an optimal multiplicity of infection (Pich et al., 2019) or cultivated the nucleofected B cells on CD40 ligand feeder cells in the presence of IL-4 as described (Wiesner et al., 2008) immediately after nucleofection. The efficiency of gene editing was investigated both at the level of nucleotide sequence and protein expression. The primary human B cells with selected genes incapable of encoding the targeted protein were used for further functional assays.

2.1.1 How to design gRNAs for efficient CRISPR-Cas9 genome editing

With the CRISPR-Cas9 system, targeting of the Cas9 nuclease to a particular locus relies on a guide RNA (gRNA) with complementary to the target DNA sequence and on the presence of a protospacer adjacent motif (PAM) sequence at the target site. Together with CRISPR genome editing, several algorithms have been developed for predicting maximal effectiveness with minimal off-target effects. In my PhD thesis, I selected crRNAs using the IDT design tool (https://eu.idtdna.com/site/order/designtool/index/CRISPR_PREDESIGN), but applied the Synthego CRISPR design tool (<https://design.synthego.com/#/>) to identify suitable gRNAs. The proposed gRNAs were analyzed further to identify target exons within their consensus coding sequences using the University of California Santa Cruz (UCSC) online genome browser (<https://genome.ucsc.edu/>). In addition to the basic criteria of gRNA design, earlier studies suggested that nucleosomes can impede Cas9 binding and cleavage (Horlbeck et al., 2016), affecting the efficiency of the CRISPR technology. To take this aspect into consideration I used available data from my lab derived from time-course MNase-seq experiments with EBV infected B cells (Mrozek-Gorska et al., unpublished) to identify nucleosome free or nucleosome depleted regions in cellular chromatin. The identification of nucleosome free regions was supported by data from ChIP-seq analysis including the histone acetylation marker (H3K27Ac) and DNase I sensitive region (Dnase C clusters) provided by UCSC. To improve knock-out efficiencies as suggested by Albanese et al. (2022), I aimed at designing pairs of gRNAs to target single genes such that the two paired gRNAs are located around 100 bp apart.

2.2 Highly efficient CRISPR-Cas9-mediated gene knockout in primary human B cells

Genetic editing with targeted nucleases allows diverse applications in experimental and therapeutic genome engineering, but an extension to primary human B cells has not been possible. Thus, almost all attempts to manipulate B cells genetically have focused on cell line models. This section of my thesis describes the detailed development of a methodology to target cellular genes in primary human B cells efficiently. Basics of this method have been published in Akidil et al. (2021).

2.2.1 Targeting the locus of cell surface protein CD46 in primary human B cells

To establish the functional knockout of genes in primary human B cells with the CRISPR-Cas9 technology, I designed RNP complexes targeting the *CD46* gene. This gene encodes a cell surface protein present on almost all cells, which is also robustly expressed in mature human B cells (Mrozek-Gorska et al., 2019 and <http://ebv-b.helmholtz-muenchen.de/>). The cell surface protein can protect cells from complement attack, it modulates adaptive immune responses in T cells and is a receptor exploited by certain bacteria and viruses. Despite these diverse functions, the survival of human B cells does not depend on its expression even *in vivo* (Fuchs et al., 2009).

The primary human B cells isolated from adenoid tissue were nucleofected with a mixture two RNP complexes containing one gRNA each. The pair of gRNAs targets two sites in the second exon of the gene locus 98 bp apart. For their *ex vivo* survival in cell culture, edited B cells were infected with wild-type (WT) EBV (6008) one hour post nucleofection. The efficiency of gene editing was investigated at the level of surface protein expression one week later with cells, which had been nucleofected with the two specific gRNAs either individually or combined Figure 2.2A. When the CD46-Cas9 RNP complexes were used individually knockout efficiencies of about 60 and 85% were observed. When both CD46-Cas9 RNP complexes were co-nucleofected knockout efficiencies regularly reached 97% and more according to measuring CD46 surface expression by flow cytometry. The analysis of the efficiency of gene editing was performed by DNA sequencing, one week after nucleofection. The efficiency of gene editing at the level of nucleotide sequence supports the protein level analysis in which maximal knockout efficiencies were reached when two specific gRNAs were used in combination (Figure 2.2B).

For primary human lymphocytes the 4D-Lonza nucleofector protocol suggests the program E0177 which might increase the efficiency of gene editing compared to my initial approach. Thus, I compared the efficiency of gene editing using the different transfection programs (Seki and Rutz, 2018). Primary human B cells from adenoid tissue were purified and the *CD46* gene was targeted with the

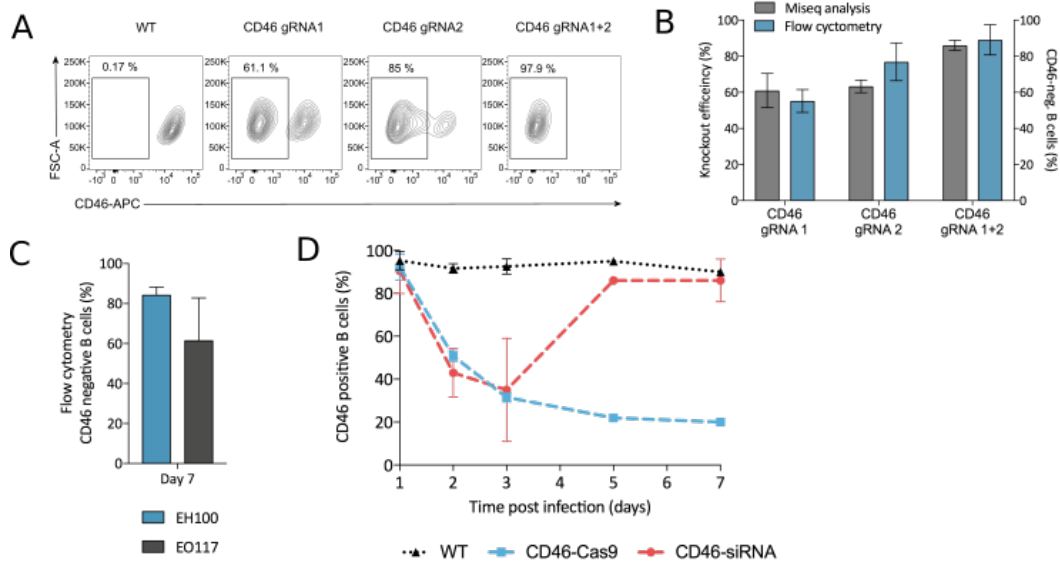


FIGURE 2.2: Highly efficient inactivation of the locus encoding the CD46 cell surface protein in primary human B cells. (A) Flow cytometry analysis of living cells for their CD46 surface expression after nucleofection with two individual Cas9 RNP complexes (gRNA1 or 2) or with both complexes targeting the *CD46* locus. (B) Knockout efficiency obtained from next generation sequencing (Miseq analysis) of the second exon of the *CD46* gene are shown together with flow cytometry analysis of CD46 protein expression as in panel A, one week after nucleofection. Mean and standard deviation from four independent biological replicates are shown. (C) Comparison of knockout efficiencies at the *CD46* locus after RNP transfection using two different nucleofection programs (EH100 and EO117) as suggested by the manufacturer (Lonza). Data are represented as mean and standard deviation of two biological and technical replicates. (D) Time course experiments indicating the percentage of CD46 positive B cells after nucleofection with CD46-Cas9 RNP complexes or with siRNAs targeting the *CD46* transcript. Mean and standard deviation from two independent biological replicates are shown.

pair of gRNAs following my protocol. When I applied the E0177 program the efficiency of gene editing at the level of CD46 surface protein expression dropped to around 60% (Figure 2.2C) as measured by flow cytometry. Therefore, the 4D-Lonza nucleofector program EH-100 was identified as the optimal protocol, in line with findings by Seki and Rutz (2018) who achieved more than 97% RNP delivery in primary human T cells.

A knockout of certain genes might be fatal to the cells such that the phenotype and function of the gene of interest cannot be studied further. On the contrary, the RNA interference (RNAi) technology provides a different means to study single cellular functions (Carthew and Erik J. Sontheimer, 2009). A small interfering RNA (siRNA) with a length of 20-25 nucleotides can regulate endo-nucleolytic cleavage of mRNAs in a sequence-dependent manner (Tomari and Zamore, 2005). siRNAs induce the specific degradation of mRNAs and inhibit their translation creating a reversible knockdown of selected proteins of interest. I wanted to check whether my new protocol for RNP-based genome editing can be also used with the siRNA technology in human primary B cells. Therefore, I identified two siRNAs using the design tool provided by IDT (https://eu.idtdna.com/site/order/designtool/index/CRISPR_PREDESIGN). The siRNAs share sequences with the two gRNAs targeting exon 2 of

CD46. As shown in Figure 2.2D, the fraction of *CD46* positive B cells dropped at day 2 with both technologies, siRNA mediated knockdown and gRNA mediated knockout. The siRNA approach showed the lowest fraction of *CD46* positive B cells after three days and the protein levels came back on day 5 post siRNA delivery as expected. With the gRNA mediated knockout of *CD46*, the protein surface levels on the B cells dropped to about 20% in the following days. Surprisingly, both approaches did not differ in their kinetics regarding the initial loss of *CD46* surface expression in the first days (Figure 2.2D). Taken together, my nucleofection protocol with primary human B cells is also applicable in combination with other genetic techniques such as the siRNA knockdown technology.

2.2.2 Knock-out efficiency is independent of the source of B cells

I was wondering whether this highly efficient protocol, which was developed using primary human B cells from adenoid tissue can be applied to B cells from other sources such as PBMCs. Towards this end, I isolated B cells from both adenoid tissue and PBMCs (as described in Section 5.1.5 and 5.1.6) with a purity of around 90% each (Figure 2.3A). The two B cell preparations consisted of about 60% naive B cells (Figure 2.3B). The purified B cells were nucleofected with the two *CD46*-Cas9 RNP complexes. According to my analysis of surface protein levels I reached a comparable knockout efficiency with B cells from both sources (Figure 2.3C). Therefore, my protocol is equally applicable to resting human B cells from sources other than secondary lymphoid organs such as adenoids.

I also wanted to know whether I could use an alternative protocol to expand the nucleofected B cells instead of infecting them with EBV. For this I cultivated primary B cells prepared from adenoid tissue on *CD40* ligand feeder cells in the presence of IL-4 as described previously (Wiesner et al., 2008). As expected, this protocol also yielded *CD46* knockout cells with superior efficiency (Figure 2.3D) indicating that EBV infection ensures the cells' *in vitro* survival, only, but does not contribute to the efficiency of gene editing using the CRISPR-Cas9 technology.

2.2.3 Kinetics of induced DNA breaks and their repair in genome edited B cells

To characterize the Cas9 mediated DNA cleavage and repair at the *CD46* locus in detail at nucleotide sequence level, I defined three different states of its exon 2 following the double-stranded DNA break (DSB). The 'intact' state is the original, unaltered DNA sequence after its targeting by *CD46*-Cas9 RNP complexes. The 'deleted state' is in place when a DNA fragment of about 98 nucleotides is lost upon the concomitant repair of two DSBs joining the distant DNA ends in exon 2 of the *CD46* locus. Lastly, DNA repair might also lead to the 'indel' state when single DSBs are

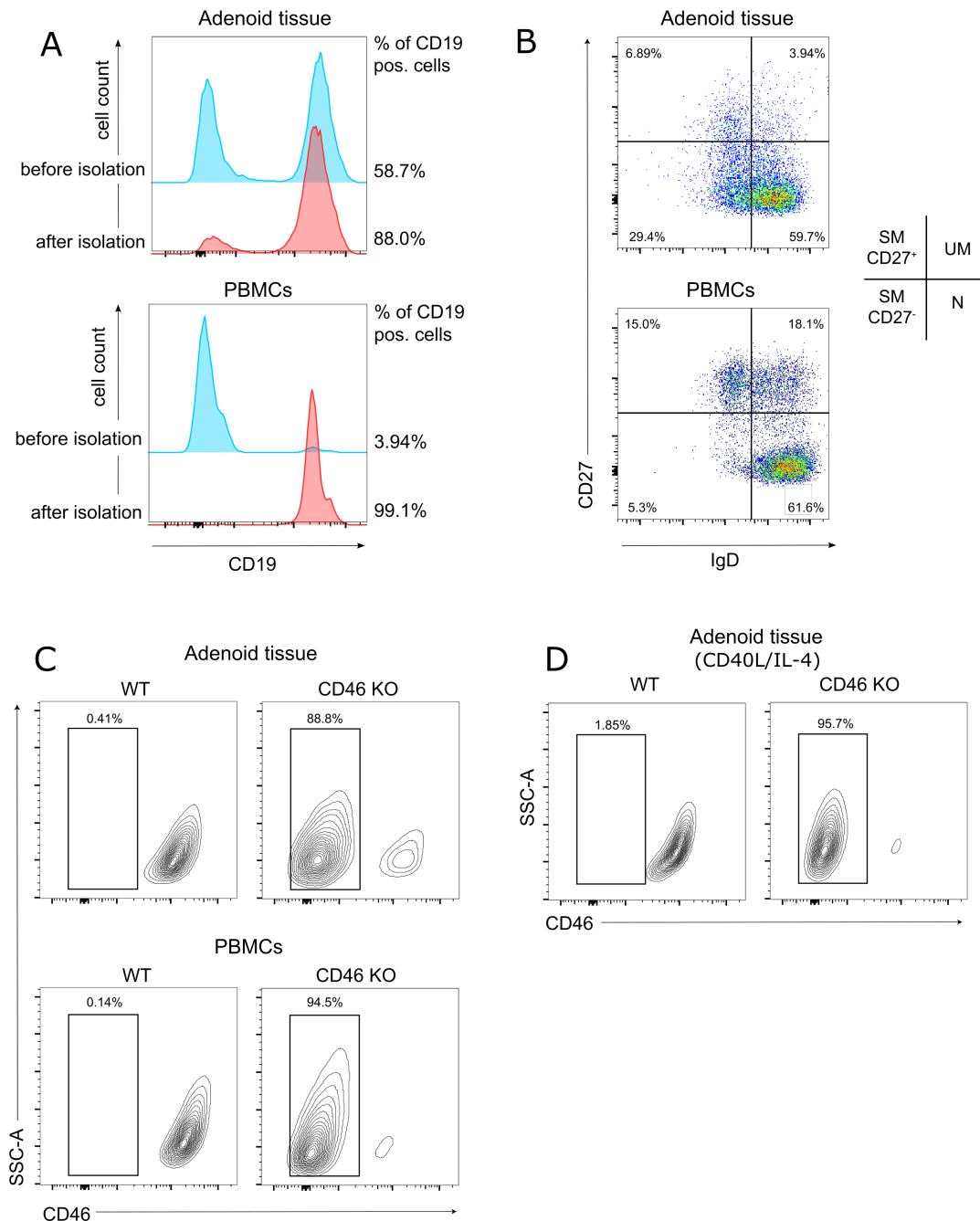


FIGURE 2.3: Comparison of human B cell subsets purified from adenoid tissue or PBMCs and their susceptibility to CRISPR-Cas9 mediated genetic alteration of the *CD46* locus. (A) B cell identity as measured by CD19 surface expression before and after B cell purification from adenoids (top) or PBMCs (bottom). (B) Flow cytometric analysis of the different subsets of B cells purified from adenoid tissues or PBMCs with antibodies directed against IgD and CD27. The nomenclature of the different B cell subsets is depicted: SM, switched memory; N, naive; UM, unswitched memory. (C) Flow cytometric analysis of CD46 surface levels on B cells obtained from adenoid and PBMC samples one week after nucleofection and infection with EBV. (D) B cells obtained from adenoid tissue after nucleofection with CD46-Cas9 RNP complexes were cultivated on irradiated CD40 ligand (CD40L) feeder cells in the presence of IL-4 for 9 days. The CD46 surface levels are shown.

repaired by the non-homologous end joining (NHEJ) pathway which often introduces small insertions or deletions at the repaired site. Different states of the DSB repaired products were visualized after next-generation sequencing of the PCR products by using the Outknocker webtool

(<http://www.outknocker.org/outknocker2.html>) (Figure 2.4A). The analysis was obtained from B

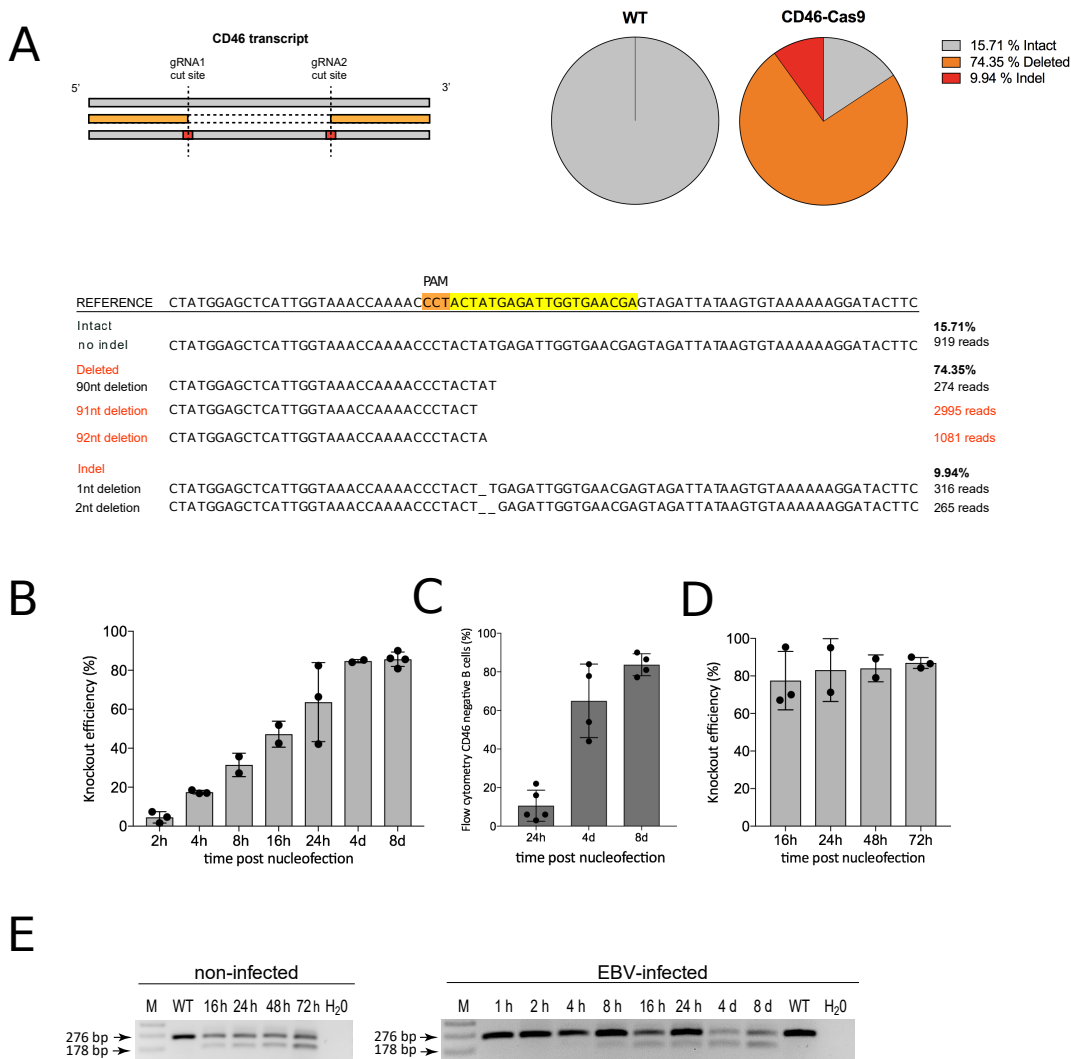


FIGURE 2.4: Kinetics of DNA strand break repair in the second exon of *CD46* in non-infected and EBV-infected primary human B cells. (A) The insertions and deletions in exon 2 of the *CD46* gene in WT EBV (6008) infected primary human B cells were analyzed 8 days post nucleofection. Cellular DNAs were PCR amplified, sequenced and analyzed with the Outknocker webtool. Reads from B cells nucleofected with the CD46-Cas9 RNP complexes (CD46-Cas9) were aligned to the hg19 reference human genome and are summarized in pie charts. Unique sequences are displayed below as examples. The target site of gRNA1, the upstream CD46 specific crRNA is highlighted in yellow within the reference sequence of the *CD46* locus; the PAM sequence is highlighted in orange. (B) The time course experiments show the knockout efficiency in the second exon of *CD46* in EBV infected primary B cells after nucleofection with two CD46-Cas9 RNP complexes. The next generation sequencing analysis was performed as shown in panel A. Knockout efficiency reached to 60% 24 h after nucleofection and increased up to 85% later days. Mean and standard deviation of independent biological replicates are shown. (C) CD46 flow cytometry analyses of primary B cells 1, 4 and 8 days post nucleofection with two CD46-Cas9 RNP complexes and subsequent infection with EBV are shown. Mean and standard deviation of independent biological replicates are provided. (D) Primary human B cells were nucleofected with the two CD46-Cas9 RNP complexes and left non-infected. At 16, 24, 48 and 72 hours later, cellular DNA of viable cells was amplified by PCR prior to next generation sequencing. Data were analyzed using the Outknocker webtool. The results showed a knockout efficiency of 70% in primary human B cells as early as 16 h after nucleofection which increased up to 90% 72 h after nucleofection. Mean and standard deviation of independent biological replicates are shown. (E) Representative agarose gels of PCR products covering exon 2 of the *CD46* locus in non-infected and EBV-infected B cells after nucleofection with two CD46-Cas9 RNP complexes at indicated time points post nucleofection. The PCR product of the intact and partially deleted exon 2 of the *CD46* locus are 276 bp and 178 bp in length, respectively, and can be visualized on agarose gels. Representative gels from three independent biological replicates from non-infected and EBV infected cells are shown.

cells nucleofected with the CD46-RNP complexes 8 days post nucleofection. Reads from B cells were aligned to the hg19 human reference genome and reads were summarized in pie charts for three different states of DNA repair. Almost 75% of the reads reflected the deleted state of the locus whereas only 9.9% of the reads showed the indel state. All in all, the knock out efficiency of the *CD46* exon 2 locus reached 84.2% 8 days post nucleofection.

To identify the kinetics of the different states, I isolated genomic cellular DNA from EBV infected primary B cells at various time points after nucleofection. At each time point, I PCR-amplified a region that encompasses exon 2 of *CD46* including the two gRNAs target sites. To study the 'indel' and 'deleted' states, I set out to determine the activity of the repair machinery via next-generation sequencing of the PCR products. The results showed a constant increase of knockout efficiencies that reached 60% 24 hours after nucleofection (Figure 2.4B). A couple of days later, knockout efficiencies plateaued at about 85%. I also analyzed the PCR products on agarose gels and found a DNA fragment of approximately 180 bp in size already 8 hours after nucleofection indicative of the deleted state (Figure 2.4E). In parallel, the loss of CD46 surface protein was studied by flow cytometry over time (Figure 2.4C). A small fraction of CD46 negative cells, about 10%, became detectable as early as 24 h after nucleofection. This fraction steadily increased to more than 85% on day 8, consistent with a moderate protein turnover of this surface receptor after the genetic knockout of *CD46*.

Next, I studied the kinetics of DSB and DNA repair in non-infected cells over time. The results showed a 70% knockout efficiency in primary human B cells 16 h after nucleofection and up to 85% 72 h after nucleofection, before the non-infected residual B cells rapidly underwent apoptosis (Figure 2.4D). I also analyzed the PCR products on agarose gels and found a DNA fragment of approximately 180 bp in size already 16 hours after nucleofection indicative of the deleted state (Figure 2.4E). Together, these observations suggested a substantial DSB activity followed by an efficient DNA repair that caused indels and deletions in the majority of non-infected primary B cells within hours after nucleofection. These results led me to conclude that Cas9 rapidly locates to its specific target site in resting primary human B cells and introduces DSBs with high efficiency. The endogenous DNA repair mechanisms are active in these primary cells independent of EBV-induced B cell activation.

2.3 Transcriptome analysis in RNP complex treated primary human B cells

A recent report showed that Cas9 remains attached to DNA ends after *in vitro* cleavage (Sternberg et al., 2014), which might result in a roadblock of transcription. Additionally, the processes of nucleofection, DSBs induced by Cas9 and their repair might induce cellular stress that could also

affect the transcriptome of the cells. To study the transcriptome and investigate possible adverse effects and, in particular, nascent CD46 transcripts I employed metabolic labeling of newly synthesized RNA with 4-thiouridine (4sU). The findings in this section have been published in Akidil et al., 2021.

2.3.1 Metabolic labeling of newly transcribed RNAs with 4sU and their analysis

The transcriptome of cells is often investigated looking at the abundance of RNA transcripts. These well-established methods reveal steady-state levels of transcripts resulting from both RNA synthesis and processing. With the emergence of next generation sequencing technologies the uridine analog 4-thiouridine (4sU), which is used as a metabolic label allows to study genome-wide RNA kinetics at high resolution (Rabani et al., 2011; Garibaldi et al., 2017). Basically, upon uptake of 4sU by eukaryotic cells the nucleotide analog is incorporated into newly transcribed RNA replacing uridine. Following isolation of total cellular RNA, the fraction of 4sU-labeled RNA is thiol-specifically separated from unlabeled RNA with high purity using streptavidin-coated magnetic beads. As a result, the newly transcribed RNA reflects the transcriptional activity of genes within the period of 4sU exposure.

As depicted in Figure 2.5A, isolated primary human B cells (2×10^7 cells) from three donors were nucleofected with the two CD46-Cas9 RNP complexes and infected with WT EBV (6008) one hour later. 23 hours after nucleofection newly transcribed RNAs were metabolically labeled with 4sU for 60 minutes. The concentration of 4sU and its incubation time with primary human B cells were based on earlier studies (Windhager et al., 2012; Rädle et al., 2013). As a control, non-nucleofected (WT) but equally EBV infected and 4sU labeled cells were prepared. The labeled RNA was thiol-specifically biotinylated and separated from unlabeled, preexisting RNA as shown in Figure 2.5B. After proper analysis and quantitation of the 4sU labeled and purified RNAs, cDNA libraries were established including cDNA amplification with specific adaptors to allow multiplex sequencing at the Heinrich Pette Institute, Hamburg, Germany. Equimolar amounts of the obtained libraries were sequenced on a Nextseq500 (Illumina) platform. From all samples 150 base-long paired-end sequence information and 15.7 to 18.6 million reads per sample were obtained. The analysis of the original RNA sequencing data was performed following the steps depicted in Figure 2.5C. The RNA-seq data obtained from CD46-Cas9 and WT B cell samples from 3 different B cell donors were initially checked for read quality with MultiQC (Ewels et al., 2016). This analysis provided a fast check of the sequencing output covering quality scores per base, GC content, overrepresented sequences and duplication levels. I identified some portions of the reads as low quality which mainly resulted from the attached adapter sequences as part of the sequencing. These contaminating sequences were

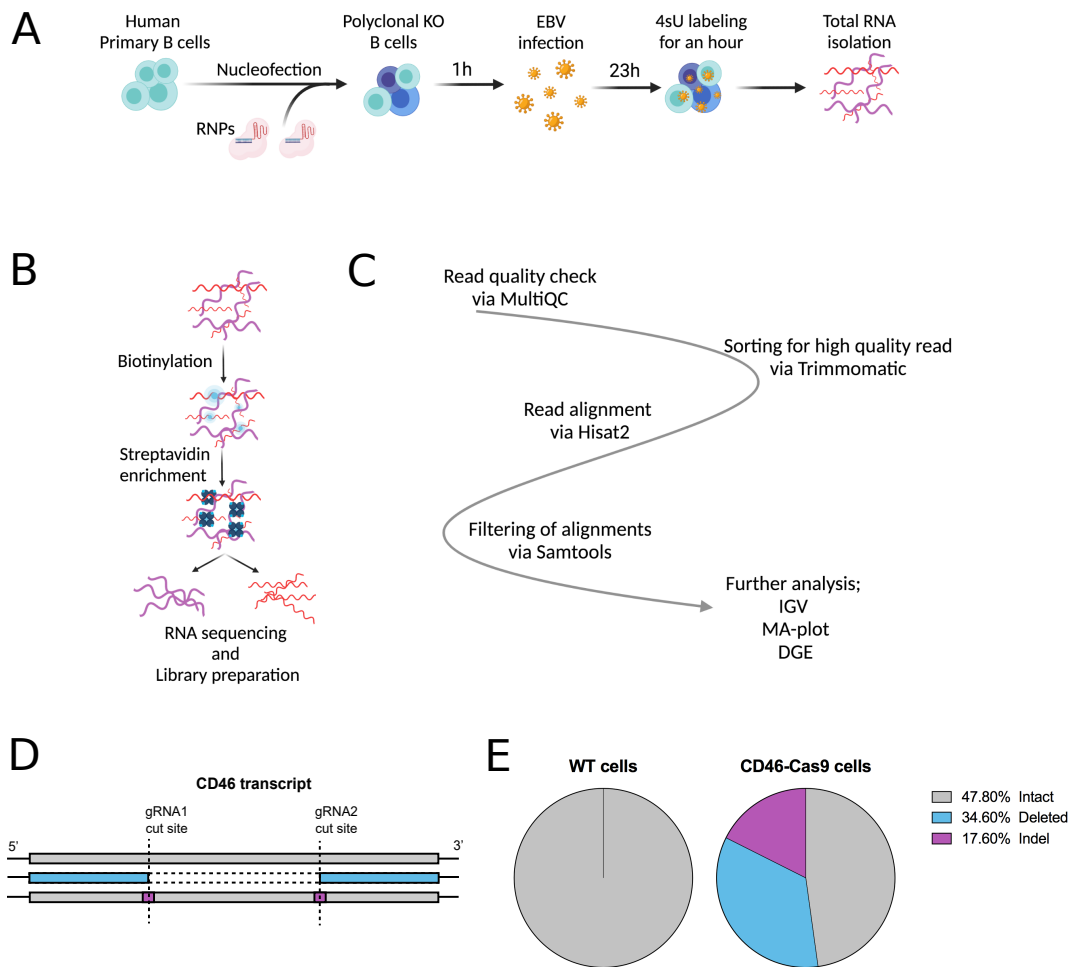


FIGURE 2.5: Transcriptional activity in the second exon of *CD46* in non-infected and EBV-infected primary human B cells. (A) Scheme of metabolic labeling of newly transcribed RNAs with 4sU. 2×10^7 primary human B cells were nucleofected with two *CD46*-Cas9 RNP complexes. Nucleofected as well as adjusted numbers of untreated (WT) B cell samples were infected with wild-type (WT) EBV. 23 hours after nucleofection, newly transcribed RNAs were metabolically labeled with 4sU for 1 hour. Total RNAs were isolated as described in Section 5.6.2. (B) Scheme of sorting the newly transcribed RNA from pre-existing and non-labeled RNA. Biotinylation of transcribed 4sU labeled RNAs and streptavidin enrichment of biotinylated RNA allowed the construction of cDNA libraries which were sequenced on a NextSeq500 (Illumina) instrument with 150 nt paired end reads. (C) The scheme illustrates the main steps for the bioinformatic analyses of the RNA-seq data (QC, quality control; IGV, Integrative Genomic Viewer; MA, mean average; DGE, differential gene expression). (D) Three schematic examples of mapped reads aligned to the hg19 reference sequence together with the two RNP complex target sites (chr1: 207,930,419-207,930,438 and chr1: 207,930,497-207,930,516) at exon 2 of the *CD46* gene. Reads with unmodified exon 2 (WT) sequences, reads with nucleotide mutations (indels, i.e. base changes or small insertions and deletions) and reads with deletions in between the two annotated RNP complex target sites shown with their relative frequencies 24 hours post nucleofection.

trimmed for leading and trailing bases with a quality threshold of 20 each using the Trimmomatic software (0.39) (Bolger et al., 2014). In the following, the reads were mapped to Human Genome 19 with Hisat2 (2.1.0), which is an alignment program for mapping next-generation sequencing reads (Kim et al., 2015). Lastly, low quality alignments were removed and file format conversion was performed by Samtools (1.10) (Heng Li et al., 2009).

The sorted reads obtained after bioinformatics processing were displayed in the Integrative Genomics Viewer (IGV) (Robinson et al., 2011). Next, the occurrence of mutations in the RNA of exon 2 of *CD46* gene was analyzed and reads were assigned to three different groups as mentioned previously; 'intact', 'deleted' and 'indel'. The reads were normalized to the total number of reads within each replicate and the mean of three independent replicates was calculated. As shown in Figure 2.5D, all reads from untreated (WT) B cell samples were identical with the reference sequence, whereas only 47.8% of the reads in CD46-Cas9 treated RNA samples were unchanged. 17.6% of the reads in these RNA libraries showed mutations whereas the remaining 34.6% documented the deletion of about 98 nucleotides as expected 24 hours after nucleofection. All in all, the experiments showed that more than 50% of exon 2 transcripts of CD46 contained indels or were deleted indicating that cleavage and repair of the template DNA were already completed and transcription of the edited gene had resumed and was functional as early as 24 hours post nucleofection.

2.3.2 Detailed analysis of 4sU labeled transcripts

Based on the preliminary analysis at the *CD46* locus as described in the previous chapter, active transcription at the Cas9 target side had resumed after DSB and DNA repair already 24 hours after nucleofection, which was unexpected. I also wanted to study the effect of gene editing at exon 2 focusing on the upstream exon 1 and *CD46* exons downstream of the Cas9 target site. Therefore, I examined the CD46 transcript and its exon-related read profiles in non-nucleofected, untreated cells and in cells 24 hours after CD46-Cas9 RNP complex nucleofection. Apparently, the overall read coverage of exon 2 RNA was reduced to about one third in nucleofected cells compared with RNA data from non-nucleofected B cell samples (Figure 2.6A). The significant drop in read coverage was also observed in the upstream exon 1 of the CD46 transcript which might result from a road blockage of the transcription machinery as the Cas9 RNP complex stays attached to DNA ends after cleavage. However, I did not observe clear differences in read coverage in the CD46 transcript downstream of exon 2 (Figure 2.6A).

To analyze whether the differences in read coverage in nucleofected and untreated cells were specific to exon 2 of the CD46 transcript, I identified exons from other transcripts (ATN1, DICER, FCRL5) with the same number of nucleotides (189 nt) for comparison. The exons of equal length did not show differences between nucleofected and untreated cells (Figure 2.6B, upper panel). In addition, profiles of the read coverage of the last exon of CD46 RNA compared with the last exons of other transcripts were comparable (Figure 2.6B, lower panel). In summary, Cas9 mediated editing of the *CD46* locus led to alterations in exon 1 and 2 of the CD46 transcript, only, but did not seem to affect other transcripts and their steady-state levels.

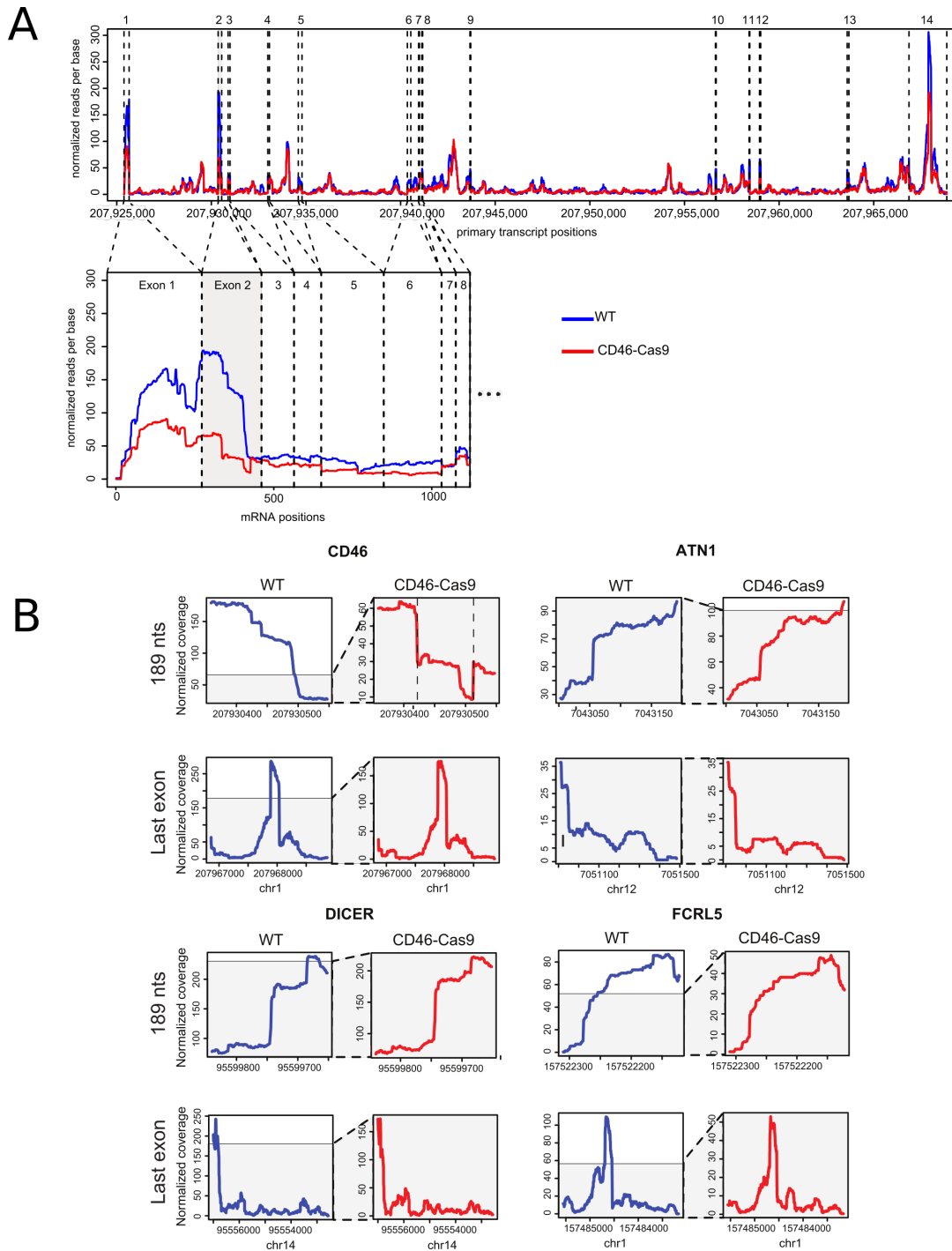


FIGURE 2.6: Plots with the read coverage of 4sU labeled transcripts show a reduced transcription of only exon 1 and 2 of *CD46* in cells 24 hours after *CD46*-Cas9 RNP complex nucleofection. (A) The plot shows the primary, unspliced transcript of the *CD46* gene on chromosome 1 together with its nucleotide coordinates and the 14 exons (dashed, vertical lines) of the *CD46* transcript (x-axis). The normalized read coverage at single nucleotide resolution is shown (y-axis) from WT cells (blue line) and *CD46*-Cas9 treated cells (red line). The lower graph depicts the mRNA data of exon 1 to 8 of the *CD46* transcript covering the two conditions. Read normalization of three pairs of biological replicates was performed. **(B)** The plots show the primary transcript positions (bp) (x-axis) vs. the normalized read coverage at single nucleotide resolution of four selected transcripts (*CD46*, *ATN1*, *DICER*, *FCRL5*). Transcript data (y-axis) from WT cells (blue line) and *CD46*-Cas9 nucleofected cells (red line) are shown. Plots indicated '189 nts' visualize the 189 nt long exons of the *ATN1*, *DICER* and *FCRL5* transcripts together with the second exon of the *CD46* transcript. Plots of the last exons of the four transcripts are shown below for comparison. The two dashed vertical lines in the plot of the second exon of *CD46* indicate the positions of the Cas9 mediated cleavage sites.

2.3.3 Studying the effect of CRISPR-Cas9 on the transcriptome of B cells

I performed a differential gene expression (DGE) analysis comparing the transcriptomes of CD46-Cas9 and WT B cell samples using the DeSeq2 package in R (Love et al., 2014). Basically, The DeSeq approach identifies differentially expressed genes based on the count number of reads mapped to each transcript. 11,782 genes were included into the analysis and after normalization, 182 genes were detected to be differentially expressed in this comparison ($\text{padj} < 0.05$) (Supplementary Table 6.1 in Appendix). The comparison was visualized in a Mean-Average (MA) plot (Figure 2.7A) indicating the \log_2 fold changes versus the mean of normalized counts for all the samples. Although the CD46 transcript does not belong to the group of differentially expressed genes, the transcription at the *CD46* locus was reduced by a factor of 0.73 in nucleofected cells as compared to control cells. In addition to CD46, I inspected the transcripts of genes involved in the different pathways of DNA repair (*RAD51AP1*, *XRCC4*, *XRCC1*, *H2AFX*, *RBBP8*, *MRE11A*, *MTOR*, *CDKN1A*, *ATM*, *XRCC5*, *XRCC6*, *MCM2*). However, none of the genes related to DNA repair showed a clear trend. This finding suggested that the nucleofected and gene-edited cells did not respond with a global stress response nor induced factors involved in DNA repair as a consequence of severed DNA strands.

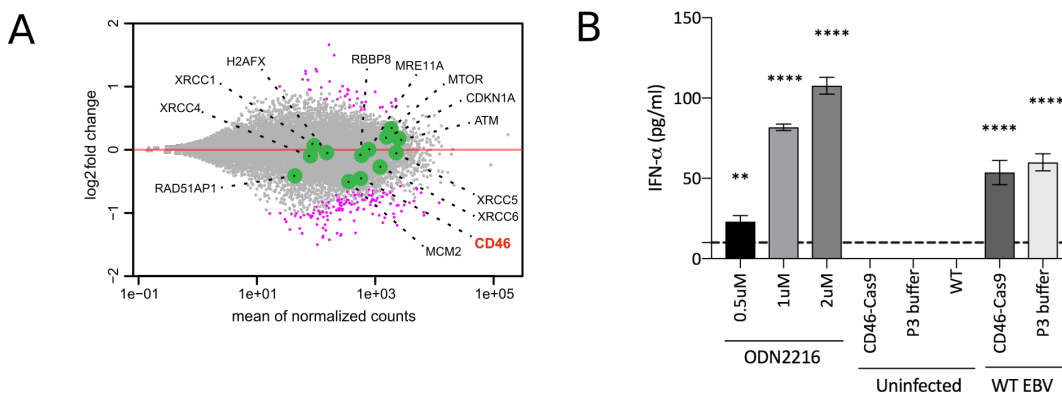


FIGURE 2.7: Nucleofection of the CD46-Cas9 RNP complexes has no major impact on the transcriptome of human B cells. (A) A mean average (MA) plot shows the differentially expressed genes comparing CD46-Cas9 vs. untreated (WT) B cell samples following EBV infection and 4sU labeling 24 hours after B cell preparation. 2-fold changes and mean of normalized read counts were plotted on the y- and x-axes, respectively. 182 differentially expressed genes are designated by magenta dots. Transcripts of the *CD46* gene and genes involved in the different pathways of DNA repair are highlighted with green dots. (B) IFN- α release of primary B lymphocytes after CD46-RNP complex or P3 buffer nucleofection with or without WT EBV infection. After 48 hours, supernatants were collected and IFN- α in the cell supernatant was measured by ELISA. As positive controls, uninfected cells were treated with different concentration of the TLR9 agonist ODN2216 for 20 hours prior to analysis. The threshold of detection was 10 pg/ml IFN- α as indicated by the dashed line. P values were calculated using the one-way ANOVA test. ****, $P < 0.0001$, **, $P < 0.01$. Mean and standard deviation of two biological and technical replicates are shown.

The group of significantly regulated genes (fold change > 2 , $\text{padj} < 0.05$) in the DGE analysis did not provide clear hints either because many individually regulated genes did not seem to share clear biological functions. To address this problem, I performed Gene ontology (GO) and a gene set enrichment analysis (GSEA) using Webgestalt (<http://www.webgestalt.org/>) to generate gene sets,

which could be differentially regulated. Such lists included, e.g., ‘nucleosome’ and ‘DNA packaging complex’ entries among other sets but their differential regulation was not convincing. From this data I concluded that Cas9 nucleofection and DNA cleavage have no global effect on ongoing cellular transcription.

My detailed transcriptomic analyses did not reveal adverse effects in cells after nucleofection of RNP complexes. As these complexes contain synthetic gRNA molecules and probably also free, non-complexed tracrRNA and crRNA, I asked whether these RNAs might trigger a type I interferon (IFN) response. To test this, B cells were nucleofected with CD46-Cas9 RNP complexes or left untreated. The next day the identical number of cells were seeded and the concentration of IFN- α , which had accumulated in the following 24 hours was measured by ELISA. As a positive control, uninfected cells were treated with different concentrations of the TLR9 agonist ODN2216, which resulted in substantial amount of IFN- α release (Figure 2.7B). EBV infected cells released low levels of IFN- α as reported previously (Bouvet et al., 2021), but IFN- α levels released from uninfected yet nucleofected cells were below the threshold level of detection (Figure 2.7B). This analysis indicated that RNP complex delivery to primary human B cells via electroporation did not induce an adverse type I interferon response in these cells.

2.4 Functional knockout of the cell cycle inhibitor *CDKN2A* encoding p16^{INK4a} and its role during EBV infection of primary human B cells

For a functional proof-of-principle, I targeted an EBV relevant cellular gene, *CDKN2A*, which encodes p16^{INK4a}, the CDK4 kinase and cell cycle inhibitor controlling cell cycle G1 progression (Allday, 2013). This gene acts as an important tumor suppressor gene, which is deleted or not expressed in various tumor types (Kim and Sharpless, 2006). I planned to validate the role of *CDKN2A* in EBV infection using my CRISPR-Cas9 approach by inactivating this gene in primary human B cells from different donors¹. Towards this aim, I designed a gRNA that targets exon 1 α of the *CDKN2A* locus. As shown schematically in Figure 2.8A, knockouts in this exon will cause frame shift mutations affecting the translation of p16^{INK4a}. I confirmed the successful genome editing at the *CDKN2A* gene locus with knockout efficiencies of about 60 to 80% one week after nucleofection as expected from a single DSB that occurred in all cells (Figure 2.8B). The successful editing of the *CDKN2A* gene allowed me to re-investigate earlier studies in the EBV field which will be represented and discussed in the next chapters.

¹Data in this section are already published in Akidil et al. (2021).

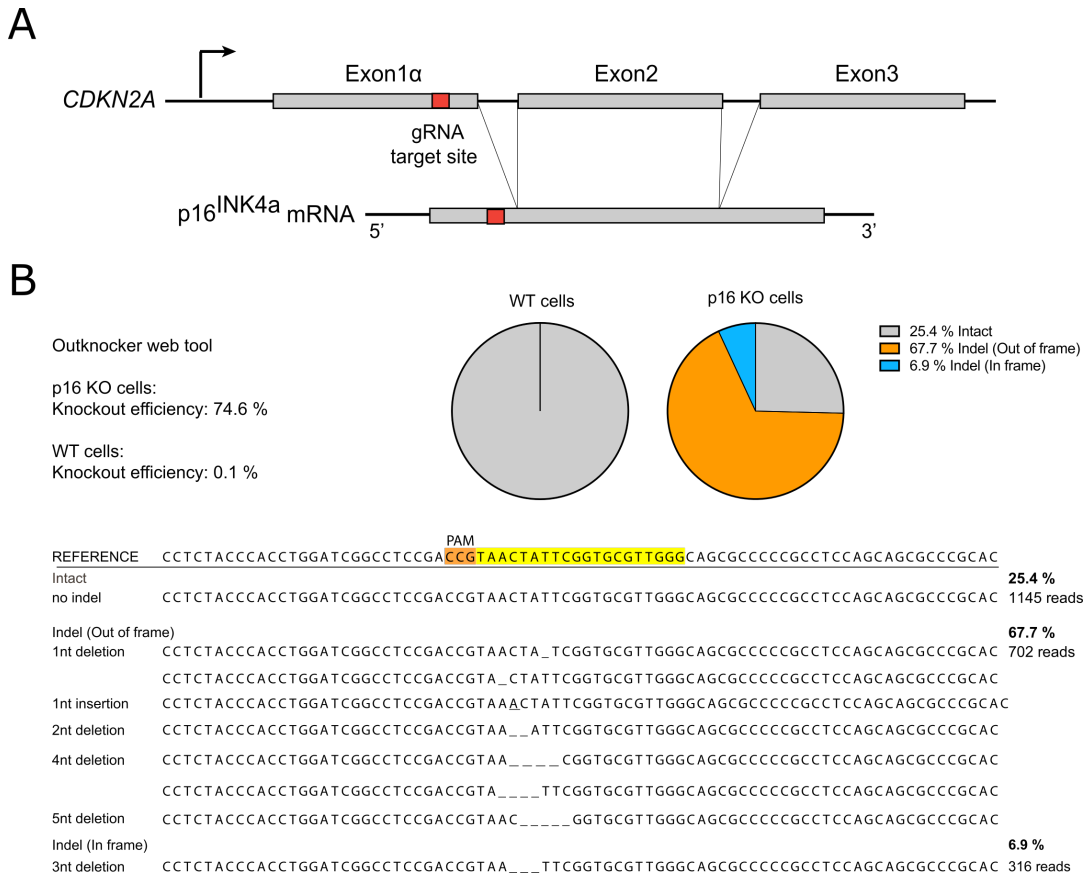


FIGURE 2.8: Next generation sequencing of the *CDKN2A* locus in p16 KO and WT cells. (A) Blueprint of the primary transcript and the spliced mRNA with the three exons of the *CDKN2A* gene encoding the p16^{INK4a} protein on chromosome 9. The target site of the RNP complex within the 1st exon (exon 1 α) (chr9:21,974,678 -21,974,827) is shown. (B) The insertions and deletions in exon 1 α of *CDKN2A* encoding p16^{INK4a} were analyzed in primary human B cells two weeks post nucleofection. Cellular DNA of the *CDKN2A* locus was PCR amplified, sequenced and analyzed with the Outknocker webtool. Reads for WT and p16 KO cells were aligned to the hg19 reference human sequence. The results are summarized in pie charts and unique read sequences are displayed below as examples. The target site of the *CDKN2A* specific crRNA and the PAM sequence are highlighted in yellow and orange, respectively, in the reference sequence.

2.4.1 p16^{INK4a} is a functional barrier to EBV driven proliferation of lymphoblastoid cells.

The previous study by Skalska et al. (2013) suggested that EBNA3C, a transcriptional repressor and latent EBV gene is responsible for epigenetic repression of *CDKN2A* in latently infected lymphoblastoid cell lines. This conclusion is mostly based on circumstantial evidence but a single infection experiment with primary B cells from an individual with a genetic lesion in p16^{INK4a} supported this conclusion (Skalska et al., 2013). Evidently, there is a need to test these earlier findings.

Towards this end, primary wild-type (WT) B cells and p16 KO cells from the same donor were mixed such that the latter comprised 10 to 20% of the total population, initially. The cells were infected with the WT EBV (6008) strain or the Δ EBNA3C (6123) mutant EBV (Pich et al., 2019) to establish four different lymphoblastoid cell lines (LCLs) from each donor. The cells were cultivated for up to 10 weeks and occasionally sampled for their cellular DNAs to analyze the *CDKN2A* knockout

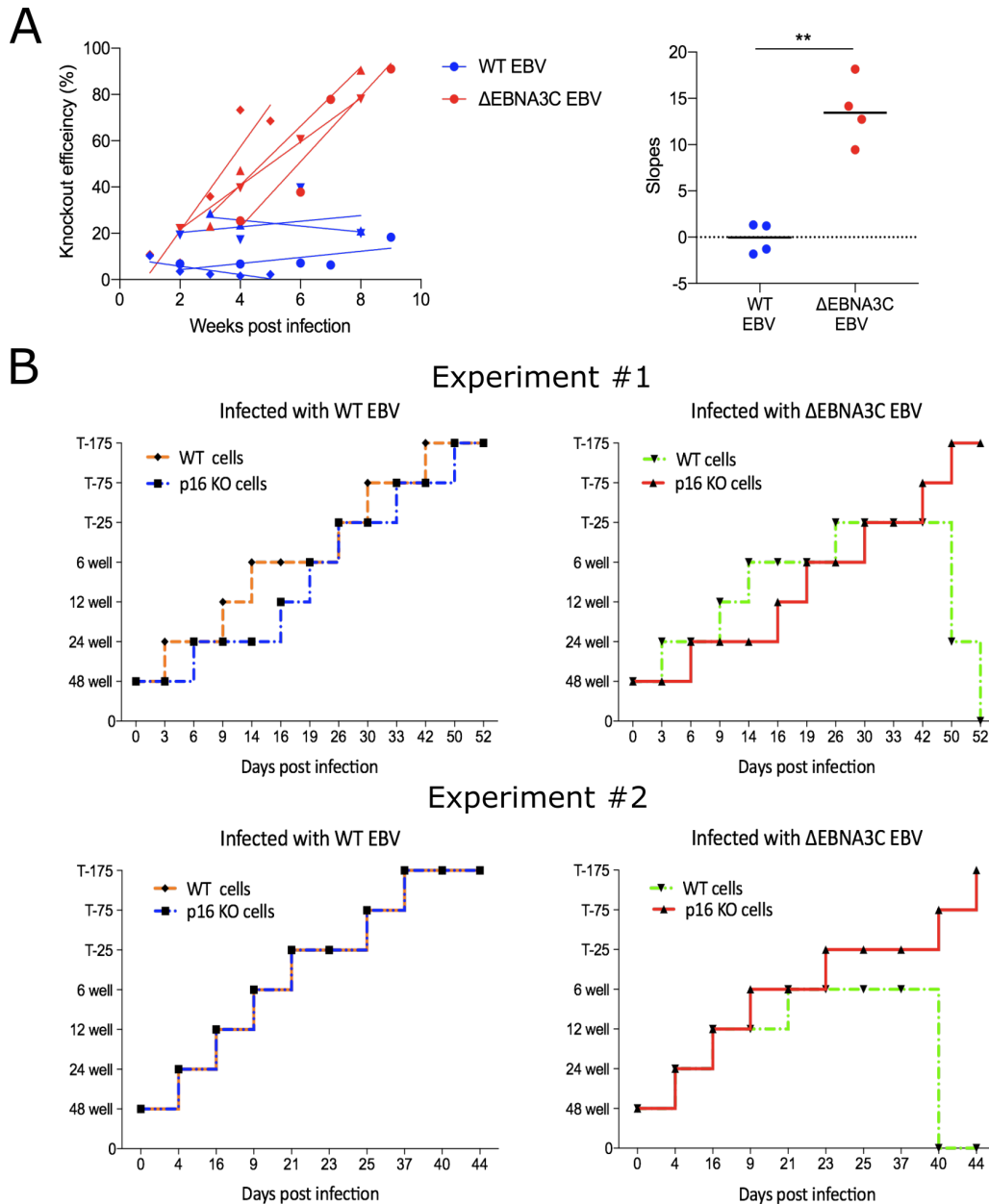


FIGURE 2.9: p16^{INK4a} is a functional barrier to EBV driven proliferation of lymphoblastoid cells. (A) The biological effect of the *CDKN2A* knockout in a time course experiment was studied. WT and p16 KO cells were mixed such that the fraction of the latter was in the order of 10 to 20%, when the cells were infected with WT or Δ EBNA3C EBV strains. The knockout status of the *CDKN2A* gene was analyzed by next generation sequencing to monitor the *CD46* locus in mixed cell populations over time. The left graph shows the statistical analysis of the time-related frequencies of *CDKN2A* negative B cells (according to identified indels) infected with WT or Δ EBNA3C EBV strains from four independent experiments. The fraction of cells with a disabled *CDKN2A* gene increased in cells infected with Δ EBNA3C EBV exceeding 80% after eight weeks, whereas the knockout status of *CDKN2A* in the population of cells infected with WT EBV did not show a clear trend. Linear regression analysis was performed with data from all four experiments to calculate the slopes of linear regression, which were transferred into a column data table and summarized in the right graph. P values were calculated using the unpaired t-test. **, $P < 0.05$. **(B)** Cell numbers of four different B cell populations were plotted as a function of days post nucleofection (x-axis) versus the format of the cell culture vessel (y-axis) starting with cells in a single well of a 48-well cluster plate. 2×10^6 B cells with an intact *CDKN2A* locus (WT cells) or cells with an edited *CDKN2A* gene (p16 KO cells) were infected with wild-type (WT) EBV (left panel) or Δ EBNA3C EBV (right panel). WT EBV infected primary human B cells developed into stably expanding lymphoblastoid cell lines irrespective of their p16^{INK4a} status (left panel). Δ EBNA3C EBV infected B cells could be expanded until about six weeks p.i., when cells with an intact *CDKN2A* gene ceased to proliferate and were lost eventually (right panel). In contrast, Δ EBNA3C mutant EBV infected p16^{INK4a} negative B cells continued to proliferate beyond this time point.

efficiencies by next generation sequencing. As shown in Figure 2.9A, cells infected with the WT EBV strain showed a constantly low fraction of cells with the inactivated *CDKN2A* gene during the course of the experiment. On the contrary, cells infected with the Δ EBNA3C mutant EBV showed a slow but gradual increase of *CDKN2A* knockout efficiencies that reached and exceeded 80% in some experiments. This observation documented a selection of *CDKN2A*-negative cells over time, when the cells were initially infected with an Δ EBNA3C mutant EBV. In the absence of EBNA3C, cells expressing p16^{INK4a} were lost because they entered a G1 block and thus ceased to proliferate as suggested previously (for a recent review see Styles et al. (2017)). Cells that lacked p16^{INK4a} and were infected with the Δ EBNA3C mutant EBV had a survival advantage and continued to proliferate even in the absence of the viral transcriptional repressor EBNA3C. This advantage then causes an enrichment of *CDKN2A*/p16^{INK4a} negative cells over time.

I also observed the proliferation of the four different cell cultures by simply tracking their expansion in cell number. I started with 2×10^6 primary B cells infected with the WT EBV strain or the Δ EBNA3C mutant EBV in a single well of a 48-well plate and continued to expand the cultures gradually to a final volume of about 100 ml in T175 cell culture flasks. WT EBV infected primary human B cells led to LCLs irrespective of their p16^{INK4a} status and reached the final culture volume about 5 to 7 weeks after the start of the experiments (Figure 2.9B, left panel). Δ EBNA3C mutant EBV infected B cells could be expanded similarly until about 5 to 6 weeks p.i., when p16^{INK4a} positive B cells ceased to proliferate and died eventually (Figure 2.9B, right panel). In contrast, p16^{INK4a} negative B cells infected with the Δ EBNA3C mutant EBV strain continued to proliferate beyond this time point (Figure 2.9B, right panel).

Together, these experiments with primary B cells confirmed that EBNA3C is essential for the repression of *CDKN2A*, a finding which is in line with reports of the Allday group. All results are consistent with p16^{INK4a} being the functional barrier to EBV-driven proliferation of LCLs. No other viral latent gene but EBNA3C plays a central function to restrain transcription of p16^{INK4a} in these cells as suggested previously (Maruo et al., 2006; Skalska et al., 2013; Styles et al., 2017).

2.4.2 p16^{INK4a} negative B cells infected with Δ EBNA3A/C EBV do not differentiate into plasma cells.

Work by others and my contribution demonstrated that p16^{INK4a} is a barrier to establish EBNA3C deficient LCLs. Interestingly, EBNA3A is dispensable in this respect (Allday et al., 2015), although it is a close relative of EBNA3C and both proteins show high overall sequence homology. Since the two viral proteins also act as epigenetic repressors of other cellular loci such as *CDKN2C* and *PRDM1* encoding p18INK4c and BLIMP-1, respectively, both EBNA3A and EBNA3C have been implicated in blocking B cell differentiation towards plasmablast and plasma cells (Styles et al., 2017). I revisited

this finding with the aim to test if human plasma cells emerge when the p16^{INK4a}-mediated block of cellular proliferation is eliminated using my p16^{INK4a} knockout strategy. Towards this end, I nucleofected mature B cells with the CDKN2A specific Cas9 complex and infected the cells with the Δ EBNA3A/C (6331) double negative EBV mutant strain (Pich et al., 2019). I expanded the cell cultures and analyzed their differentiation by flow cytometry to assess B cell phenotypes using diag-

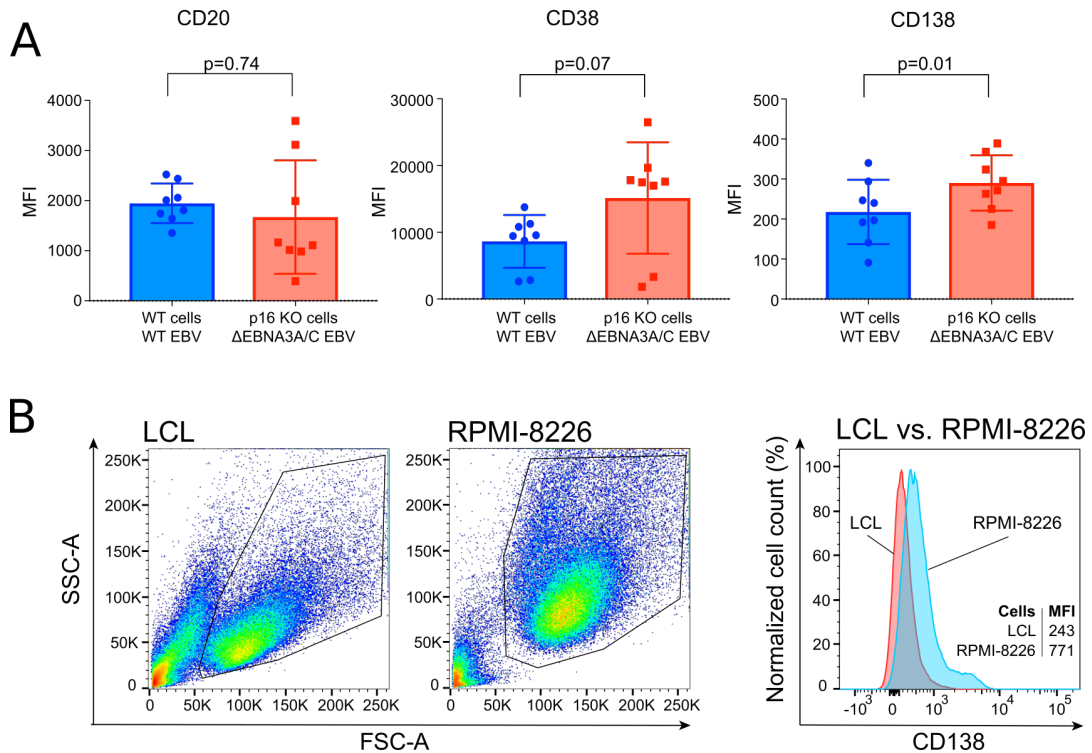


FIGURE 2.10: p16^{INK4a} negative B cells infected with Δ EBNA3A/C EBV do not differentiate into plasma cells. (A) p16 KO cells infected with Δ EBNA3A/C EBV and WT cells infected with WT EBV were analyzed by flow cytometry for the surface markers CD20, CD38 and CD138 indicative of plasma cells. The graph summarizes the mean fluorescence intensities (MFI) of the markers of living cells in 8 independent biological experiments two months post infection. Mean and standard deviations are shown. The significance of MFI values of the immunophenotypic surface proteins was calculated using the Wilcoxon matched-pairs signed rank test. (B) CD138 expression in the RPMI-8226 cell line compared to its expression in an EBV-infected lymphoblastoid cell line (LCL). The left and middle panels show forward and sideward scatter data of an established EBV-infected lymphoblastoid cell line (LCL) and the RPMI-8226 cell line, respectively. The right panel shows the expression level of CD138 in both cell lines. The population of RPMI-8226 cells (blue) express higher levels of CD138 together with a CD138^{high} subpopulation as compared to LCLs (red). Cell numbers were normalized as indicated (y-axis).

nostic and paradigmatic cell surface markers (Robillard et al., 2014). B cells from the same donors infected with the WT EBV strain served as control (Figure 2.10A).

The immunophenotypic characteristics of plasma cells include surface expression of CD138, elevated levels of CD38, a general marker of lymphocytic activation, and down-regulation of CD20 (Robillard et al., 2014). The multiple myeloma cell line RPMI-8226, which expresses high levels of CD138 and contains a typical small subpopulation of CD138^{high} cells (Figure 2.10B), as reported previously (Maïga et al., 2014; Païno et al., 2014), served as positive control.

I prepared and infected primary B cells as described above, cultivated them for up to two months and evaluated their immunophenotypic surface pattern. I found that cells infected with the two viruses did not show substantially different levels of the three surface markers CD20, CD38 and CD138. Even though Δ EBNA3A/C mutant EBV infected cells had a trend towards lower levels of CD20 and higher levels of CD38 and CD138 as compared to WT EBV infected cells, the levels were either not significantly different in case of CD20 and CD38 or very low in case of CD138 and without a discernable CD138^{high} subpopulation as seen in RPMI-8226 cells. Thus, my results appear to differ from reported work in which EBNA3A/C was found to block plasma blasts or plasma cell differentiation in LCLs (Styles et al., 2017).

2.5 Histone chaperones and their role in the early phase of EBV infected B cells.

Virions of EBV contain a single linear copy of double-stranded DNA of about 170 kbps, which is epigenetically naive. Cytosine residues in viral DNA are unmethylated and free of histones, but the DNA circularizes quickly and acquires nucleosomes within 48 hours after infection and prior to the first round of cellular DNA replication and EBV-induced cell division. Almost nothing is known how viral DNA acquires cellular histones and nucleosomes and which cellular factors drive this process. Likely, nucleosome acquisition is driven by cellular histone chaperones, which load histones on the incoming viral DNA for its chromatinization. In this chapter of my thesis, I investigated this hypothesis applying the CRISPR-Cas9 technology in primary human B cells.

2.5.1 Does the survival of EBV infected B cells depend on certain histone chaperones?

To identify the potential role of histone chaperones for the survival of EBV infected B cells, I first screened gRNA combinations for an efficient knockout of cellular genes encoding the histone chaperones *CHAF1B* (the core component of the CAF-1 complex), *HIRA*, *DAXX* and *ATRX* (Supplementary Figure 6.1A-D in Appendix). As depicted in Figure 2.1, isolated B cells were nucleofected with RNP complexes and infected with WT EBV (6008) or cultured on CD40 ligand feeder cells in the presence of IL-4 one hour after nucleofection. After 3 and 10 days, total DNA was isolated, amplified by PCR, sequenced and the knockout efficiencies were calculated (Supplementary Figure 6.1E in Appendix). In Figure 2.11A, the fraction of cells with an inactivated gene reached almost 100% but the knockout efficiency of *ATRX* was lower and in a range from 70 to 85%. In case of *HIRA*, *DAXX* and *ATRX* the knockout efficiencies at the targeted loci appeared stable with no apparent counterse-

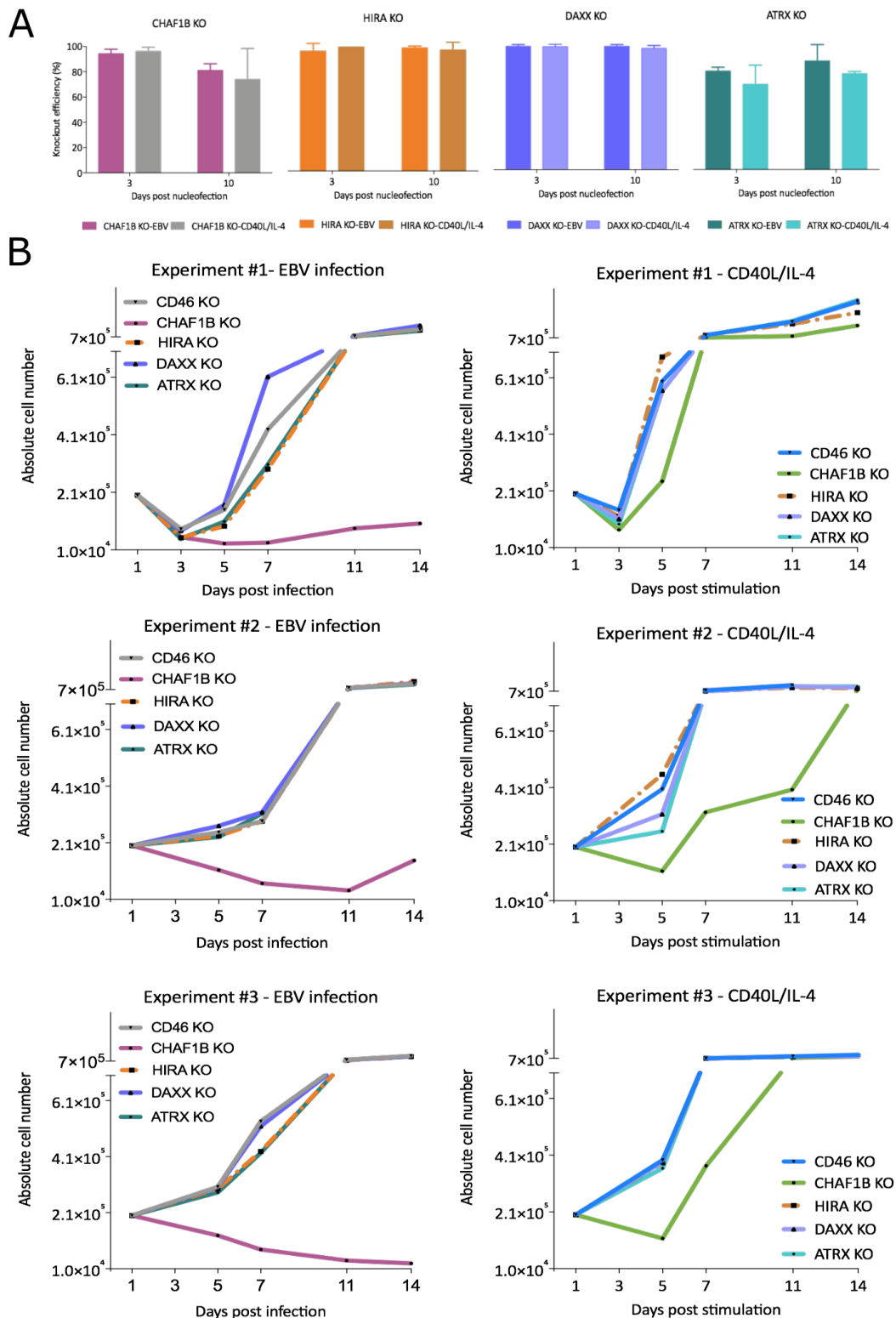


FIGURE 2.11: Functional analysis of four different histone chaperones in primary B cells after CRISPR-Cas9 knockout and infection with EBV. As in Figure 2.1, primary B cells were nucleofected with RNP complexes directed against *CHAF1B*, *HIRA*, *DAXX* and *ATRX*. Subsequently, the cells were infected with wild-type (WT) EBV or plated on irradiated CD40 ligand (CD40L) feeder cells in the presence of IL-4. **(A)** Knockout efficiencies of the targeted exons of *CHAF1B*, *HIRA*, *DAXX*, *ATRX* genes as determined by Sanger sequencing. DNA samples were collected and analyzed on day 3 and 10 after nucleofection. Mean and standard deviation from four independent biological replicates are shown. **(B)** Only *CHAF1B* is essential for the survival of EBV infected B cells. The number of proliferating B cells in samples infected with EBV or activated with CD40L/IL-4 were recorded by flow cytometry at the indicated time points after nucleofection. Three independent experiments with B cells from three different donors are shown.

lection for the unaltered gene, but cells with the *CHAF1B* knockout showed a noticeable gain of unaltered cells on day 10 after nucleofection. Similar results were obtained when the nucleofected cells were cultivated on CD40 ligand feeder cells in the presence of IL-4. The results so far suggested that an inactivation of the four histone chaperone genes is efficient to study the phenotypes of the cells in detail.

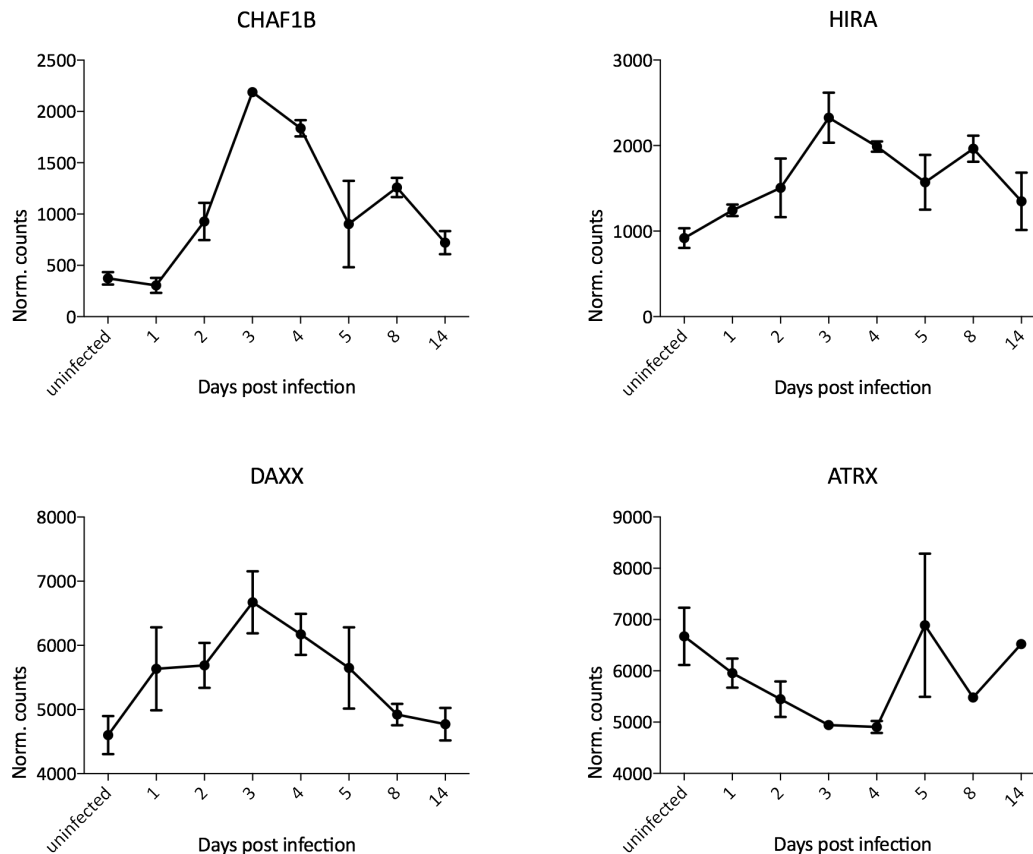


FIGURE 2.12: Transcripts of the histone chaperones CHAF1B, HIRA, DAXX and ATRX in primary human B cells infected with wild-type (WT) EBV. The transcriptomes of uninfected and EBV-infected B cells were analyzed by RNA sequencing at the indicated time points as described previously (Mrozek-Gorska et al., 2019). The panels show the transcription levels of the cell-cycle dependent histone chaperone CHAF1B and the cell-cycle independent histone chaperones HIRA, DAXX and ATRX. Normalized read counts were plotted over time. The data were derived from a publicly available source (<http://ebv-b.helmholtz-muenchen.de/>).

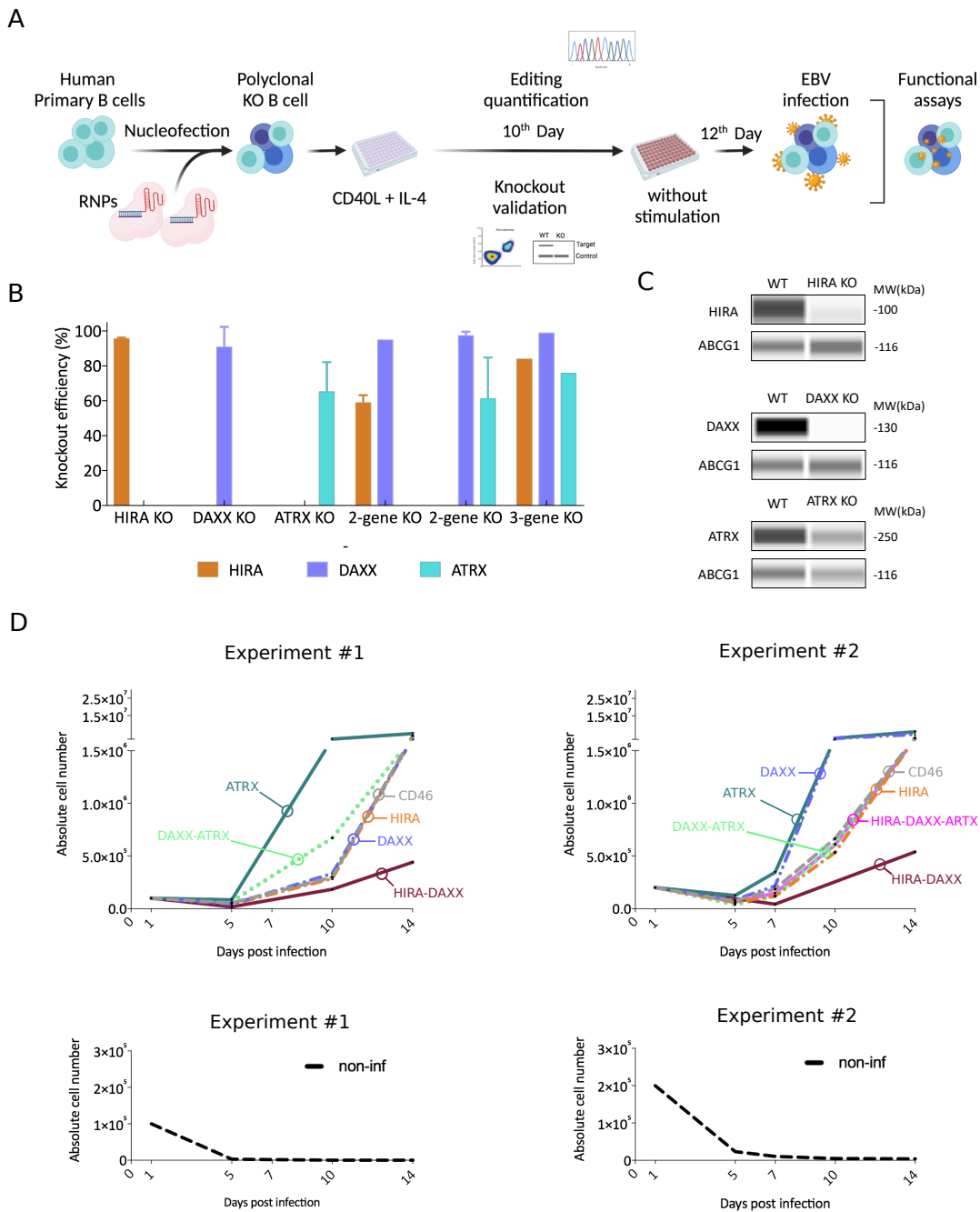
In a second approach, I counted the absolute number of viable lymphocytes and emerging B blasts by flow cytometry with calibrated allophycocyanin (APC) beads as a volume standard to investigate the fitness of the cells (Figure 2.11B). I nucleofected primary B cells with the four different sets of RNP complexes targeting the histone chaperone genes *CHAF1B*, *HIRA*, *DAXX* and *ATRX*. CD46-RNP complex nucleofection served as a control. One hour after nucleofection, the cells were infected with WT EBV (6008) or cultured on CD40 ligand feeder cells supplemented with IL-4. 24 hours later, the cells from each treatment were counted and 2×10^5 cells were seeded in single wells of a 48-well plate. At different time points after nucleofection (Figure 2.11B), the number of cells across conditions was

determined by flow cytometry. Biological replicates with B cells from three different donors showed that the individual knockout of the replication-independent histone chaperones *HIRA*, *DAXX* and *ATRAX* had no discernible phenotype. This finding suggested that the three histone chaperones are dispensable or have redundant, complementing functions for the survival of EBV infected primary human B cells and the establishment of viral latency. On the contrary, *CHAF1B* seemed to be critical for the survival of EBV infected B cells but less so when the cells were left uninfected and were plated on CD40L feeder cells together with IL-4 (Figure 2.11B).

The strong phenotype observed in EBV infected and *CHAF1B* knockout cells is accompanied by a strong induction of the gene as shown in a recent transcriptomic analysis of EBV infected primary human B cells (Figure 2.12, see also <http://ebv-b.helmholtz-muenchen.de/>). *CHAF1B*'s mRNA is weakly expressed in resting primary B cells but the transcripts increase rapidly upon EBV infection (Figure 2.12) and prior to the first round of cellular DNA replication. In contrast, mRNA levels of the three replication-independent histone chaperones *HIRA*, *DAXX* and *ATRAX* did not show a clear trend or an early upregulation (Figure 2.12).

Knockout experiments targeting the replication-independent histone chaperones *HIRA*, *DAXX* and *ATRAX* indicated that they are dispensable for the survival of EBV infected primary human B cells, but persisting protein levels of these histone chaperones could still provide functionality in cells with their inactivated individual genes in the critical initial phase of infection. My current protocol (Figure 2.1) does not take this possibility into account. To deplete these histone chaperones prior to EBV infection, I modified the established protocol as depicted in Figure 2.13A. The isolated B cells were nucleofected with RNP complexes targeting *CD46*, *HIRA*, *DAXX* and *ATRAX* individually or in various combinations. Subsequently, the cells were cultured on CD40 ligand feeder cells supplemented with IL-4 for 10 days. Knockout efficiencies were analyzed after PCR amplification of the targeted loci via Sanger sequencing. As shown in Figure 2.13B, the knockout efficiencies of individual knockouts were similar and comparable to my earlier experiments on day 10 after nucleofection as shown in Figure 2.11A. Even when I combined two or three RNP complexes targeting *HIRA*, *DAXX* and *ATRAX*, the observed knockout efficiencies at the three loci were comparable with experiments in which individual genes were targeted (Figure 2.13B). Taken together, my protocol can successfully target up to three genes in primary B cells with knockout efficiencies exceeding 70% at the low end and up to 100%.

After the knockout of a gene of interest functional alterations become apparent only after the pre-existing protein pool has been depleted. Parameters that contribute to protein loss are individual protein turnover rates, subcellular localizations and corresponding half-lives (Mathieson et al., 2018). Consequently, I assessed the reduction of all three proteins, *HIRA*, *DAXX* and *ATRAX* 10 days after the knockout of their encoding genes as show in Figure 2.13C. The *HIRA* and *DAXX* proteins were



undetectable by immunoblotting 10 days post nucleofection. The decrease in protein level of ATRX was calculated almost 50% with the Compass SW (simple western) software tool. The differences probably reflect the different efficiencies of knockout and the half-lives of the three proteins.

Ten days after nucleofection and propagation on CD40L feeder cells, I removed the activated B cells and transferred them on plastic for two days to re-establish their resting state prior to their infection with WT EBV (6008). 24 hours after infection, 2×10^5 cells were seeded per well and time point for their subsequent analysis. As a negative control, the cells were kept uninfected and were cultivated without CD40L and IL-4 stimulation. The total numbers of B cells infected with EBV were recorded by flow cytometry together with the uninfected controls in two different experiments as shown in Figure 2.13D.

ATRX and DAXX interact to load H3.3 onto DNA (Lewis et al., 2010). Their interaction is compromised in the early phase of EBV infection because BNRF1, a tegument protein and component of virions was reported to displace ATRX and DAXX (Tsai et al., 2014; Tsai et al., 2011; Huang et al., 2016). The action of BNRF1 is believed to prevent chromatinization and epigenetic repression of the incoming viral DNA supporting sustained transcription of latent viral genes. My experiments shown in Figure 2.13D are in conflict with this earlier report. EBV infected B cells with an *ATRX* knockout accumulated more rapidly than *CD46* knockout cells in experiments with cells from two different donors, despite the level of ATRX protein was reduced by half, only, prior to EBV infection (Figure 2.13C). Similarly, the knockout of *DAXX* was congruent with (experiment 1) or showed higher cell numbers (experiment 2) than control cells (Figure 2.13D). A double knockout of *ATRX* and *DAXX* had a comparable phenotype indicating that both histone chaperones have no supportive function in B cells in the early phase of viral infection. On the contrary, ATRX even seemed to have a regulatory role because its knockout led to higher initial cell numbers in my two experiments.

Next, the HIRA complex appeared to be dispensable as well (Figure 2.13D), but a double knockout of both *HIRA* and *DAXX* led to a much reduced number of surviving cells after EBV infection. This finding suggested that HIRA and DAXX have similar, i.e, trans-complementing functions which are important in the early phase of EBV infected B cells. Interestingly, in the triple knockout of *HIRA*, *DAXX* and *ATRX*, the latter appeared to revert the phenotype seen in the double knockout of *HIRA*-*DAXX* because cells with the triple knockout proliferated similarly as control cells. This conclusion is consistent with the phenotype of the single *ATRX* knockout as revealed in Figure 2.13D.

My experiments described in this chapter identified HIRA and DAXX to provide redundant yet critical functions for the survival of EBV infected B cells. The knockout of *CHAF1B* resulted in an even more dramatic phenotype with a rapid and detrimental loss of viable cells in the early days in EBV infected cells, only, but not in the same cells plated on CD40L feeder cells in the presence of IL-4 (Figure 2.11). In the next chapters of the Result Section, I concentrated on the molecular

characterization of the *CHAF1B* knockout and the identification of pathways that lead to cell death in these EBV infected primary human B cells.

2.5.2 Regulation of the cellular metabolism in *CHAF1B* knockout B cells

Basic components for nucleic acid biosynthesis, protein synthesis or other biochemical processes are very crucial for all processes in the cell. To prepare for rapid cycling and cell division of the proliferating cells starting at day 3 post infection, EBV infected B cells activates their cellular metabolic pathways as indicated by their increased glucose uptake and mitochondrial activities (Mrozek-Gorska et al., 2019). I was curious whether the strong phenotype observed in EBV infected and *CHAF1B* knockout B cells (Figure 2.11B) could result also in metabolic phenotypes in the cell population. Toward this aim, B cells were isolated from PBMCs and nucleofected either with CD46- or CHAF1B-RNP complexes. One hour after nucleofection, the cells were either infected with WT EBV (B95.8) or cultured with CD40 ligand feeder cells supplemented with IL-4. (The EBV B95.8 strain was chosen because it does not encode the fluorescence marker gene *GFP* which would interfere with my following analyses.) At certain time points post treatment, the cells were incubated with the glucose analogue 2-NBDG (2-[N-(7-nitrobenz-2-oxa-1,3-diazol-4-yl) amino]-2-deoxy-D-glucose), TMRE (tetramethylrhodamine ethyl ester) and Annexin V, to analyze glucose uptake, mitochondrial activity and occurrence of pro-apoptotic cells, respectively.

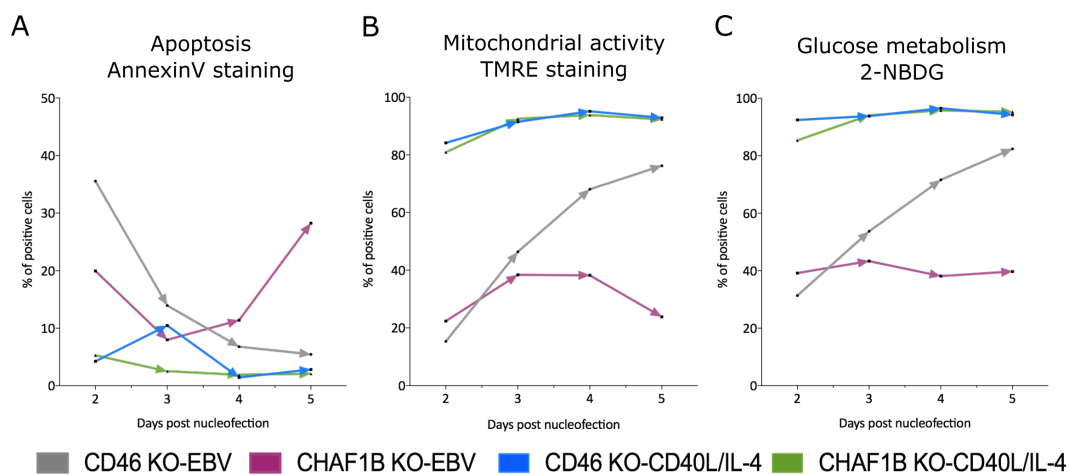


FIGURE 2.14: Reduced metabolic activity and fitness of B cells after *CHAF1B* KO when infected with EBV. B cells were nucleofected with CD46- or CHAF1B-RNP complexes and infected with EBV or plated on CD40L feeder cells in the presence of IL-4. The metabolic state of the B cells was recorded by flow cytometry analyzing their mitochondrial activity and glucose uptake with TMRE and 2-NBDG, respectively. Annexin V was used to identify pro-apoptotic cells. The cells were infected with the B95-8 EBV strain with an MOI of 0.1. The experiments show the mean of two biological replicates. **(A)** Annexin V binding is shown. **(B)** The fraction of TMRE positive cells was identified at the indicated time points post infection. 2×10^5 cells were incubated with 100 nM TMRE for 30 min prior to their analysis by flow cytometry. **(C)** Uptake of the glucose analogue (2-NBDG) is shown in the first days of treatment. 2×10^5 cells were incubated with 100 μ M 2-NBDG for an hour at 37°C prior to flow cytometry.

The fluorescently labelled (FITC) deoxyglucose analogue 2-NBDG is a substrate of the cellular glucose transporter, is taken up actively and phosphorylated by the cellular hexokinase 1 (HK1) (Zou et al., 2005). Thus, cellular 2-NBDG incorporation mimics the very first steps of glycolysis. TMRE is a red-fluorescent, positive-charged dye that accumulates in active mitochondria due to their negative charge and polarized membranes (Crowley et al., 2016). Therefore, cells with depolarized mitochondrial membranes cannot incorporate TMRE to emit its red fluorescence. Human B cells incorporate TMRE but two distinct subpopulations, TMRE_{high} (PE) and TMRE_{low} (PE) are regularly observed in preparations of resting primary B cells (Mrozek-Gorska et al., 2019). Annexin V binds to exposed phosphatidylserine residues (PS), which translocate from the cytoplasmic side of the plasma membrane to the cell surface in pro-apoptotic cells (Lakshmanan and Batra, 2013).

To address the metabolic state in primary B cells nucleofected with RNP complexes directed against *CHAF1B* or *CD46*, I infected the cells with EBV or plated them on CD40L feeder cells in the presence of IL-4. I analyzed the binding of Annexin V, stained the cells with TMRE and determined their uptake of the glucose analogue 2-NBDG.

Only about 5% of the CD40L/IL-4 activated B cells were Annexin V positive on day 2 after nucleofection and this fraction decreased in following days independent of the status of *CHAF1B* (Figure 2.14A, Supplementary Figure 6.2 in Appendix). In contrast, 20 to 35% of the EBV-infected cells were Annexin V positive on the second day. The fraction of Annexin V binding *CD46* knockout cells dropped in following days, but *CHAF1B* knockout cells showed a rapid increase of Annexin V positive cells especially on day 5 after nucleofection and infection.

My analysis in Figure 2.14B is based on the fraction of TMRE_{high} cells, which increases rapidly in primary B cells infected with EBV (Supplementary Figure 6.3 in Appendix)(Mrozek-Gorska et al., 2019). The CD40L/IL-4 activated B cells showed about 80% TMRE_{high} cells already on the second day. This level remained constantly high over time and was independent of the *CHAF1B* status. On the other hand, only 20% of EBV infected B cells with a *CD46* knockout belonged to the TMRE_{high} population early after infection but this fraction reached almost the same high level as CD40L/IL-4 activated B cells on day 5 post infection (Figure 2.14B). In sharp contrast, EBV-infected *CHAF1B* knockout cells did not show this dynamic and the fraction of TMRE_{high} cells on day 5 even dropped to the level already seen on day 2 (Figure 2.14B).

The dynamics of glucose uptake in cells nucleofected with *CD46*- or *CHAF1B*-RNP complexes was similar and irrespective of the *CHAF1B* status, when the cells were plated on CD40L feeder cells supplemented with IL-4. Already on the second day the cells showed a very efficient glucose analogue uptake, which did not increase further (Figure 2.14C, Supplementary Figure 6.4 in Appendix). In contrast, only about 40% 2-NBDG positive cells were observed after infection with EBV on the second day. The fraction of 2-NBDG positive cells constantly increased in the control cells

but in *CHAF1B* knockout cells the fraction of cells that took up the glucose analogue 2-NBDG stayed constant throughout the observation period (Figure 2.14C).

Taken together, the knockout of *CHAF1B* resulted in a drastically lower metabolic activity in EBV infected cells according to my TMRE and 2-NBDG stainings and a substantial increase in the number of apoptotic cells. Very much in contrast, *CHAF1B* knockout cells did not show similar phenotypes when activated via CD40L/IL-4 signals suggesting that CHAF1B is a critical factor for cellular homeostasis in the early phase of EBV infection but dispensable when the primary B cells are activated via the two signaling pathways genuinely triggered by CD4⁺ T helper cells in a germinal center reaction.

2.5.3 EBV infected, *CHAF1B* knockout B cells arrest in the early S phase.

The CAF-1 replication-dependent histone chaperone is specifically associated with the transport of newly synthesized histones and their deposition directly behind the replication forks and onto newly synthesized DNA (Shibahara and Stillman, 1999; Verreault, 2003). The well-established role of CHAF1B in cell cycle regulation and the phenotypes in *CHAF1B* knockout cells infected with EBV have raised my interest to investigate the effect of CHAF1B depletion in the cell cycle of B cells.

To understand the proliferation defect, I analyzed the cell cycle of primary B cells nucleofected with CD46- or CHAF1B-RNP complexes and infected with EBV or activated with CD40L/IL-4 on different days post nucleofection. Actively cycling cells incorporate 5-ethynyl-2'-deoxyuridine (EdU), a thymidine analog, into newly synthesized DNA (Pereira et al., 2017). When EdU incorporation was combined with staining of total DNA (FxCycle Violet stain), the different phases of the cell cycle could be analyzed more accurately (Figure 2.15A). SubG1 phase cells are defined by a DNA content lower than a complete set of chromosomes ($n=2$) compared to the G0/G1 phase population of cells. Cells in S phase show an increase in the EdU signal and total DNA content. Lastly, cells in G2/M do not incorporate EdU, but show a twofold higher DNA content ($n=4$) compared to G0/G1 cells.

Four conditions of B cells were investigated. Primary B cells were either nucleofected with CD46- or CHAF1B-RNP complexes and activated by EBV infection or stimulation with CD40L/IL-4. The cells were analyzed on day 2, 3, 4, 5 and 7 post nucleofection (Figure 2.15B, C). The cell cycle analysis revealed that CD46-RNP complexes treated B cells infected with WT EBV (6008) entered the S phase on day 3 post infection, similar to cells stimulated with CD40L/IL-4. In *CD46* knockout cells, the fraction of G2/M phase cells increased more rapidly in EBV infected samples on day 4 and 5 compared to cells stimulated with CD40L/IL-4. The comparison suggested that the latter passed through S more slowly and accumulated less in G2/M than EBV infected cells. As discussed previously (Figure 2.7), the *CD46* knockout did not cause any adverse effect regarding B cell survival and their cycling.

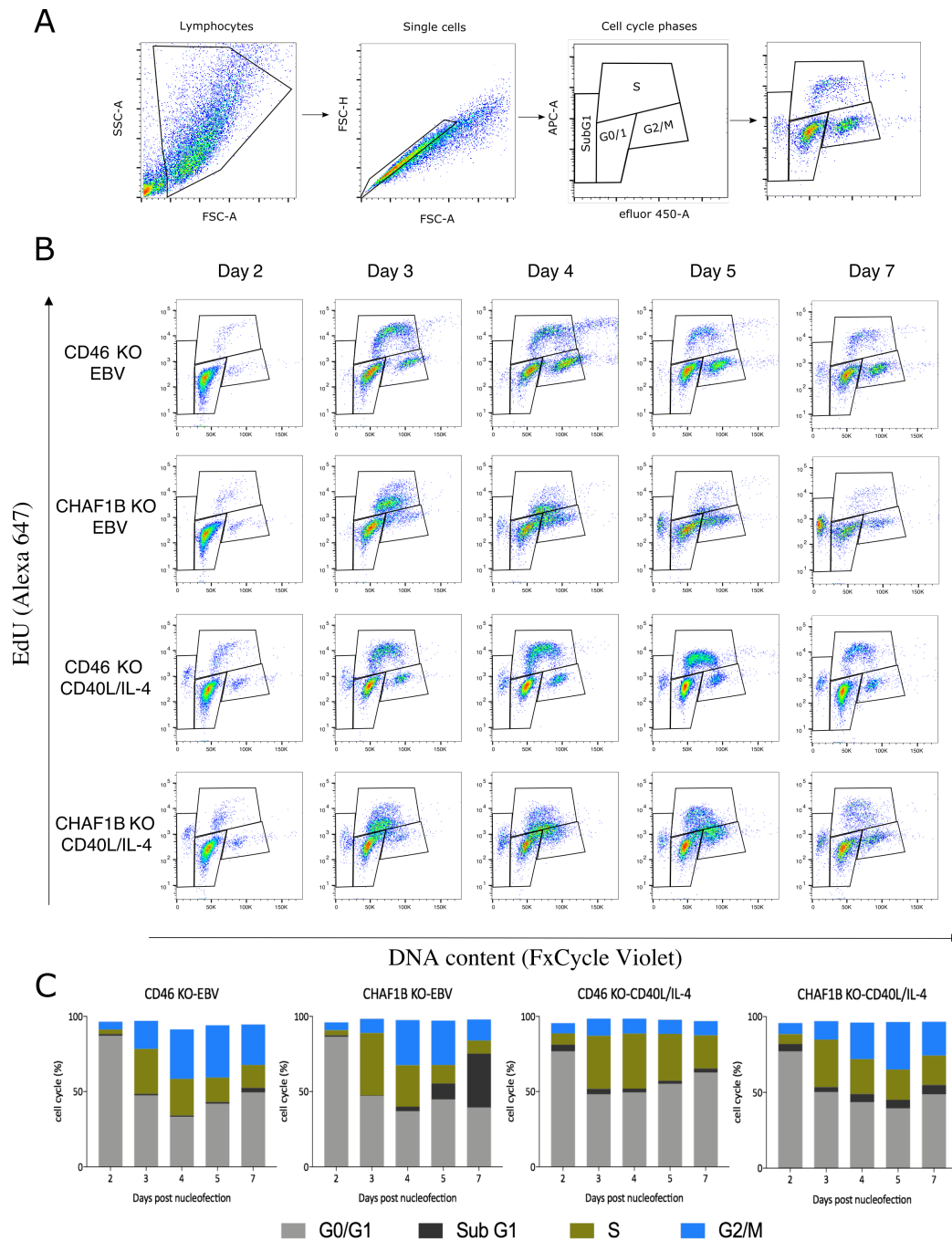


FIGURE 2.15: CHAF1B depleted and EBV infected B cells arrest in early S phase. Cell cycle analysis of B cells nucleofected with CD46- and CHAF1B-RNP complexes and either infected with EBV or plated on CD40L feeder cells in the presence of IL-4. Prior to harvest, 100 μ M EdU (final concentration) was added to the cells for 1 hour. **(A)** Gating example of B cells infected with EBV for 7 days. Shown are cells in the lymphocyte gate, the gating of single cells and subpopulations of cells indicating cells in sub G1, G0/G1, S, or G2/M. **(B)** Time course analysis of EBV infected or CD40L/IL-4 activated cells of one representative experiment. The assay was performed with primary B cells nucleofected with CD46- or CHAF1B-RNP complexes recording the cell cycle distribution 2, 3, 4, 5 and 7 days after nucleofection. **(C)** Summary of cell cycle analyses of 3 biological replicates of EBV infected samples and 2 biological replicates of CD40 ligand feeder cells supplemented with IL-4. Mean values of the four different cell cycle fractions are shown as indicated.

In *CHAF1B* knockout cells, the fraction of S phase cells was increased on day 3 post EBV infection compared to *CD46* knockout cells (Figure 2.15B, C), but, paradoxically, fewer *CHAF1B* knockout

cells reached the G2/M phase on that day. On day 5, the fraction of SubG1 cells increased rapidly in EBV infected *CHAF1B* knockout cells but not in CD40L/IL-4 stimulated cells. On day 7, many EBV infected *CHAF1B* knockout cells accumulated in SubG1 indicative of cell death and nuclear disintegration. Importantly, the strong phenotype of *CHAF1B* knockout cells when infected with EBV did not emerge in CD40L/IL-4 activated B cells. Although these cells did not incorporate as much EdU as *CD46* knockout cells especially on day 4, they resumed S phase cycling and showed only a small fraction cells in SubG1 on day 5. My results revealed that EBV infected *CHAF1B* knockout cells started the cell cycle and entered S on day 3 post infection, but seemed to arrest in early S, did not progress further but started to die rapidly on day 4 and 5 post infection in contrast to CD40L/IL-4 stimulated *CHAF1B* knockout cells.

2.5.4 *CHAF1B* knockout results in high γ -H2A.X levels, DDR and DRS in EBV infected but not in CD40L/IL-4 stimulated B cells.

The cellular response to DNA damage involves a series of events that lead to either cell cycle arrest or apoptosis. One of these events is the phosphorylation of the histone variant H2A.X at the serine residue 139 (γ -H2A.X) (Rogakou et al., 1998), which is a well-known effect of a DNA damage response (DDR) signal that involves recognition and repair of double-strand breaks. However, DNA replication stress (DRS) also triggers γ -H2A.X formation during ongoing DNA replication even in the absence of DNA damage (Ward and Chen, 2001; Saldivar et al., 2017). A recent study from our lab (Pich et al., 2019) showed that EBV infection causes DNA replication stress during the rapid cycling of B cells on day 4 and 5 post infection, but does not induce a DNA damage response per se. With the guidance of this previous study, I wished to identify the cause of the severe cell cycle phenotype in *CHAF1B* knockout B cells infected with EBV (Figure 2.15). I investigated the phosphorylation of H2A.X by flow cytometry over time using my scheme of four conditions shown in this figure.

Towards this aim, primary B cells were nucleofected with *CHAF1B*- or *CD46*-RNP complexes and cultivated on CD40 ligand (CD40L) feeder cells in the presence of IL-4 or the cells were infected with WT EBV (6008). Phosphorylation of the histone variant H2A.X was analyzed in the four different sets of cells at the indicated time points (Figure 2.16A). Independent from culturing conditions and the targeted gene, γ -H2A.X levels were very low for the first 2 days (not shown data). On day 3 with the onset of DNA synthesis, the global levels of γ -H2A.X increased considerably in the population of EBV infected cells compared to CD40L/IL-4 stimulated cells. The dramatic difference between *CHAF1B* and *CD46* knockout cells became obvious on day 5 when normal B cells infected with EBV undergo very rapid rounds of DNA replication and cell division (Pich et al., 2019). The functional loss of *CHAF1B* with its role in loading histones downstream of replication forks seems to be critical

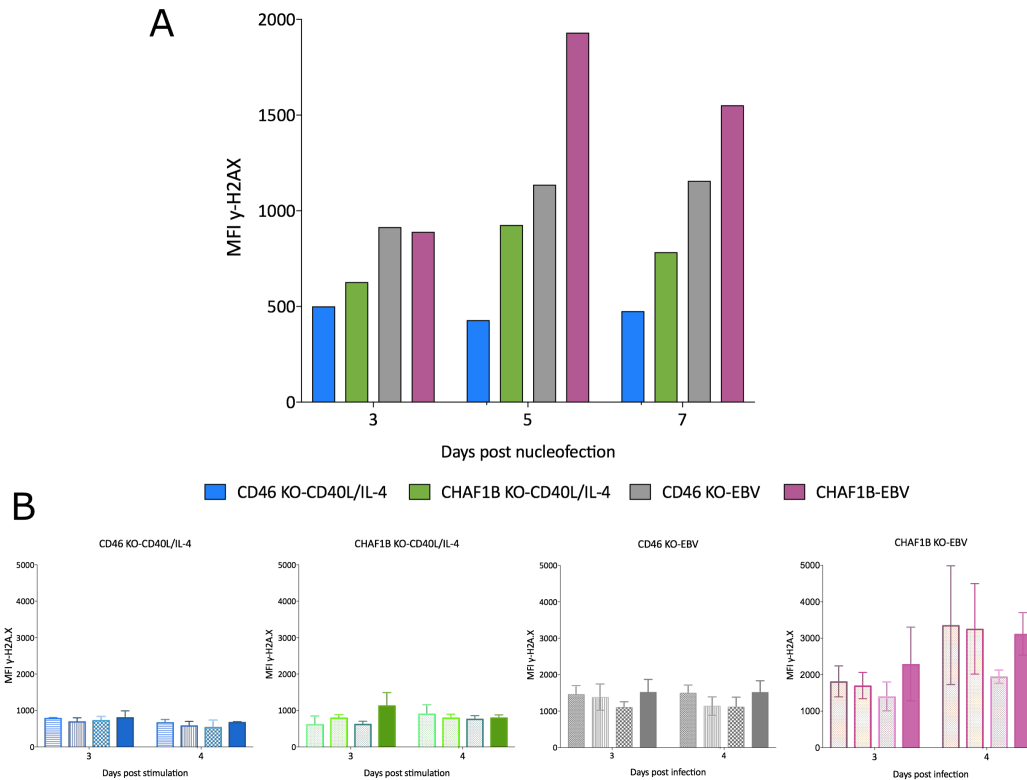


FIGURE 2.16: EBV infected, CHAF1B depleted primary B cells show high γ -H2AX levels indicative of DDR and DRS. (A) Primary B cells nucleofected with CHAF1B-RNP complexes were cultivated on CD40 ligand (CD40L) feeder cells in the presence of IL-4 (green bars) or infected with EBV (red bars). As controls B cells were nucleofected with CD46-RNP complexes and cultivated on CD40L feeder cells in the presence of IL-4 (blue bars) or infected with EBV (grey bars). Phosphorylation γ -H2A.X was analyzed by flow cytometry in fixed and permeabilized cells and mean fluorescence intensities (MFI γ -H2A.X) of the four different populations are provided 3, 5 and 7 days post nucleofection. One representative experiment is shown. (B) The experimental setup is identical to that in panel A except that the cells were treated with an ATM inhibitor (KU-55933; an DDR inhibitor) or an ATR inhibitor (AZ20; an DRS inhibitor) or a combination of both for 1 h prior to their fixation and 3 or 4 days post nucleofection as indicated. The results of two independent experiments are summarized.

to cope with EBV induced stress responses. On day 7 after infection when a lymphoblastic cell population is established, mean fluorescence intensities of γ -H2A.X levels dropped slightly in *CHAF1B* knockout cells infected with EBV but also in cells stimulated with CD40L/IL-4 cells. However, the number of infected and viable cells was consistently very low on that day compared to CD40L/IL-4 stimulated cells (Figure 2.11B).

To discriminate between DDR and DRS as the source of the elevated γ -H2A.X signal in EBV infected *CHAF1B* knockout cells, I repeated the previous set of experiments and analyzed the effects of an ATM (KU-55933; an DDR inhibitor) and an ATR inhibitor (AZ20; an DRS inhibitor) and a combination of both inhibitors as described in Materials and Methods. ATM counteracts DDR caused by DNA strand breaks, whereas ATR reduces DRS caused by stretches of RPA-coated single-stranded DNA (ssDNA) at stalled replication forks (Cimprich and Cortez, 2008). As shown in Figure 2.16B, the four different populations of B cells were kept untreated or were treated with the DDR and DRS inhibitors alone or in combination for one hour prior to their γ -H2A.X staining. Since the *CHAF1B*

depleted populations showed highest genotoxic stress levels already on day 5 after nucleofection and activation (Figure 2.16A), I decided to study earlier time points (day 3 and 4). Similar to the previous set of experiments, primary B cells cultured on CD40L feeder cells in the presence of IL-4 generally showed lower γ -H2A.X levels in contrast to EBV infected cells. Remarkably, γ -H2A.X levels in *CHAF1B* knockout cells did not differ much on day 3 and 4 from levels in *CD46* knockout cells when both cells were stimulated with CD40L/IL-4 (Figure 2.16B). In contrast and in EBV infected cells, phosphorylation of H2A.X was higher in *CHAF1B* knockout cells compared with *CD46* knockout cells used as a control.

The application of the DDR (KU55933) or DRS (AZ20) inhibitors suggested that the high level of γ -H2A.X in unmodified and EBV infected cells resulted from DRS in S and G2/M phase cells (Figure 9B in Pich et al., 2019). In *CD46* knockout cells, AZ20 but not KU55933 reduced the level of γ -H2A.X slightly on day 4 post infection (Figure 2.16B, second panel from the right). This finding is in stark contrast to the situation in *CHAF1B* knockout cells on days 3 and 4 post infection, when KU55933 in combination with AZ20 lowered the γ -H2A.X levels in EBV infected B cells considerably (pink bars; rightmost panel in Figure 2.16B). Taken together, both DDR and DRS combined contributed to the high levels of γ -H2A.X in EBV infected *CHAF1B* knockout cells on day 3 and 4 post infection. Only in *CHAF1B* deficient cells, EBV caused a high genotoxic stress level as indicated by DNA damage and replication stress responses that presumably led to the imminent cell death of EBV infected cells, only. The stress level in cells activated by CD40L/IL-4 was considerably lower and did not result in a substantial numeric loss of B cells (Figure 2.11B).

2.5.5 Control of immediate early EBV genes in the absence of *CHAF1B*

In the early days of EBV infection, many lytic viral genes are spontaneously expressed, which are epigenetically suppressed within a few days post infection (Kalla et al., 2010). Among these early expressed lytic genes is BZLF1, a viral master regulator that can induce EBV's lytic phase in latently infected B cells. In the early, so-called pre-latent phase of EBV infection BZLF1 fails to throw this switch, because CpG methylation of viral DNA is a prerequisite to induce the lytic phase of EBV. CpG methylation of the viral genome, however, is a late process and takes weeks to completion (Supplementary Figure S3 in Kalla et al., 2010).

In primary B cells, *CHAF1B* could nevertheless act as a histone chaperone that regulates early lytic gene expression and prevents the untimely expression of certain viral genes with (geno-) toxic functions in the pre-latent phase. I studied the expression of the early viral BMRF1 gene, which is downstream and a direct target of BZLF1 using an EBV strain that expresses the rat *CD2* gene under the control of the BMRF1 promoter. CD2 is found on the surface of B cells infected with this EBV reporter when the BMRF1 promoter is active (Kalla et al., 2010). This experiment was meant to clarify

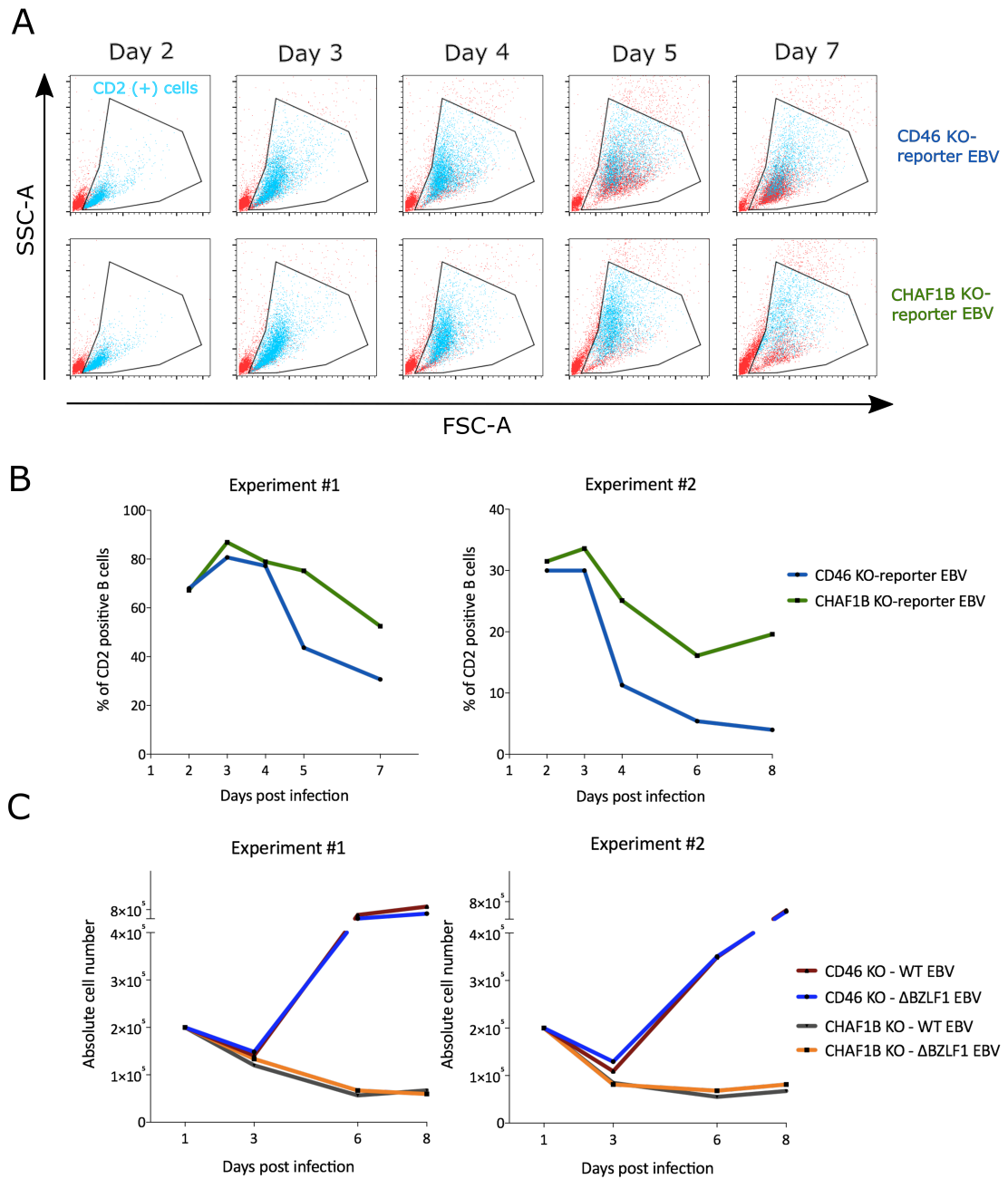


FIGURE 2.17: In *CHAF1B* knockout cells EBV infection leads to marginally higher expression of the early EBV gene *BMRF1*, but neither the induction of EBV's lytic phase nor *BZLF1* have a critical role in the survival of *CHAF1B* knockout cells. (A) B cells were nucleofected with CD46- or CHAF1B-RNP complexes prior to their infection with a reporter EBV strain (3875), in which the early viral *BMRF1* promoter controls the expression of rat CD2 on the surface of the infected cells (Kalla et al., 2010). Lymphocyte gates of the EBV infected cell population are shown in red according to forward (FSC-A) and sideward (SSC-A) scatter criteria 2 to 7 seven days post infection as indicated. In a back-gating mode, blue CD2 positive cells are shown as they emerge primarily on day 5 and 7 post infection. One representative experiment is shown. (B) Two independent experiments with B cells nucleofected with Cas9-RNP complexes directed against *CD46* or *CHAF1B* and infected with the *BMRF1* reporter EBV strain (3875) are shown. The fraction of intact, CD2 positive B cells was analyzed on the indicated days post infection, as detailed previously. (C) *BZLF1* expression early in infection does not play a role in *CHAF1B* knockout, EBV infected B cells. Primary B cells were nucleofected with CD46- or CHAF1B-RNP complexes prior to their infection with WT (6008) or Δ BZLF1 (3283) mutant EBV strains. The number of proliferating B cells was recorded by flow cytometry at the indicated time points after nucleofection and infection. Two experiments with B cells from two different donors are shown.

the presumed role of CHAF1B as a repressive epigenetic factor of viral lytic genes. Toward this aim, B cells were nucleofected with CD46- or CHAF1B-RNP complexes and infected with the rat CD2 reporter EBV strain (3875) or WT EBV (6008). CD2 positive B cells that indicate the activation of the early lytic BMRF1 gene were visualized as shown in Figure 2.17A-B and compared to CD2 negative cells. Already on day 2 post infection, most of the cells in the lymphocyte gate expressed CD2 and the maximum of CD2 positive cells was seen on day 3 in two independent experiments. Later, CD2 expression dropped rapidly in CD46 knockout cells but CHAF1B knockout cells consistently showed a higher percentage of CD2 positive cells on the following days suggesting that CHAF1B has an axillary role in the silencing of early lytic genes.

The elevated expression of the early promoter of the BMRF1 gene raised the question whether the prolonged expression of BZLF1, the master regulator of EBV's lytic phase, might play a role in the inferior survival of CHAF1B knockout cells. Toward this aim, primary human B cells were infected with WT EBV (6008) or the mutant (3283) EBV strain with an inactivated BZLF1 gene and the absolute number of cells was recorded by flow cytometry with the aid of APC beads at the indicated time points (Figure 2.17C). My analysis of two experiments with B cells from two different donors showed that BZLF1 does not have a role in the survival of CHAF1B knockout cells. In contrast to a previous study (Kalla et al., 2010), BZLF1 did not contribute to the proliferation of resting B cells in the early phase of infection because the number of cells infected with WT EBV (6008) or the BZLF1 knockout (3283) strain did not differ. Importantly, the BZLF1 negative EBV strain did not rescue the proliferation of B cells devoid of CHAF1B (Figure 2.17C).

Taken together, the early expression of viral lytic genes does not seem to contribute to the genotoxic stress seen in B cells with a CHAF1B knockout.

2.5.6 Viral DNA accumulates in CHAF1B knockout cells and leads to cell death of EBV infected B cells

Based on the fact that CHAF1B loads histones on replicating DNA, I hypothesized that EBV DNA might replicate uncontrolled in B cells devoid of CHAF1B and thus might induce genotoxic stress and cell death, eventually. To scrutinize this hypothesis, I determined the molar quantity of viral DNA in B cells nucleofected with CD46- and CHAF1B-RNP complexes after their infection with WT EBV (6008) in a time course experiment. I designed primers to amplify viral DNA at two EBV loci (origin of plasmid replication (*oriP*) and the C promoter (*Cp*) and two cellular DNA gene loci (*FHIT* and *GUSB*). Total nuclear DNA was isolated from the cells on the indicated days post infection (Figure 2.18) and amplified by qPCR with primer pairs specific for viral loci (*oriP* and *Cp*) and cellular genes (*FHIT* and *GUSB*) (Figure 2.18). The ratio of viral versus cellular DNA stayed stable in EBV infected, CD46 knockout cells but dropped by almost a factor of two when the cells underwent their first cell

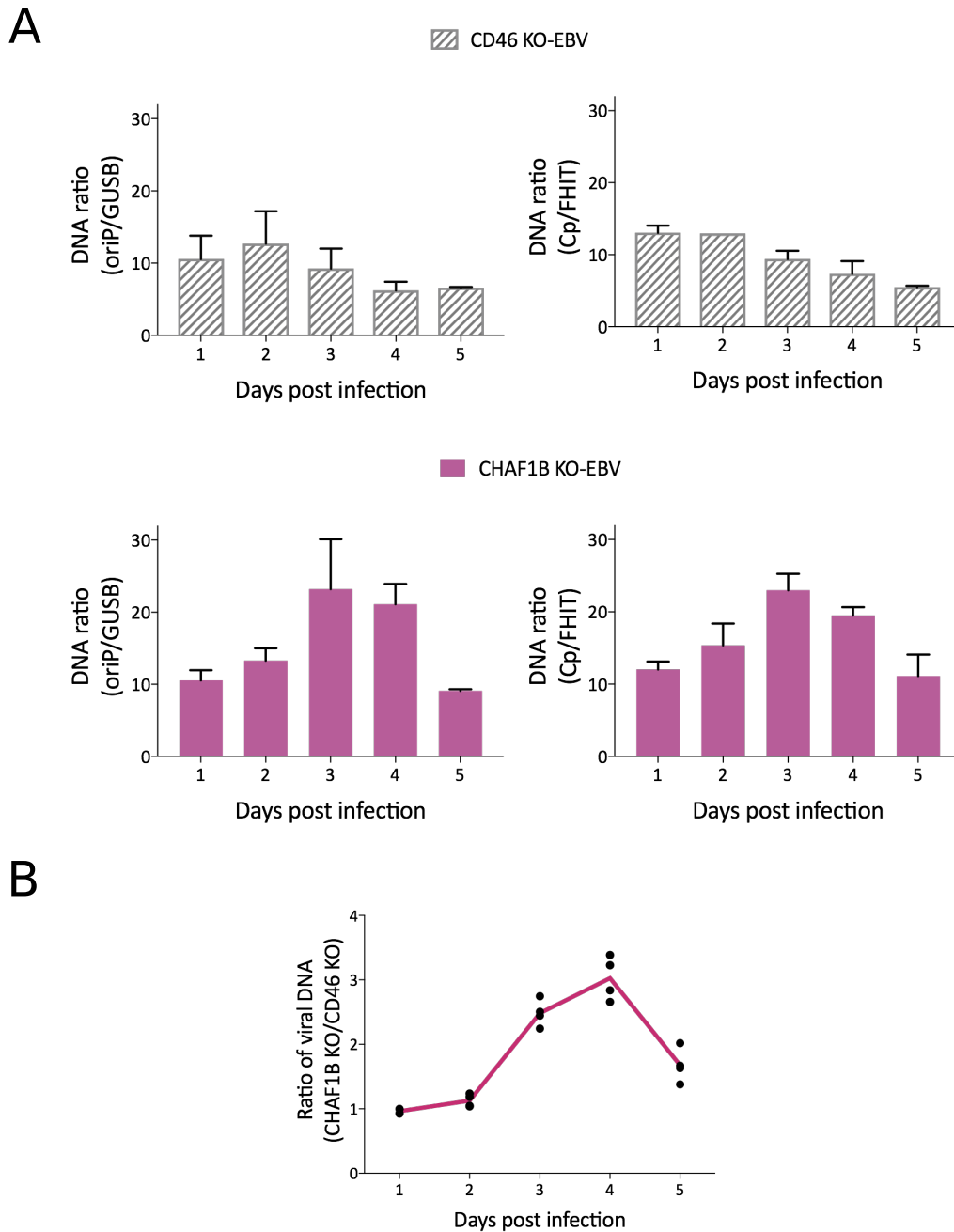


FIGURE 2.18: Viral DNA accumulates in CHAF1B depleted and EBV infected B cells. B cells were nucleofected with CD46- or CHAF1B-RNP complexes prior to their infection with WT (6008) EBV. At the indicated time points after infection, total nuclear DNA was isolated and tested by qPCR analysis with primer pairs specific for two viral and two cellular genes (*oriP*, *Cp* and *FHIT*, *GUSB*, respectively). **(A)** The ratios of viral versus cellular DNA were calculated. DNA quantification was based on the $\Delta\Delta C_t$ -method correcting for primer efficiencies. Mean and SDs of two technical replicates of one biological replicate are shown **(B)** Ratios of viral DNA of CHAF1B-RNP versus CD46-RNP complex nucleofected B cells on different days post infection are shown summarizing the two independent experiments in panel A.

division on day 4 (Figure 2.18A) as reported (Pich et al., 2019). On the opposite, in *CHAF1B* knockout cells viral DNA accumulated, most probably due to unlicensed viral DNA replication starting on day 3 post infection. The ratios of viral versus cellular DNA in *CHAF1B* knockout cells over time are shown in Figure 2.18B. The ratio reached its highest level on day 4 (Figure 2.18B) and prior to the

appearance of pro-apoptotic cells on day 5 after infection (Figure 2.14A).

The data suggested that viral DNA accumulates in infected B cells devoid of CHAF1B and triggers a massive genotoxic DNA damage response probably because the newly replicated DNA is free of histones and nucleosomes, which is a known cause of DDR. How and why viral DNA over replicates in this situation is elusive but certainly worth investigating.

Chapter 3

Discussion

3.1 Scope and aims of my thesis

Human hematopoietic stem cells and their derivatives of the myeloid and lymphoid lineages are important targets for gene correction using the CRISPR-Cas9 technology. One prominent example is the site-specific insertion of chimeric antigen receptors (CARs) or T cell receptors (TCRs) in primary T cells for their adoptive transfer back into the patient. In contrast to T cells, human B cells are very sensitive, difficult to handle and short-lived *ex vivo* preventing their genetic modification with the CRISPR-Cas9 approach. Genome editing in B cells has been achieved in established B cell lines (Cheong et al., 2016) or pre-activated human B cells (Wu et al., 2018), but efficient protocols for the genetic manipulation of primary human B cells have not been available. The lack of efficient gene editing tools for these cells has been a major roadblock for research on Epstein-Barr virus and its gene vector derivatives, which reach high infection and transduction rates in resting primary human B cells (Hellebrand et al., 2006). As a result, there is an apparent need to establish a genome editing protocol of the CRISPR-Cas9 technology in B cells to investigate the role of cellular factors and to study EBV's biology in its human target B cells.

In my thesis, I focused on establishing the CRISPR-Cas9 mediated technology of gene knockouts in resting primary human B cells. To ensure their *ex vivo* survival, the cells were activated subsequently by infecting them with EBV (or mutant derivatives) or by culturing them on CD40 ligand (CD40L) feeder cells in the presence of IL-4. I have successfully reached very high knockout efficiencies using Cas9 RNP complexes in primary human B cells. I further optimized and applied my protocol to human B cells derived from different sources such as adenoids or peripheral blood using different culturing conditions for their survival. My interest was also in the kinetics of cellular repair functions at double stranded breaks induced by the Cas9 endonuclease and the resumed transcription after Cas9 mediated gene editing and ensuing locus repair. Eventually, I provided a functional proof-of-principle in human B cells targeting an EBV relevant cellular gene, *CDKN2A* encoding p16^{INK4a}.

My initial interest was also on epigenetic processes, which potentially regulate viral DNA and its chromatinization after EBV infection of resting primary B cells. I studied the role of several histone chaperones in the chromatinization of the incoming viral DNA using my optimized protocol of CRISPR-Cas9 genome editing. I found a very specific phenotype of EBV infected B cells devoid of one particular histone chaperone, CHAF1B, and identified the molecular pathway that causes this compelling phenotype in EBV infected B cells.

3.2 Genome editing in primary human B cells with the CRISPR-Cas9 technology

The CRISPR-Cas9 technology has evolved into an essential tool for genome manipulation in various mammalian cells and cell lines, but the technology has its limits when it comes to studying the biology of cells that cannot be easily maintained in culture *ex vivo*. Therefore, primary human B cells have received little attention in the field of gene manipulation although they are involved in numerous biological processes, autoimmunity and infectious diseases. In recent years, our laboratory has been unsuccessful in genetically manipulating primary human B cells very much in contrast to established B cell lines (Maier et al., 2005; Feederle et al., 2004). Thus, until now, it was not possible to study the potential role of cellular factors of B cells in the context of EBV's biology. The very high efficiency of genetic manipulation of primary B cells with my protocol is a considerable step forward following pioneering work in primary human T cells (Hendel et al., 2015; Schumann et al., 2015; Hultquist et al., 2016; Seki and Rutz, 2018).

Genome editing in primary human B cells has been challenging due to the cell's rapid apoptosis upon genetic manipulation and cultivation *in vitro*. My optimized protocol minimizes the time of the cells in the electroporation buffer (P3 Primary Cell Nucleofector Solution). Pre-cooling of the cuvette prior to nucleofection and supplementing the cells with pre-warmed cell culture medium containing 20% fetal calf serum (Chicaybam et al., 2017) after nucleofection were essential steps towards obtaining high number of recovered cells following genome editing. As a result, I obtained a consistently high *CD46* knockout efficiency in primary human B cells with a cell viability between 70 and 80% after nucleofection (data not shown). Additionally, I showed that the RNP-complex treatment does not affect cellular transcription globally (Figure 2.7A). I could also show that the delivery of gRNAs as part of the RNP-complex does not induce an adverse innate immune response (Figure 2.7B) which supposedly arise when lentiviral vectors are used for the delivery of gRNAs (Caeser et al., 2019).

The optimized knockout efficiency and enhanced cell viability depend on the targeted gene locus and the design of the gRNAs. I followed the scheme proposed by Clarke et al. (2018) and designed

the upstream and downstream CD46-Cas9 RNP complexes to target the non-template and template orientations of the upper and lower DNA strands, respectively. Remarkably, this strategy induced an efficient deletion together with frame shift mutations that led to a functional *CD46* knockout exceeding 85% and more at the level of DNA editing and loss of CD46 surface expression (Figure 2.2B). Similarly, when I targeted other cellular genes with single or a combination of different Cas9 RNP complexes I regularly observed frame shift mutations in the order of 80% (Figure 2.8B and 2.11A) suggesting that nearly all cells in the B cell population can be reached using my nucleofection protocol.

I optimized the conditions and parameters of my genome editing protocol in B cells using the cell surface protein CD46 as a model. CD46 is a single-span, type I transmembrane protein that acts as cell surface receptor and modulator of adaptive immune responses in T cells (Seya and Atkinson, 1989). Since CD46 protein is consistently expressed on other hematopoietic cells (Cattaneo, 2004), my genome editing protocol for the *CD46* gene can be easily transferred to optimize genome editing in cell types other than human B cells. In fact, a recent study by Albanese et al. (2022) showed a highly efficient genome editing of the *CD46* gene in resting human CD4⁺ T cells with over 80% viability and 90% of editing efficiency. While optimizing the knockout efficiencies for other cellular targets, I ran the *CD46* gene in parallel which put me into the position to monitor possible problems that can arise during nucleofection and in downstream steps.

In my knowledge, targeting several genes simultaneously in primary human B cells has not been established, previously. With my protocol, I could successfully inactivate two and three genes with high knockout efficiencies in a single round of nucleofection (Figure 2.13). In principle, targeting multiple genes in one go can be a game changer in analyzing and dissecting entire cellular pathways or processes with multiple players that have redundant or (partly) overlapping functions. The latter aspect is nicely demonstrated in Figure 2.13, where I discovered the overlapping, probably complementing functions of HIRA and DAXX in the pre-latent phase of viral infection.

I could successfully apply the CRISPR-Cas9 gene editing protocol to resting B cells from peripheral blood or adenoid tissue documenting that the protocol can be used with human B cells from different sources (Figure 2.3). Additionally, my protocol also reached high knockout efficiencies in non-infected B cells (Figure 2.4D) contrary to a previous study in which the authors concluded that activated human B cells are much more amenable to Cas9-mediated gene editing compared to resting B cells with only about 20% knockout efficiency (Wu et al., 2018). These results indicated that EBV does not promote, support or enable gene editing but is only the driver of B cell survival and proliferation, which starts four days post infection (Pich et al., 2019). Lastly, delivery of the RNP complex by electroporation did not show any effect on the cellular transcriptome (Figure 2.7A), which was a concern because B cells are immune cells which can potentially sense synthetic RNA molecules

and induce an interferone response or suffer from adverse effects due genetic instability such as double strand breaks in its chromosomal DNA. Together, the data demonstrated that Cas9-mediated gene editing is fully functional and efficient in resting primary human B cells and overcomes major limitations of previous reports. Similar to functional analysis in primary human CD4⁺ T cells investigating the role of host factors in HIV infection (Hultquist et al., 2016), my efficient protocol also allows to study the functional interactions between EBV and its primary host B cells.

3.3 Kinetics of double stranded break repair and transcription at the site of gene editing

The CRISPR-Cas9 editing technology is a powerful tool but it also induces single double-strand breaks (DSB) in the genome of the cell (Cong et al., 2013; Mali et al., 2013). In all cells, DSB need to be repaired to ensure the genetic stability of the cell. The main pathway for the repair of DSBs is non-homologous end joining (NHEJ), which directly rejoins the two DNA ends leading to insertions or deletions at the severed site (Lieber, 2011). As a consequence, insertions and deletions at nucleotide level at and in the proximity of the cut site of the CD46-RNP complexes could be observed as in Figure 2.4A. Although the repair process of Cas9-induced DSBs has been only partially characterized, little is known about the kinetics of the Cas9 mediated generation of DSBs and their repair *in vivo*. Time-course studies in mammalian cells showed that DSBs are repaired with a half-life of 10-60 min, however these bulk measurements lack the resolution required to follow DSB repair at single loci (Wang et al., 2013). Additionally, the previous studies had been conducted in cell lines that were metabolically active and cycling at the time when Cas9 was introduced into the cells. These analyses also did not consider the activity of Cas9 and repair rates of DSBs in resting primary human cells such as lymphocytes.

My sequencing analysis of the targeted *CD46* locus recorded the accumulation of insertions and deletions and thus the repair rates of double stranded breaks over time. Already 2 hours post-nucleofection of Cas9-RNP complexes into primary human B cells, I could observe insertions and deletions (Figure 2.4A) similar to findings of an earlier study (Rose et al., 2017). Subsequently, indels accumulated and reached knockout efficiencies of about 60% 24 h after nucleofection (Figure 2.4A). Interestingly, I noticed additional insertions and deletions up to four days after nucleofection, which might reflect different scenarios; (1) Some Cas9 complexes might need more time to localize into the nucleus and find their target sites, (2) DSBs might be introduced slowly or after a certain lag time, (3) the repair of these DSBs might be slow or delayed for unknown reasons in some cells, (4) the state of chromatin might vary from cell to cell and modulate cleavage and repair kinetics at the Cas9

target site (Horlbeck et al., 2016; Brinkman et al., 2018). These aspects are interesting but it would require additional effort and time to address them experimentally.

During DNA repair of the *CD46* locus transcription probably ceases but the intact template is transcribed thereafter and the transcripts can be translated if they encode the functional CD46 protein. 24 hours after nucleofection less than 20% of the cells were CD46 negative according to flow cytometry of the surface protein (Figure 2.4C) even though more than 60% of the cells showed insertions and deletions as in Figure 2.4A. This discrepancy is almost certainly due to slow protein turnover rates and corresponding longer protein half-lives but also transcription of the repaired template after Cas9 cleavage might be delayed. To address this uncertainty and to study the possible impact of transcription rates at the repaired locus, I performed metabolic labeling of newly synthesized RNA using the 4sU analogue in primary human B cells (Figure 2.5A-C). Metabolic labeling with 4sU in combination with next-generation sequencing offers the possibility to study genome-wide RNA kinetics at high resolution in cells (Rädle et al., 2013). Up to date next generation sequencing of 4sU-labeled and biochemically enriched RNA was accomplished only in established cell lines (Friedel et al. (2009); Windhager et al. (2012)) but not in primary human B cells. To my knowledge, this technique has not been applied previously following Cas9-RNP complex mediated genome editing to address my question of interest. My 4sU-RNA sequencing experiments on RNA derived from CD46-RNP complex nucleofected primary human B cells provided detailed insight into ongoing transcription at the target site 24 hours after introducing the Cas9 RNP complex into these primary B cells. Surprisingly, more than 50% of newly transcribed CD46 mRNAs contained indels or showed the characteristic deletion in exon 2 at this time of RNA sampling (Figure 2.5D) similar to the fraction of insertions and deletions (60%) at the *CD46* locus (Figure 2.4A). These results indicated that the severed template was rapidly repaired and cleared to resume transcription within hours following delivery of the Cas9 RNP complexes. On the other hand, the reduced read coverage in the upstream exon of the *CD46* gene indicated a possible road blockage to transcription machinery as the Cas9 complex probably stayed attached to DNA ends after cleavage (Figure 2.6A) as claimed by Richardson et al. (2016). However, this hypothesis has to be studied further. The situation is complex since the maximum knockout efficiency in the *CD46* locus typically exceeded 85% one week after nucleofection indicating that the CD46-Cas9 RNP complex has remained active for several days in these cells contrary to a previous report in which the authors used established human cells (Kim et al., 2014). The time it takes to cleave and repair the model locus in combination with the individual protein half-life are factors that can explain the small fraction of surface CD46 negative B cells 24 hours after nucleofection (Figure 2.4B).

3.4 CRISPR-Cas9 genome editing identifies functions of cellular genes relevant for EBV

Since 1998 the genome of Epstein-Barr virus can be genetically manipulated at will (Delecluse et al., 1998) and the many mutant viruses which have emerged since then were instrumental to our understanding of the virus' biology. Very much in contrast, EBV's human target B cells have been refractory to any genetic modification. If these very sensitive target cells could be manipulated genetically, systematic studies might identify pathogen relevant cellular functions of the host cell. For example, gene editing in human primary T cells identified co-receptors of Human immunodeficiency virus type 1 (HIV-1) (Liu et al., 2017) or life cycle related host factors (Hultquist et al., 2016) for treating the Acquired immunodeficiency syndrome (AIDS) caused by HIV. So far, efforts to identify and characterize host-pathogen interactions in EBV infection have relied on the already cumbersome genetic manipulation of immortalized B cell lines of human or animal origin *in vitro* (Maier et al., 2005; Feederle et al., 2004). To prove that my RNP-based genome editing protocol in primary human B cells can be used for EBV-related functional studies in primary human B cells, I targeted an EBV relevant cellular gene, *CDKN2A*, encoding the cell cycle inhibitor p16^{INK4a} (Gil and Peters, 2006). Focusing on *CDKN2A*, I employed my novel protocol and studied two pathways of EBV's complex biology in primary human B cells. EBNA3A and C, two related EBV genes, have been reported to act as mediators of epigenetic repression of several cellular gene loci in latently EBV infected B cells. Among them is *CDKN2A* that reportedly blocks proliferation of latently EBV-infected B cells in the absence of EBNA3C's repressive epigenetic functions (Maruo et al., 2006; Skalska et al., 2013; Styles et al., 2017). As shown in Figure 2.9, my *CDKN2A* knockout results corroborated this notion with primary B cells from six donors recapitulating a rare situation with B cells from a p16^{INK4a} deficient individual (Skalska et al., 2013).

In my further analyses, I investigated yet another biological function in B cells that EBNA3A and EBNA3C together supposedly regulate. A paper by the Allday laboratory reported that EBV-infected lymphoblastoid B cells differentiated spontaneously and acquired a plasma cell-like phenotype in the absence of EBNA3A and C using conditional EBNA3 alleles (Styles et al., 2017). In this scenario EBNA3A and EBNA3C together epigenetically repressed a number of cellular genes, which are presumed drivers of terminal B cell differentiation. Consequently, the authors discussed and proposed that *in vitro* EBV infected B cells might differentiate beyond the state of lymphoblasts into proliferating plasmablasts and fully differentiated functional plasma cells in the absence of both EBNA3A and EBNA3C and an inactivated *CDKN2A* allele, i.e., in B cells devoid of the cell cycle regulator p16^{INK4a}. This is because p16^{INK4a} acts as a roadblock precluding the cycling and differentiation of pre-plasmablasts to plasmablasts and plasma cells, eventually (Styles et al., 2017). Since plasma cells

are expected to release authentic human antibodies *in vitro*, they have a promising translation potential. I put this interesting hypothesis to the test (Nutt et al., 2015) but I did not find clear evidence that EBNA3A and C together block differentiation of lymphoblasts to pre-plasmablasts, plasmablasts or plasma cells (Figure 2.10). My finding suggested that EBV-infected and activated B cells do not follow the proposed pathway to differentiate into plasma cells spontaneously *in vitro*.

Taken together, this protocol enables robust gene editing in primary human B cells and the functional characterization of host cell encoded factors, which are critical to establish or maintain viral latency.

3.5 The role of histone chaperones in the biology of EBV infected B cells

The cellular host provides EBV with critical epigenetic functions to help establish viral latency and regulate viral transcription. Epigenetically naive viral DNA enters the newly infected B cell but the DNA quickly acquires nucleosomes with mainly repressive marks. Eventually, the viral genome is characterized by large, densely CpG methylated areas (Woellmer and Hammerschmidt, 2013; Woellmer et al., 2012). These time-controlled epigenetic modifications are essential both for the persistence of the virus in the host cell and for its escape from latency to start the virus' productive, lytic phase. The acquisition of cytidine methyl groups on viral DNA takes weeks to completion (Kalla et al., 2010), whereas the recruitment of nucleosomes on EBV DNA is accomplished in B cells within 48 h post-infection (Mrozek-Gorska et al., unpublished). At the moment, our knowledge on how EBV DNA acquires chromatin in the pre-latent phase of infection and which cellular factors might be involved is very limited. In my PhD work, I was interested in the role of cellular histone chaperones which likely are instrumental for the chromatinization of the incoming EBV DNA. Epigenetic control of the viral genome probably is a critical step, because viral transcription appears to be almost global and undirected initially but needs to be tailored to express only certain sets of latent viral genes, eventually. Toward this aim, I screened for histone chaperones such as *HIRA*, *DAXX*, *ATRX* and *CHAF1B* and for their contribution to B cell survival and proliferation in the pre-latent phase of EBV infection.

Replication-independent histone chaperones

We know from our previous and ongoing work that nucleosomes occupy EBV DNA early on suggesting that nucleosome assembly takes place long before the onset of EBV-induced cellular DNA replication (Mrozek-Gorska et al., 2019 and unpublished data). Given this scenario, replication-independent histone chaperones are most likely involved in the early steps of chromatinization.

Within this group of histone chaperones, HIRA as a loader of the histone variant H3.3 seems to regulate the latency of alpha- and beta-herpesviruses such as herpes simplex virus and cytomegalovirus, respectively (McFarlane et al., 2019; Albright and Kalejta, 2016) and also to maintain HIV latency (Gallastegui et al., 2011). In contrast to the expected role of HIRA in the establishment of EBV latency in B cells, my results indicated that HIRA is not an essential factor in B cells in the early days of EBV infection (Figure 2.11B and 2.13D). Additionally, HIRA mRNA levels do not change as dramatically as CHAF1B mRNA during the first days of EBV infection (Figure 2.12) suggesting that HIRA might not be involved in the critical pre-latent phase of EBV. Otherwise, a recent paper by Zhang et al. (2020) suggested that HIRA has a role in the maintenance of latency as its knockdown triggered lytic reactivation and production of infectious EBV virus. These studies were performed with Akata cells, which are Burkitt lymphoma cells established years ago. The cells are latently EBV infected, divide rapidly and thus do not recapitulate the early steps of infection in B cells prior to their entry into the first cell division after EBV infection. Although HIRA does not seem to have any role in EBV infected B cells, its contribution in the chromatinization of other herpesvirus genomes appears to be solid (Rai et al., 2017).

It is also plausible that other histone chaperones, e.g. DAXX and ATRX complexes may have key functions in loading H3.3 onto incoming EBV genomes prior to mitosis in newly infected cells. Given my data, DAXX and ATRX histone chaperones are not essential for the survival of EBV infected B cells in the early days of infection and do not contribute to the establishment of latency (Figure 2.11B and 2.13D). On the contrary, it has been postulated that BNRF1, an EBV tegument protein contained in virus particles promotes selective viral gene expression in the pre-latent phase of EBV infection. BNRF1 disrupts the interaction of DAXX with the SWI/SNF-like chromatin remodeler ATRX (Tsai et al., 2014). The authors interpreted their findings to mean that BNRF1 prevents epigenetic repression of latent viral genes and contributes to the success of establishing viral latency. In my experiments, the phenotype of B cells devoid of DAXX did not differ compared to *CD46* knockout cells. Although normally H3.1 and H3.3 histones associate exclusively with their cognate chaperone systems (HIRA and DAXX, respectively), CAF-1 might have taken over the role of both HIRA and DAXX in my knockout experiments (Figure 2.13D). Biochemical evidence supports this interpretation as CAF-1 co-purified with H3.3 in the absence of DAXX and HIRA (Drané et al., 2010; Lewis et al., 2010). Additionally and at low level, H3.3 histones are known to be loaded onto DNA also by the replication-dependent machinery in *Drosophila* cells (Ahmad and Henikoff, 2021; Schwartz and Ahmad, 2005). This possibility needs further investigation regarding the role of CAF-1 in EBV infected B cells.

Even more controversial is the phenotype of *ATRX* knockout B cells after infection with EBV, because these cells proliferated more rapidly than *CD46* knockout cells which served as control (Figure 2.13D). Although ATRX has been reported to be important for H3.3 placement on both cellular and

viral genomes (Cabral et al., 2018), a direct examination of the role of ATRX in rapidly proliferating and EBV infected B cells is needed here. Interestingly, the double knockout of *DAXX* and *ATRX* did not alter the survival and expansion of EBV infected B cells in my experiments (Figure 2.13D). Even the triple knockout of *DAXX*, *ATRX* and *HIRA* did not have a phenotype in EBV infected primary human B cells (Figure 2.13D). This finding, however, has to be confirmed with B cells from additional donors to support and strengthen my findings.

DAXX or *HIRA* deposit histone H3.3 in diverse biological processes ranging from gene activation to heterochromatin silencing. Based on my analysis, depletion of both replication-independent histone chaperones, *HIRA* and *DAXX* showed a clear reduction of cell numbers and surviving EBV infected B cells (Figure 2.13D). As cells with single knockouts of *HIRA* or *DAXX* did not show a phenotype (Figure 2.13D), this finding indicated that *HIRA* and *DAXX* might have redundant, complementing functions on EBV DNA. My view is supported as both *HIRA* and *DAXX* were found to be involved in H3.3 deposition in proliferating senescent cells (Corpet et al., 2014). However, the knockout of both functions might also have a detrimental effect on the survival of EBV infected B cells for other, unknown reasons. Clearly, more work is needed to identify the direct cause of this drastic phenotype.

Replication-dependent histone chaperones

The CAF-1 complex preferentially loads H3.1/H4 histone tetramers onto newly synthesized or damaged host DNA, but whether it is important for H3.1 loading onto the incoming EBV genomic DNA and the establishment of viral latency is unknown. In my analysis, the knockout of *CHAF1B*, the main player of S phase linked CAF-1 function, resulted in reduced cell proliferation, prevented the establishment of latent infection in B cells and caused acute cell death. EBV strongly upregulates *CHAF1B* expression in newly infected primary human B cells prior to first mitosis (Figure 2.12, see also <http://ebv-b.helmholtz-muenchen.de/>). Other subunits of the CAF-1 complex are *CHAF1A* that binds directly to *CHAF1* and *RBBP4*, which are also both upregulated together with *CHAF1B*. This finding, which is unique compared to the regulation of other histone chaperones suggests that CAF-1 has an important role in the pre-latent phase of infection. Similar to the upregulation of all three CAF-1 components, *EBNA2* and *EBNA-LP*, which together drive the EBV induced early reprogramming of infected B cells are also massively upregulated very early during infection (Mrozek-Gorska et al., 2019). All latent viral genes, *EBNA1*, *EBNA2*, *EBNA3A* and *EBNA3B*, *EBNA3C*, *LMP1*, *LMP2A* and *LMP2B* were also significantly upregulated in *CHAF1B* knockout B cells upon EBV's lytic reactivation (Zhang et al., 2020) suggesting that CAF-1 may also be important in chromatin regulation in this phase of EBV's life cycle.

This mentioned CAF-1 might implement epigenetic silencing of viral DNA using H3.1/H4 histone tetramers that cover the entire viral genome. In support of this idea, an earlier ChIP-Seq analysis

by Zhang et al. (2020) looking for histone 3.1 versus 3.3 occupancy on EBV DNA suggested that latent EBV genomes may be broadly occupied by H3.1 containing nucleosomes, most likely loaded in a DNA replication-dependent manner during S phase (Volk and Crispino, 2015; Volk and Crispino, 2015). Lack of epigenetic repression in the absence of CHAF1B might abrogate silencing of viral lytic genes and thus prevent a stable virus-host relationship and the successful establishment of latency.

Viral transcription appears to be promiscuous and undirected in the pre-latent phase, because a number of lytic viral transcripts are found expressed but mostly at low levels. Among them is BMRF1 which BZLF1, the viral master switch and transcription factor transactivates directly via BZLF1 binding sites in the BMRF1 promoter (Kalla et al., 2010; Wen et al., 2007). In Burkitt lymphoma cell lines, CHAF1B depletion seems to induce the immediate early genes BZLF1 and BMRF1 suggesting that CAF-1 also supervises the maintenance of EBV latency (Zhang et al., 2020). Additionally, CHAF1B depletion decreased histone 3.1 occupancy at the promoter of the immediate early gene BZLF1 and late gene BLLF1. Although these studies cannot explain the role of CHAF1B in the pre-latent phase of EBV infection, I hypothesized that CHAF1B regulate early lytic genes such that its absence activates a leakage pathway supporting the expression of lytic genes (Kalla et al., 2010). As depicted in Figure 2.17, CHAF1B seems to be involved in early lytic BMRF1 gene suppression starting on day 3 or 4 after infection, although BMRF1 reporter levels did not increase dramatically in *CHAF1B* knockout cells compared with control cells. In addition, using a knockout BZLF1 viral mutant, the phenotype of *CHAF1B* knockout EBV infected B cells did not differ from the same cells infected with wild-type EBV (Figure 2.17C). The somewhat prolonged expression of lytic viral genes cannot cause the drastic phenotype observed in EBV infected *CHAF1B* knockout cells.

CAF-1 is known to be an important histone chaperone in all eukaryotic cells from yeast to multicellular organisms given its role in DNA replication and cell proliferation (Xu et al., 2010). It was therefore surprising to learn that *CHAF1B* knockout B cells, when stimulated with CD40 ligand and IL-4 did not show drastic phenotypic alterations very much in contrast to the same cells infected with EBV. A possible explanation is provided by a paper in which the HIRA complex was shown to incorporate H3.3 at replication sites when replicative H3.1 incorporation was impaired (Ray-Gallet et al., 2011). This finding speaks for an alternative, salvage pathway and is further supported by experiments with CAF-1 depleted cells in which newly synthesized DNA was partially protected against MNase digestion suggesting that nucleosome assembly during DNA replication in vertebrate cells is mediated by a so far undefined activity (Takami et al., 2007). If HIRA provided the alternative assembly pathway in CD40L/IL-4 stimulated *CHAF1B* knockout cells, it might be insufficient to cope with the need to rapidly and load histones on replicating viral DNA because these virally infected cells undergo very fast cell divisions starting on day 4 post infection. In summary, my experiments which used two different B cell activation protocols in *CHAF1B* knockout cells identified a distinct

and very peculiar role of CHAF1B during EBV infection and reprogramming of B cells by this virus.

CAF-1, the replication-dependent histone chaperone interacts with proliferating cell nuclear antigen (PCNA). Both complexes co-localize at replication foci in early S of the cell cycle. In human cells, devoid of CAF-1 the cells arrested in early and mid S with a DNA replication defect (Figure 2.15B) in contrast to the situation in yeast (Hoek and Stillman, 2003). In my analysis of *CHAF1B* knockout cells that had been activated by either EBV infection or CD40L/IL-4 signals the cells showed a similar defect in S phase by the time cells entered the cell cycle on day 3 (Figure 2.15B). In CD40L/IL-4 activated cells this phenotype persisted until day 4 but the cells resumed their normal cycling thereafter. In contrast, EBV infected *CHAF1B* knockout cells ran into a cell cycle block and a complex stress syndrome with extreme levels of phosphorylated H2A.X and signs of DNA replication stress and DDR starting on day 4 post infection (Figure 2.16B). The induced stress resulted in a high rate of apoptotic cells and cells with reduced metabolic activity at day 5 post infection and later (Figure 2.14). As a result, the cells failed to overcome this barrier and showed an increase in their subG1 fraction on day 7 post infection (Figure 2.15C). This surprising phenotype seen only in EBV infected human B cells devoid of *CHAF1B* required further analysis to understand its molecular cause.

In the nucleus of latently infected cells, EBV's genomic DNA is maintained as extrachromosomal plasmids that replicate via *oriP*, the viral plasmid origin of DNA replication (Chiu and Sugden, 2018). EBNA1, a latent viral factor binds *oriP* within nucleosome-free or poor regions within two parts of *oriP*, the family of repeats and the dyad symmetry element (Middleton and Sugden, 1994; Wysokenski and Yates, 1989). Additionally, EBNA1 as a viral factor in trans, mediates tethering of viral DNA to cellular perichromatin to maintain the partitioning of viral genome copies in resting and proliferating cells. This DNA synthesis is imperfect meaning that only about 85% of EBV plasmids are synthesized in each cell cycle and partitioned to the daughter cells (Nanbo et al., 2007). In addition to *oriP*, additional loci (eg. Raji ori) function as origins for EBV genomes only after they are established in certain proliferating cells (Wang and Bill, 2008), although EBNA1 does not bind to these sites indicating that they are unlikely to participate in the partitioning of EBV genomes. In contrary, a recent paper from my lab (Pich et al., 2019) demonstrated that the rapid cycling of EBV infected cells starting four days after EBV infection does not depend on EBNA1, suggesting that viral DNA replication must rely on the cellular machinery, only. Therefore, I hypothesized that EBV DNA might enter into a phase of over-replication in an unlicensed manner in the absence of CAF-1 in the early phase of infection. Consequently, the accumulation of nucleosome-free viral DNA might cause genotoxic stress followed by cell death in the early phase of EBV infection. My qPCR analysis (Figure 2.18) comparing the ratio of viral and cellular DNA in the absence of CHAF1B supports this hypothesis. It thus seems as if CHAF1B controls the replication of viral DNA most probably

by loading nucleosomes downstream of the replication fork onto newly replicated DNA. How this function is molecularly implemented is speculative.

3.6 Outlook

This thesis provides efficient means to manipulate primary human B cells genetically using *in vitro* assembled Cas9 ribonucleoprotein complexes. This new technology also enables studies into the functional interactions between EBV and its primary host B cell. Especially, highly efficient genome editing in the target B cells of EBV allowed me to study the potential role of histone chaperones in the survival of EBV infected B cells. In this context, I identified the CAF-1 histone chaperone complex as a cellular factor that controls viral DNA replication in the pre-latent phase of infection. My results might encourage others to invest further into genetic engineering of primary human B cells. My findings also raise a set of questions related to EBV's biology which have to be investigated and answered in more detail in the future.

3.6.1 Possible improvements for genome editing of primary human B cells for future immunotherapeutic strategies.

Methods in B cell engineering bring us closer to explore and test B-cell based therapies in the clinic. Similar to T cells, a system based on B cells from peripheral blood, which are genetically engineered, expanded in culture and then reintroduced back to the donor patient would be an excellent platform for gene therapy. The limiting factor for CRISPR based therapy is the off-target activity of the Cas9 nuclease which might be resolved in the near future.

The CRISPR/Cas9 system has also been engineered to selectively modify genomes of adenovirus and herpes simplex virus type 1 (HSV-1) in freshly infected human cells in which the virus undergoes lytic replication (Bi et al., 2014; Diemen et al., 2015). For instance, targeting essential genes of HSV-1 with multiple gRNAs prevented the production of infectious particles from infected human cells. Similarly, targeting vulnerable EBV target sites with the CRISPR approach would help to clear EBV from latently infected and EBV-transformed human tumor cells. Although currently EBV vaccines are pacing their way, CRISPR-based gene editing would present a brand-new therapeutic approach to eliminate all EBV infected cells if one could devise a B cell specific delivery of Cas9 RNP complexes.

3.6.2 How does the CAF-1 complex control EBV's DNA replication in the pre-latent phase?

My CRISPR-Cas9 knockout screen aimed at elucidating the role of several histone chaperones in EBV's pre-latent phase of infection. Unexpectedly, the screen identified the CAF-1 histone chaperone

to have a critical role in the early survival of EBV infected B cells. Additional experiments identified a link between CAF-1, viral DNA replication and ensuing genotoxic stress in the absence of CHAF1B. The molecular nature of this linkage is currently elusive and requires detailed investigations. Given the work by Pich et al. (2019) the viral EBNA1 protein, which is known to act on the plasmid origin of viral DNA replication has no role during pre-latency. This finding puts cellular factors in the spotlight, which are known to be involved in the regulation of EBV DNA replication. They include ORC members, MCMs, PCNA and others. It is unclear where viral DNA replication initiates in the pre-latent phase of infection and whether onset of DNA replication is properly licensed or, in particular in *CHAF1B* knockout cells occurs in an unlicensed manner. It is equally uncertain, whether the CAF-1 complex acts on EBV DNA and at viral replication forks as it does on cellular DNA. At first glance it now appears as if viral DNA replication differs fundamentally from cellular, licensed DNA replication in the early phase of viral infection. This difference is certainly interesting but challenging to address experimentally.

3.6.3 Where and when do histone marks on viral DNA occur during the early phase of infection?

A comprehensive study on the kinetics of nucleosome acquisition and assembly on the incoming EBV DNA in the early phase of viral infection has been recently completed (Mrozek-Gorska et al., unpublished). My experimental work complements and extends this finding and gives insight into the role of histone chaperones in the pre-latent phase of infection. Along with the CRISPR edited histone chaperones, chromatin immunoprecipitation (ChIP) experiments are needed to identify the contribution of single histone chaperones in depositing H3.1 or H3.3 histones onto incoming, epigenetically naive EBV DNA. An additional uncertainty concerns the posttranslational histone modifications which turn most of EBV's genomic DNA into repressed chromatin as indicated by the characteristic H3K27me3 histone mark. It is equally unclear when EZH2, the relevant histone methyltransferase starts to implement this modification on H3 histones on viral DNA. In this context, a recent study showed that in the absence of CHAF1A, H3K9me3 marks on chromosomally integrated HIV-1 provirus DNA are reduced suggesting that CAF-1 might have an additional role in placing or directing specific histone marks (Geis et al., 2022). Additional experiments are needed to address these very interesting but unexplored questions and possibilities.

Chapter 4

Materials

4.1 Plasmids

p509 and p260 plasmids were used to induce EBV's lytic cycle in HEK293 2089 cells for production of wild type EBV. For lytic phase reactivation, the p509 plasmid expresses the BZLF1 gene under the control of CMV promoter (Hammerschmidt and Sugden, 1988). Virus titer was increased with expression plasmid p2670 encoding the viral BALF4 gene under the control of the CMV promoter.

4.2 Virus supernatants

All supernatants are established and referred in previous study (Pich et al., 2019).

TABLE 4.1: Virus Supernatants

EBV supernatant	Description
B95-8	Wild type EBV derived from the marmoset B-lymphoblastoid cell line (B95-8) (Miller et al., 1972)
wt/B95.8 (2089)	Wild type EBV: F plasmid (pMBO131) with eGFP, 13 miRNAs and hygromycin resistance gene in B95-8 DNA.
r-wt/B95.8 (6008)	Wild type EBV: restored deleted miRNAs and puromycin resistance gene in 2089
Δ EBNA3C (6123) mutant	Mutant EBV: knockout of EBNA3C by carrying two in-frame stop codons in exons 1 and 2 of EBNA3C
Δ EBNA3A/C (6331) mutant	Mutant EBV: knockout of EBNA3A and 3C with insertional mutagenesis of EBNA3A
Δ BZLF1 (3283) mutant	Mutant EBV: knockout of BZLF1 by introducing a stop codon after amino acid 56
CD2 reporter EBV (3875)	Reporter EBV: The rat CD2 gene encompassing amino acid residues 1–233 of the rat CD2 coding region was expressed from the viral BMRF1 promoter and introduced into the backbone of the recombinant EBV plasmid p2089 (Kalla et al., 2010).

4.3 Antibodies

TABLE 4.2: Monoclonal antibodies

Specificity	Host	Application	Supplier/ Cat No.
CD46	Mouse/IgG1	FACS	Biologend, #352405
CD19	Mouse/IgG1	FACS	eBioscience, #48-0199-42
CD20	Mouse/IgG2b	FACS	BD, #556633
CD38	Mouse/IgG1	FACS	eBioscience, #25-0389-42
CD138	Mouse/IgG1	FACS	Invitrogen, #17-1389-42
CD2	Mouse/IgG2a	FACS	HMGU Monoclonal Antibody Core facility
H2AX	Mouse/IgG1	FACS-IC	BD, #560447
IgD	Mouse/IgG2a	FACS	BD, #555778
HIRA	Rabbit	WB	Novus Biologicals, NBP3-04894
DAXX	Rabbit	WB	Novus Biologicals, NBP1-85309
ATRX	Rabbit	WB	Novus Biologicals, NBP1-83077
ABCG1	Rabbit	WB	Abcam, #ab52617

4.4 Eukaryotic cell lines

TABLE 4.3: Common cell lines

Cell lines	Description
Raji	Human EBV positive Burkitt's lymphoma cell line (Pulvertaft, 1964)
HEK293	Human epithelial embryonic kidney cell line (Graham et al., 1977)
LL8	Murine fibroblasts stably transfected with human CD40L (Wiesner et al., 2008)
LCL	Lymphoblastoid cell line derived from B cells transformed with EBV
Elijah	EBV-negative Burkitt lymphoma cell line (Rowe et al., 1985)

4.5 Oligonucleotides

TABLE 4.4: PCR and sequencing primers

Name	Application	Sequence (5' to 3')
CD46-fwd	Gel electrophoresis	CTGTACTACCTGCTGCCAGACC
CD46-rev	Gel electrophoresis	ATAACAGGCGTCATCTGAGACAGG
CD46-fwd	Miseq-single end seq	ACACTCTTTCCCTACACGACGctcttccgatct CTGTACTACCTGCTGCCAGACC
CD46-rev	Miseq-single end seq	TGACTGGAGTTCAGACGTGTGctcttccgatct ATAACAGGCGTCATCTGAGACAGG
CD46-fwd	Miseq-paired end seq	ACACTCTTTCCCTACACGACGctcttccgatct GACCACAGTCCATGGCTGATG
CD46-rev	Miseq-paired end seq	TGACTGGAGTTCAGACGTGTGctcttccgatct CATCACCGTAGTGGAATATGTACCC
CDKN2A-fwd	Miseq-single end seq	ACACTCTTTCCCTACACGACGctcttccgatct CGTCCTCCAGAGTCGCCC
CDKN2A-rev	Miseq-single end seq	TGACTGGAGTTCAGACGTGTGctcttccgatct CTGCGGAGAGGGGGAGAG
CHAF1B-fwd	Sanger seq	AGATGGGATTTTACTGTGTTAGC
CHAF1B-rev	Sanger seq	TAAAGTTAAGGTAAGTTAGGGCC
HIRA-fwd	Sanger seq	GGGAGTTTTTTCAGGTTGGTTA
HIRA-rev	Sanger seq	AATTAAACAGCGTCTCAGAAATG
DAXX-fwd	Sanger seq	CTCGATCTCATCTACAACCTTGG
DAXX-rev	Sanger seq	AAGAAGTTTCTCTAAGGAATCCC
ATRX-fwd	Sanger seq	CACGACTTACAGTATGGCTATATT
ATRX-rev	Sanger seq	CTGCTCTCTGAATAAAATAAATGGT

TABLE 4.5: qPCR primer

Name	Sequence (5' to 3')
Cp-fwd	ACAAGGGGACAAGTGTGGCA
Cp-rev	TGACTGGTGGGGGGCATC
FHIT-fwd	GCACCTGATGTTAAGCCGGA
FHIT-rev	CTGCCCCGACGAGAAACAAGA
Orip-fwd	GCCCACCGTGCTCTCAGC
Orip-rev	TCAAACCACTTGCCCACAAAAC
GusB-fwd	GTGCTGGGGAATAAAAAGGGG
GusB-rev	ACTCGGGGAGGAAGGGACAC

TABLE 4.6: crRNAs for genome editing

Target gene	Naming in the text	Sequence (5' to 3')	PAM sequence	Supplier
CD46	CD46-gRNA1	TCG TTCACCAATCTCATAGT	AGG	IDT/Synthego
CD46	CD46-gRNA2	TTTGTGATCGGAATCATAACA	TGG	IDT/Synthego
CDKN2A	CDKN2A-gRNA	CCCAACGCACCGAATAGTTA	CGG	IDT
CHAF1B	CHAF1B-gRNA1	UAUCAUACACAUCUUCUAAG	TGG	Synthego
CHAF1B	CHAF1B-gRNA2	AUCAUAUGGGAUGUCAGCAA	AGG	Synthego
HIRA	HIRA-gRNA1	UCACAUCUGAAAAGAAGACAG	TGG	Synthego
HIRA	HIRA-gRNA2	CUUGGUCAAAGGGUUGACAU	GGG	Synthego
DAXX	DAXX-gRNA1	UGCAGGGUCAACGCCUACGU	GGG	Synthego
DAXX	DAXX-gRNA2	AAGAGAAGAGCUCGGCUCCA	AGG	Synthego
ATRX	ATRX-gRNA1	UGAAAGCAAGUUGAAUACAU	TGG	Synthego
ATRX	ATRX-gRNA2	UGAUUCAUUGCAAGUCGUGG	AGG	Synthego

4.6 Cell culture media

TABLE 4.7: Media and media supplements for cultivating eukaryotic cell lines.

Medium	Application	Supplier
α -thioglycerol	Antioxidant reagent as an additive to the media	Sigma Aldrich, Germany
Ciprobay	Antibiotics used as an additive to the media	Bayer Vital, Germany
Penicillin/Streptomycin	Antibiotics used as an additive to the media	Gibco, UK
RPMI 1640 Medium	Cell culture medium used for cultivation of all cell lines	Gibco, UK
Sodium Pyruvate	Antioxidant reagent as an additive to the media	Gibco, UK
Sodium Selenite	Antioxidant reagent as an additive to the media	Gibco, UK
Trypsin-EDTA	0.05% solution used for cell dissociation from the cell culture dish	Gibco, UK
Fetal calf serum	Fetal calf serum	Sigma Aldrich, Germany
Bambanker	Cell freezing medium	NIPPON Genetics Europe
Puromycin	Antibiotics used for cell culture selection	Merck (Calbiochem) Germany
Interleukin-4	Inducing B cell proliferation	Miltenyi Biotech GmbH, Germany
Defibrinated sheep blood	Removal of T cells	Thermo Scientific Oxoid
Bradford reagent	Protein lysate quantification	Merck

4.7 Enzymes and other chemicals

TABLE 4.8: The list of enzymes and other chemicals used in this thesis

Enzyme/Chemical	Supplier
2-NBDG	Thermo Scientific, USA
4sU	Sigma Aldrich
Agarose	Invitrogen, Karlsruhe, Germany
AZ20	Sigma-Aldrich
Biotin-HPDP	Pierce
Cas9 V3 protein	Lonza
Cell Lysis Buffer	Thermo Scientific, USA
Ethanol (absolute, pure)	Merck, Darmstadt, Germany
EDTA	Thermo Fisher Scientific
Ethidium bromide	Roth, Germany
Ficoll Hypaque	PAN Biotech, Germany
FxCycle TM Violet stain	Thermo Scientific, USA
FACS APC beads	Calibrite; Becton, Dickinson
Gene Ruler (1 kb and 100 bp plus)	Thermo Scientific, USA
Glycogen	Thermo Scientific, USA
KU 55933	Sigma-Aldrich
LightCycler 480 SYBR Green I Master mix	Roche Diagnostics, Germany
NP-40 (IGEPAL)	Sigma-Aldrich, Munich, Germany
Q5 Polymerase	New England Biolabs, USA
PBS	Biochrome AG, Berlin
Polyethylenimine Max (PEI Max)	Sigma-Aldrich, Munich, Germany
TMRE (Mitostatus)	BD Pharmigen, USA
Trizol Reagent	Thermo Scientific, USA

4.8 Commercial Kits

TABLE 4.9: Commercial Kits

Product	Supplier
Annexin V-Cy5 Apoptosis Kit	BioVision
B cell isolation kit II, Human	Miltenyi Biotec GmbH, Germany
Click-iT TM EdU Cell Proliferation Kit	Thermo Fisher Scientific
Fix/Perm kit	Thermo Fisher Scientific
IFN- α pan Human ELISA development Kit	MabTech
QIAMP DNA Mini Kit	Qiagen, Hilden
Qubit sdDNA HS Assay Kit	Thermo Fischer Scientific, USA
P3 Primary Cell 4D-Nucleofector X Kit S	Lonza
Nucleospin Gel and PCR Clean-up	Macherey-Nagel, Germany
66-440 kDa Separation Module, 8 x 13 Capillary Cartridges	Bio-techne, Protein simple, USA
Anti-Rabbit Detection Module	Bio-techne, Protein simple, USA

4.9 Material and devices

TABLE 4.10: Material and devices

Product	Supplier
Agilent 2100 Bioanalyzer	Agilent Technologies
Bioruptor Standard Sonicator	Diagenode, Belgium
DNA High Sensitivity Chip	Diagnostic Roche
FACS Fortessa	BD Biosciences, USA
FACS Canto	BD Biosciences, USA
Lonza 4D Nucleofector Core and X Units	Lonza
Light Cycler 480	Diagnostic Roche
MACS LS Columns and Separator	Miltenyi Biotec GmbH, Germany
Nanodrop spectrophotometer system	Thermo Fischer Scientific, USA
Phase Lock Gel Heavy Tubes	QuantaBio
RNeasy MinElute column clean up	Qiagen
Nextera XT DNA Library Preparation Kit	Illumina
SMART-Seq v4 Ultra Low Input RNA	Clontech Laboratories
Qubit 2.0 Fluorometer	Thermo Fischer Scientific, USA
MACs Streptavidin Microbeads	Miltenyi
Wes instrument	Bio-techne, Protein Simple, USA

4.10 Software packages and web tools

TABLE 4.11: Software packages and web tools

Name	Application	Supplier/Source
Flowjo Software	Post-acquisition FACS analysis	Becton Dickinson, USA
Microsoft Office 2017	Processing Text, tables and presentation processing	Microsoft, USA
TIDE	Calculation of knockout efficiency	https://tide.deskgen.com
Biorender	Creation of Diagrams in Figures	https://biorender.com/
GraphPad Prism	Data analysis	Graphpad Software, USA
MacVector 15.5	Nucleic acid visualization, primer design	MacVector, USA
RStudio Version 1.2.5001	Integrated Development Environment for R	RStudio Inc., USA
Mendeley Desktop 1.17.12	Literature citation	Mendeley Inc., USA
Compass software v 4.0	Visualization and quantitative analysis for each protein	Bio-Techne, USA
Integrative genomics viewer (IGV) 2.5.9	Visualization of NGS data	http://software.broadinstitute.org/software/igv/

Chapter 5

Methods

5.1 Working with eukaryotic cells

5.1.1 Cultivation of suspension and adherent cells

Eukaryotic cells were treated in class II biosafety laminar flow hoods and cultured at 37°C with 95% humidity and 5% CO₂. Centrifugation of the cells was performed at 300 g for 10 min. Raji, HEK293, B95-8 cells and LCLs were cultured in RPMI 1640 medium supplemented with 8% FCS, 100 µg/ml streptomycin, 100 U/ml penicillin, 1 mM sodium pyruvate, 100 nM sodium selenite, and 0.43% α -thioglyceroles.

HEK293 virus producer cells were cultured with additional 1 µg/ml puromycin on 13 cm dishes until the confluency of the cells reached 80%. The cells were detached from the 13 cm dishes using a Trypsin-EDTA 0.05% solution and were resuspended in fresh medium prior to their transfer to new dishes. The suspension cells were cultivated and kept at an average density of 5×10^5 cells/ml at the start of the culture.

LL8 feeder cells were cultured in RPMI 1640 supplemented with 10% FCS, 4 mM L-glutamine, 100 U/ml penicillin, 100 µg/ml streptomycin, and 100 nM sodium selenite. LL8 feeder cells are murine fibroblasts L929 stably transfected with the human CD40L gene that binds CD40 and induces an internal signaling cascade in B cells (Wiesner et al., 2008).

5.1.2 Long-term storage of cells

Cells for long-term storage were collected in 1 ml freezing medium (Bambanker) and around 5×10^6 cells were transferred to a single pre-cooled vial. The vials were stored at -80°C for a week. Afterwards, the vials were transferred to a liquid nitrogen tank for long-term storage.

To re-culture frozen cells, the frozen cells were thawed at 37°C in a water bath and immediately washed with 50 ml of pre-warmed medium. The cells were resuspended in 5 ml fresh medium

and cultured overnight. On the following day, the medium was replaced with selection medium containing appropriate antibiotics if required.

5.1.3 Cell number calculation

An aliquot of the cell culture was mixed with Trypan blue 1:2 to 1:10 depending on the cell density and 10 μ l of this suspension was counted using a Neubauer hemacytometer. Dead cells were identified by their Trypan blue staining. Live cells located within four large squares were counted and the cell concentration was calculated considering the geometry of the hemacytometer:

$$\text{Cells/ml} = (\# \text{ of live cells counted} \times \text{dilution factor} \times 10^4)/4$$

The absolute number of viable lymphocytes and B blasts in suspension cultures was counted by adding a known number (usually 20,000 per sample) of calibrated allophycocyanin (APC) beads (Calibrite; Becton, Dickinson) as a volume standard to the cell culture medium. The flow cytometer was usually set to count 5,000 APC beads (one fourth of the total volume of the probe).

5.1.4 Irradiation of CD40L expressing LL8 stimulator cells

CD40L expressing LL8 feeder cells were provided by the group of Andreas Moosmann. Briefly, trypsinized cells were washed, resuspended in medium and irradiated with 180 Gy at the radiation facility. 10^6 cells were seeded per one full plate with 96, 48, 24, 12, or 6 wells.

5.1.5 Isolation of B cells from adenoid biopsies

Primary B cells were isolated from adenoid biopsies of anonymous donors received from the Clinic Grosshadern. The adenoid tissues were rinsed with PBS several times using a 100 μ m cell strainer and transferred to a sterile petri dish. Adenoid tissues were mechanically chopped with two sterile scalpels in PBS. The cell suspension was filtered through a 100 μ m strainer while washing them with additional PBS. Depending on the adenoid size, this procedure was repeated several times to recover a maximum number of cells. The volume of the collected cells was increased to 30 ml with PBS. 0.5 ml defibrinated sheep blood was added to deplete T cells in the next step. The cell suspension was underlayered with 15 ml Ficoll Hypaque and the samples were centrifuged at 500 g for 30 min. Cells were carefully collected from the interphase and transferred to a new 50 ml tube. The cell suspension was washed three times in a total volume of 50 ml PBS and centrifuged with decreasing sedimentation forces (450, 400 and 300 g) for 10 min each. At the last centrifugation step, erythrocytes were lysed by resuspending the cell pellet in 5 ml red blood cell lysis buffer (154 mM NH_4Cl ; 9.98 mM KHCO_3 ; 0.127 mM ETDA, pH 8.0). The cell pellet was resuspended in fresh,

pre-warmed complete cell culture medium supplemented with Ciprobay (1:200 dilution) to control bacterial contamination.

5.1.6 Isolation of B cells from PBMCs

B cells were isolated from fresh LRSCs (Leukoreduction system chambers) obtained from the Clinic Grosshadern after plateletpheresis procedures. The blood cell sample was diluted 1:6 or more with PBS and underlayered with 15 ml Ficoll Hypaque in a 50 ml Falcon tube. The samples were centrifuged at 500 g for 30 min. PBMCs were carefully collected from the interphase and transferred to a new 50 ml tube. The cell suspension was washed three times in a total volume of 50 ml PBS and centrifuged with decreasing sedimentation forces (450, 400 and 300 g) for 10 min each. The cell pellet was resuspended in fresh medium and B cells were isolated using the B cell isolation kit II as described in manufacturer's protocol (Miltenyi) using MACS sorting with an LS column.

5.1.7 Virus supernatant production from HEK293 6008 and B95-8 cell lines

To obtain virus stocks, different HEK293 producer cell lines established in our lab (6008, 6123, 6331, 3283, 3875) (Pich et al., 2019) were transiently transfected with expression plasmids encoding BZLF1 (p509) and BALF4 (p2670) to induce EBV's lytic cycle. Briefly, cells were seeded onto 13 cm dishes to reach 80% confluency. The next day, the cells were transfected using 6 µg p509 and 6 µg p2670 plasmid DNAs (Neuhierl et al., 2002) mixed with 72 µl of a 1 mg/ml stock solution of polyethylenimine in water (pH 7.0) in 2.4 ml plain RPMI1640 cell culture medium and incubated for 15 min at RT. The mix was dropped onto HEK293 producer cell lines in fully supplemented cell culture medium without puromycin and the transfected cells were incubated for 3 days at 37°C with 95% humidity and 5% CO₂. Cell culture supernatants were collected and centrifuged for 8 min at 300 g and then at 1,200 g for 8 min. The virus stocks were stored at 4°C and used to determine the virus concentration with Raji cells.

For collecting EBV virus stocks from B95-8 cells (from the institute's cell strain collection), the cells were cultivated at higher density to increase the fraction of cells that spontaneously reactivate and release virus into the medium. The spent cell culture medium was collected and centrifuged at 300 and 1200 g for 10 min to remove cellular debris. The virus stocks were stored at 4°C and used to determine the virus concentration.

5.1.8 Determination of the virus titer

To titer the virus stocks (harvested from lytically induced HEK293 cells), 1×10^5 Raji cells (obtained from the Leibniz Institute DSMZ, Braunschweig) were incubated with different volumes of

virus stocks at 37°C for 3 days in a 24-well plate. The percentages of GFP-positive cells were determined by flow cytometry using a BD FACS Canto instrument (BD Bioscience). The percentages of GFP-positive Raji cells was plotted against the volume of the added supernatant. The linear regression equation was calculated as previously described (Steinbrück et al., 2015) for the linear part of the graph using GraphPad Prism. The titer defined as “Green Raji Units/ml” was calculated by the linear regression formula:

$$\text{Titer(GRU/ml)} = ((ax1000\mu\text{l}+b)/100) \times 10^5$$

To titer the virus stocks obtained from supernatants of B95-8 cells, Elijah cells were infected with defined volumes of B95.8 virus stock and wt/B95.8 (2089) EBV stock with a calibrated concentration in GRU per milliliter. The cells were incubated with different supernatants for 3 hours at 4°C under rotation and washed twice with PBS. Later, the cells were stained with a directly coupled antibody directed against the viral envelop protein gp350, which binds to viral particles attached to the Elijah cells. A linear regression equation was calculated on the basis of the applied amounts of wt/B95.8 (2089) EBV stock with the known titer versus the fractions of gp350-positive cells infected with B95.8 virus stock, which allow to calculate the concentration of the B95.8 virus stock in question.

5.1.9 EBV infection of primary human B cells and generation of LCL

Virus supernatants were incubated with primary B cell suspension at an optimal multiplicity of infection (MOI) of 0.1 ‘green Raji units’ overnight as described (Steinbrück et al., 2015). The following day, the virus supernatant was replaced with fresh medium after centrifugation of the cell suspension at 300 g for 10 min.

5.1.10 B cell activation using CD40 ligand feeder cells together with IL-4

B lymphoblasts were generated by plating isolated primary human B cells on irradiated CD40 ligand feeder cells in the presence of 2 ng/ml IL-4 as described by Wiesner et al. (2008).

5.1.11 IFN- α release assay and quantitation by ELISA

For ELISA assays, B cells nucleofected with CD46-Cas9 RNP complexes or P3 buffer were cultured with or without EBV infection at 37°C for 20 h. On the next day, the cells were counted and 2×10^5 cells were plated in 96 well cluster plates in a volume of 200 μl cell culture medium. After 48 h, cell supernatants were collected and their IFN- α content was quantified using the IFN- α pan Human ELISA development Kit from MabTech.

5.2 Flow cytometry measurements

5.2.1 Staining of B cell surface markers for flow cytometry

B cells were collected at different time points after infection and stained with antibodies specific for the cell surface markers CD19 (eFluor450 conjugated, diluted 1:50), CD20 (PE-conjugated, diluted 1:100), CD38 (PECy7-conjugated, diluted 1:300), CD138 (APC-conjugated, diluted 1:50), CD46 (APC-conjugated, diluted 1:50) and CD2 (unconjugated, Ox34, mouse IgG-2A). For staining, the cells were washed with and resuspended in 50 μ l FACS staining buffer (PBS, 0.5% BSA, 2 mM EDTA). The samples were incubated with the antibodies at 4°C in the dark for 20 min. The host, suppliers and catalog numbers of the antibodies are provided in Table 4.2. Cells were washed with 1 ml of FACS staining buffer and resuspended in 200 μ l of the same buffer for their FACS analysis. Flow cytometry data were collected on a FACS Canto II (BD) or FACS Fortessa (BD) instrument. The data were analyzed with the FlowJo software (version 10.4).

5.2.2 Cell cycle analysis

Primary B cells were nucleofected with Cas9-RNP complexes and infected with a virus stock or plated on CD40 ligand feeder cells with IL-4. The cells were incubated at a density of 10^6 cells/ml overnight. On the following day, the cells were counted for their absolute cell number and around 2×10^5 cells were plated for each time point in 96 well cluster plates. Prior to cell harvest on day 2, 3, 4, 5 and 7 after infection, the infected cells were pulsed with a final concentration of 10 μ M EdU for 1 h at 37°C. Afterwards, the harvested cells were washed once with wash buffer (PBS with 1% BSA) and resuspended in 100 μ l Click-IT fixative solution prior to their incubation for 15 min at RT. The samples were stored in freezing medium (90% FCS, 10% DMSO) at -80°C until all samples from different time points were collected.

Prior to FACS analysis, freshly thawed samples were washed in wash buffer (PBS and 1% BSA) and resuspended in 100 μ l 1x Click-IT permeabilization and wash reagent. For each sample Click-IT EdU reaction cocktail (PBS, Copper protectant, fluorescent dye Alexa 647 picolyl azide and 1x Click-IT EdU buffer additive) prepared and incubated with for 30 min at RT in the dark. After washing the samples with 1 ml 1x Click-IT permeabilization and wash reagent, cells were resuspended in 400 μ l of the same buffer and incubated with 1 μ l of Fxcycle Violet stain for 30 min at RT in the dark. The analysis was done with a BD Fortessa instrument.

5.2.3 Staining with 2-NBDG, TMRE and Annexin V following their analysis

Primary B cells were nucleofected with Cas9-RNP complexes and infected with a virus stock or plated on CD40 ligand feeder cells with IL-4. The cells were incubated with a density of 10^6 cells/ml overnight. On the following day, the cells were counted for their absolute cell number and around 2×10^5 cells were plated for each time point in 96 well cluster plates. At the day of analysis, the cells were re-suspended in 200 μ l of glucose-free medium supplemented with 1% FCS and 100 μ M of the glucose analogus 2-NBDG (2-[N-(7-nitrobenz-2-oxa-1,3-diazol-4-yl) amino]-2-deoxy-D-glucose) was added to the prepared samples for 1 hour at 37°C. Thirty minutes into the incubation, the samples were transferred to polypropylene FACS tubes and mixed with 100 nM TMRE (tetramethylrhodamine ethyl ester). The samples were incubated further for 30 min at 37°C. In the next steps, the cells were washed with FACS buffer two times to remove the uncoupled dye. Finally, the cells were resuspended in 500 μ l Annexin V staining buffer and incubated with APC-coupled Annexin V for another 10 min in the dark. The co-stained cells were measured using a FACS Fortessa flow cytometer analyzing 2-NBDG uptake in the FITC channel, TMRE incorporation in the PE channel and Annexin V bound cells in the APC channel. The fluorescence spillovers were corrected prior to measurements by using compensation controls. Measurements were performed daily for the first eight days after infection.

5.2.4 Intracellular staining of γ -H2A.X for flow cytometry

Primary B cells were nucleofected with Cas9-RNP complexes and infected with a virus stock or plated on CD40 ligand feeder cells with IL-4. The cells were treated with a DDR inhibitor (KU 55933 at a final concentration of 10 μ M), DRS inhibitor (AZ20 a final concentration of 2 μ M) or a combination of both inhibitors or they were left untreated for an hour at 37°C. In parallel, the activity of the DDR inhibitor KU 55933 was controlled by treating the cells with 85 μ M etoposide together with the DDR inhibitor for an hour at 37°C. Intracellular flow cytometry staining was performed with fixed cells using the Fix Perm kit (Thermo Fisher Scientific). Briefly, cells were washed and re-suspended in FACS staining buffer (PBS, 0.5% BSA, 2 mM EDTA). Cells were fixed by adding 100 μ l of Fix Perm medium A for 15 min in the dark at RT. The fixed cells were washed with FACS staining buffer and the pellet was re-suspended in 1 ml freezing medium (90% FCS, 10% DMSO) to be stored at -80°C until all samples from different time points were collected. At the time of analysis, the cell pellets were thawed and washed with FACS staining buffer (PBS, 0.5% BSA, 2 mM EDTA). The samples were re-suspended in 100 μ l of Fix Perm medium B and stained with 2 μ l of H2AX specific

mouse monoclonal antibody-conjugated Alexa Fluor 647 for 20 min at 4°C. After another washing step with 1 ml staining buffer, the samples were measured using a FACS Canto flow cytometer.

5.3 Nucleic acid related techniques

5.3.1 Genomic DNA purification from eukaryotic cells

Genomic DNA was isolated from eukaryotic cells by using the QIAamp DNA Mini Kit (Qiagen) following the manufacturer's instructions. Purified DNA was eluted in 50 µl elution buffer and the concentration was measured with the Nanodrop spectrophotometer system (Thermo Fisher).

Optionally, genomic DNA was isolated by using lysis buffer instead. The cells were re-suspended in 20 µl lysis buffer (0.2 mg/ml proteinase K, 1 mM CaCl₂, 3 mM MgCl₂, 1 mM EDTA, 1% Triton X 100, 10 mM Tris pH 7.5) supplemented with 20 ng/ml proteinase K. The reactions were incubated at 65°C for 10 min and at 95°C for 15 min in a PCR thermocycler. The lysates were stored at -20°C.

5.3.2 Nuclear-associated compartment fractionation by NP-40

Nuclear DNA the cells was separated as previously described (Galvis et al., 2017). Briefly, about 2×10^5 cells were collected at 4°C and washed with 1 ml PBS. The pelleted cells were resuspended in 200 µl of TMK buffer (25 mM Trish-HCl (pH 7.4), 5 mM KCl, 1 mM MgCl₂) and 150 µl of TMK buffer supplemented with 1% NP-40 was added. The suspension was incubated on ice for 5 min with occasional vortexing. The nuclei were pelleted by centrifugation (parameter here) and the supernatant with the cytoplasmic fraction was removed without disturbing the nuclear pellet. The pellet was suspended in 500 µl of S1 buffer (0.25 M Sucrose, 10 mM MgCl₂) and layered over 500 µl of S2 buffer (0.35 M Sucrose, 0.5 mM MgCl₂). The suspension was pelleted and resuspended in 300 µl of PBS. Nuclear DNA isolation was performed by using the QIAamp DNA Mini Kit (Qiagen) following the manufacturer's instructions.

5.3.3 Polymerase chain reaction (PCR)

PCR reactions were performed using 5 µl of the cell lysate or about 100 ng of DNA samples in a final total volume of 25 µl that included primers, dNTPs, reaction buffer, GC-enhancer buffer and 0.25 µl of Q5 Hot Start High-Fidelity DNA Polymerase (NEB, Massachusetts, USA). Amplification was done after an initial phase of denaturation (95°C, 5 min) in 32 cycles composed of 98°C, 62°C, and 72°C for denaturation, annealing and elongation and for 20 sec, 30 sec, and 40 sec, respectively. To perform next generation sequencing, PCR products were run on a 1.2% preparative agarose gel and the products were cleaned up using the Nucleospin Gel and PCR-clean-up columns (Machery-Nagel).

For next generation sequencing using a MiSeq benchtop sequencing system (Illumina), two-step PCR barcoding scheme was performed. Briefly, 6 μ l of PCR products were transferred to a second round of PCR amplification using barcode primers that were sample specific for subsequent DNA sequencing. The PCR reaction was run on a 1.5% preparative agarose gel, size-separated and bands of the expected lengths were eluted and quantified using a Nanodrop spectrophotometer system (Thermo Fisher). Primers used are listed in Table 4.4.

5.3.4 Quantitative real time PCR (qPCR)

The qPCR-standard protocol from our laboratory was used to quantify the viral and cellular DNA with a Roche LightCycler480 II device and LightCycler 480 SYBR Green I Master (Roche) reagent according to the manufacturer's instructions. 2 μ l of sample volume was combined with 8 μ l of the master mix for each well. The master mix contained 5 μ l LightCycler 480 SYBR Green I Master, 1 μ l 10 μ M forward primer and reverse primer and 1 μ l PCR grade H₂O. The cycle conditions are listed in Table 5.1

TABLE 5.1: LightCycler 480 cycling conditions

Analysis mode	Cycles	Segment	Temp(°C)	Ramp Rate(°C/s)	Time hold	Acquisition mode
None	1	Pre-incubation	95	4.4	10 min	none
Quantification	45	Denaturation	95	4.4	3 sec	none
		Annealing	63	2.2	10 sec	none
		Extension	72	4.4	20 sec	single
Melting curves	1	Denaturation	95	4.4	5 sec	none
		Annealing	65	2.2	1 min	none
		Melting	97	0.1	-	continuous
None	1	Cooling	40	2.2	30 sec	none

The primer efficiencies were calculated from the standard curves with the dilutions of defined amounts of the respective PCR product. Two replicates for each DNA, target and standard dilution were analyzed in parallel. The relative quantification of viral target genes to cellular genes was calculated by $2^{-\Delta\Delta C_t}$ method provided by the Roche LightCycler 480 and corrected for primer efficiencies. Primers used are listed in Table 4.5.

5.4 CRISPR/Cas9 mediated genome editing

5.4.1 sgRNA design for CRISPR/Cas9 mediated genome editing

crRNAs for CRISPR/Cas9 experiments were designed by using IDT website (<https://eu.idtdna.com/>) and gRNAs were designed by using Synthego's website (<https://www.synthego.com/>). The

choice of gRNAs was detailed in the Results section 2.1.1 of the thesis. crRNAs with tracrRNA were ordered from Integrated DNA Technologies, Inc, whereas gRNAs were ordered from Synthego.

5.4.2 Assembly of ribonucleoprotein (RNP) complexes

Chemically synthesized tracrRNA and crRNAs were obtained from IDT and were dissolved in Nuclease-free Duplex Buffer (IDT) at 200 μM . 5 μl of crRNA and tracrRNA each were mixed 1:1 to reach a final concentration of 100 μM . To form the gRNA complex the mixture was incubated at 95°C for 5 min in a pre-heated PCR cyclor and slowly cooled down to room temperature by switching the instrument off. This step of gRNA assembly was not performed when we obtained chemically synthesized gRNAs from Synthego. Briefly, gRNAs were dissolved in Nuclease-free 1X TE buffer (Synthego) to reach a final concentration of 100 μM .

To form RNP complexes, 6.5 μl of a 62 μM Cas9 V3 protein (1081059; Integrated DNA Technologies) was added to 10 μl of the gRNAs and the mix was diluted with PBS (0.22 μm mesh size filtered) to a final volume of 50 μl . The mixture was incubated at room temperature for 10 min to form RNPs at a final concentration of 8 μM Cas9. The sequences of the crRNAs and gRNAs are provided in Table 4.6.

5.4.3 Nucleofection of primary human B cells with RNP complexes

2×10^6 freshly isolated primary B cells were washed in PBS and resuspended in 20 μl P3 Primary Cell Nucleofector Solution buffer prepared with Supplement 1 buffer (Lonza) according to the manufacturer's instructions (P3 Primary Cell 4D-Nucleofector X Kit S). Cells were mixed with 5 μl of the RNP mixture by gently pipetting and were transferred to pre-cooled (4°C) 16 well Nucleocuvette Strips (Lonza). Primary human B cells were nucleofected using the EH100 program of Lonza's protocol. 100 μl prewarmed non-supplemented RPMI1640 medium was added to the cells, which were incubated for 15 min at 37°C. The cells were transferred to a single well of a 24-well cluster plate and complete prewarmed cell culture medium containing 20% FCS was added to a final volume of 220 μl to allow cell recovery. The cells were incubated at 37°C, 5% CO₂ for 1 h before they were infected with EBV.

5.4.4 Next generation sequencing and knockout quantification

Sanger sequencing was performed by Eurofins and data obtained in ABI sequencer file format was analyzed using the Synthego ICE analysis tool (<https://ice.synthego.com/#/>). Next generation

sequencing was performed using MiSeq benchtop sequencing system (Illumina). Data were obtained in FASTQ format and analyzed using the Outknocker 2.0 web tool (<http://www.outknocker.org/outknocker2.htm>; **Schmid-Burgk**).

5.5 Protein Biochemistry

5.5.1 Whole cell protein lysate preparation

B cells (2×10^5) were collected, washed with PBS and kept on ice for 30 min followed by freezing at -80°C . Cell pellets were thawed on the day of experiment, mixed with 20 μl of $1 \times$ Cell Lysis Buffer (Cell signaling Technology 9803) freshly supplemented with 1 mM PMSF, incubated on ice for 10 min and sonicated with a Bioruptor Sonicator (on HIGH setting, 4×5 min, on ice). The cellular debris was removed by high speed centrifugation for 20 min at 4°C and the supernatants were transferred to new tubes for their long term storage at -80°C .

5.5.2 Protein concentration measurement

The protein concentration was determined with the Bradford protein assay based on the standard dilutions using bovine serum albumin (BSA) ranging from 0-12 μg in 1 ml of $1 \times$ ready to use Bradford reagent. 4 μl of lysate sample was mixed with Bradford reagent and incubated for 5 min at RT prior to measuring their absorption at 595 nm. The average absorption values were taken for the measured standard dilutions and samples. Protein concentrations of the samples were calculated using the BSA standard curve.

5.5.3 WES platform western blotting

After cell lysis and protein quantification as described above, 0.6 μg of total protein from knock-out and wild-type cells was analyzed by capillary electrophoresis and immunodetection using the WES system (Bio-technie). Briefly, the lysates were analyzed with antibodies directed against ABCG1, HIRA, DAXX and ATRX. The primary antibodies are listed in Table 4.2. Preparation of the antibodies and lysates were performed based on manufacturer's instructions. Protein separation was performed using 66-440 kDa (Protein Simple, SM-W006) separation module with pre-filled plates and capillary cartridges. Immunodetection of the proteins of interest was completed using the anti-rabbit detection module. The Wes instrument was set for 90 min incubation with the primary antibodies. The data analysis and quantification (area under the curve) were performed using Compass for SW software (version 4.0).

5.6 4sU-RNA Seq experiment

5.6.1 Metabolic labeling of newly transcribed RNA with 4sU

Previously published 4sU protocols (Garibaldi et al., 2017; Sun and Chen, 2018) were adjusted to our conditions and used for metabolic labeling of newly transcribed RNAs. 4sU (Sigma Aldrich) was added to the culture medium at a final concentration of 100-200 μM and incubated at 37°C for 1 hour. At the end of labeling, the cells were centrifuged and washed with cold PBS. For RNA extraction, the cell pellet was homogenized in 1 ml of 4°C cold Trizol reagent by vortexing and passing the lysate through a 25G needle 8-10 times. The samples were vigorously vortexed for 15 sec and incubated for 2-3 min at room temperature. The lysate was transferred into a prepared 5PRIME Phase Lock Gel – Heavy and Light (Quantabio) and centrifuged at 12,000 g for 15 min at 4°C to separate RNA, DNA and proteins into different phases. The upper phase containing RNA was carefully transferred to a new sterile RNase-free tube and combined with an equal volume of isopropanol and 0.1 volume of 5 M NaCl. The mixture was incubated for 10 min at RT and precipitated RNA was collected at 12,000 g at 4°C for 10 min. The pellet was washed with 1 ml of 80% of ethanol and spun at 5,000 g for 5 min at 4°C and air-dried for 2-3 min at room temperature. The pelleted RNA was rehydrated in 20-40 μl of RNase-free water.

To biotinylate the newly transcribed and 4sU labeled RNAs, 100 μg of total RNA was incubated with biotin-HPDP (Pierce) at a final concentration of 0,2 mg/ml in biotinylation buffer (final concentration; 10 mM Tris pH 7.4, 1 mM EDTA) while agitating in the dark for at least 2 h. The identical volume of phenol-chloroform-isoamyl alcohol was mixed with the biotinylated RNA sample, which was later purified by using Phase Lock Gel Heavy Tubes. The upper RNA containing phase was precipitated by adding an equal volume of isopropanol and 0.1 vol of 5 M NaCl followed by incubation at room temperature for 10 min. After centrifugation, the pellet was washed with 500 μl of 80% of ethanol and centrifuged (20,000 g, 5 min, 4°C). Biotinylated RNA was resuspended in 100 μl RNase-free water at a final concentration of 1 $\mu\text{g}/\mu\text{l}$.

5.6.2 RNA isolation

4sU-biotinylated RNA was separated from unlabeled RNA using streptavidin beads and magnetic sorting. RNA samples were denatured at 65°C for 10 min followed by rapid cooling on ice for 5 min. RNA was incubated with 200 μl of μMACs Streptavidin Microbeads (Miltenyi) for 15 min at room temperature while agitating. The columns were placed in an OctoMACS Separator magnetic stand and were equilibrated with wash buffer (100 mM Tris-HCl pH 7.4, 10 mM EDTA, 1 M NaCl, 0.1% Tween 20). RNA samples with beads were loaded onto the column to enrich for 4sU-biotinylated RNA molecules. The flow through with mostly unlabeled RNA was reloaded twice onto

the column. The column was washed 2 times with 200 μ l of pre-warmed (55°C) wash buffer. The interactions between 4sU-biotinylated RNA and streptavidin beads were resolved by washing the column with 100 μ l of 100 mM freshly prepared DTT in water. Elution steps were repeated twice with the addition of 100 μ l of 100 mM DTT. Unlabeled and labeled RNA molecules were recovered by ethanol precipitation using 0.1 volume of 3 M NaOAc (pH 5.2) and 3 volumes of cold absolute ethanol. To recover labeled RNAs efficiently, 3 μ l of glycogen (20 mg/ml, Thermo Fisher Scientific) was added prior to precipitation. The samples were incubated overnight at -20°C. Precipitated RNAs were collected by centrifugation at 20,000 g for 20 min at 4°C. The RNA pellet was rehydrated with an appropriate volume of RNase-free water and stored at -80°C. Total RNA concentration and the quality of the samples were determined using an Agilent 2100 Bioanalyzer (Agilent Technologies) prior to generating the libraries for next generation sequencing.

5.6.3 Library preparation and sequencing

Library preparation and sequencing of data were performed at the Heinrich Pette Institute, Hamburg, Germany. After isolation of total RNA its integrity was analyzed with the RNA 6000 Pico Chip on an Agilent 2100 Bioanalyzer (Agilent Technologies). Prior to library generation, RNA was subjected to DNase I digestion (Thermo Fisher Scientific) followed by RNeasy MinElute column clean up (Qiagen). RNA-Seq libraries were generated using the SMART-Seq v4 Ultra Low Input RNA Kit (Clontech Laboratories) according to the manufacturer's recommendations. cDNA final libraries were generated utilizing the Nextera XT DNA Library Preparation Kit (Illumina). Concentrations of the final libraries were measured with a Qubit 2.0 Fluorometer (Thermo Fisher Scientific) and fragment lengths distribution was analyzed with the DNA High Sensitivity Chip on an Agilent 2100 Bioanalyzer (Agilent Technologies). All samples were normalized to 2 nM and pooled to become equimolar. The library pool was sequenced on the NextSeq500 (Illumina) with 2x150 bp (paired end), with 15.7 to 18.6 mio reads per sample.

5.7 Bioinformatic analysis

5.7.1 Quality control and data normalization

The quality control and data normalization of 4sU-RNA Seq experiment were performed with the help of Alexander Buschle. The FastQ-sequences were analyzed with MultiQC (v1.7) (Ewels et al., 2016) for quality issues and trimmed with Trimmomatic (0.39) (Bolger et al., 2014) for leading and trailing bases with a quality threshold of 20 each. The reads were mapped to the Human Genome 19 with Hisat2 (2.1.0) (Kim et al., 2015) and file format conversion and sorting was done with Samtools (1.10) (Li et al., 2009). Since the targeted exon 2 of CD46 comprises 189 nucleotides, other exons with

the same number of nucleotides were identified for comparison. The data from the genes comprising exons of 189 nts were extracted with Samtools' view command, indexed with Samtools' index, and the coverage for each base was calculated with Samtools' depth -a -r. Both normalization and visualization were done in R (R Core Team, 2018). For normalization the samples were downsampled to the total number of mapped reads. The mean was applied to three independent replicates for visualization.

5.7.2 Gene set enrichment analysis (GSEA)

Gene ontology (GO) and gene set enrichment analysis (GSEA) were done using Webgestalt (<http://www.webgestalt.org/>). The differentially regulated list of genes can be found in Table 6.1.

5.7.3 Accession number and Data availability

RNA-seq NGS files are deposited on ArrayExpress (Kolesnikov et al., 2015) using the web-based submission tool Annotare 2.0 (<https://www.ebi.ac.uk/fg/annotare/login/>). The data files of interest can be downloaded via <https://www.ebi.ac.uk/arrayexpress/> using the following accession numbers: RNA-seq: <https://www.ebi.ac.uk/arrayexpress/experiments/E-MTAB-9531>

5.8 Statistical Analysis

All statistical analyses were performed using the Prism software v7.0 (GraphPad Software, San Diego, CA). Prior to the analysis, graph kurtosis was analyzed to ensure normal or non-normal distribution of the data. Based on the distribution analysis; the Wilcoxon signed-rank test was used for comparisons between samples. Data are reported as mean and SEM.

Chapter 6

Appendix

TABLE 6.1: **Differential gene expression (DGE) analysis comparing the transcriptomes of CD46-Cas9 and WT B cell samples.** 182 genes were identified to be differentially expressed ($\text{padj} < 0.05$) based on the count number of reads mapped to each transcript represented in this table.

Gene	padj	Gene	padj
H3F3B	0.0495853586509852	IFIT5	0.0205249820474698
EXOC6B	0.0495722573540268	ZFYVE9	0.0205249820474698
FAM26F	0.0494844708609299	CKS2	0.0199227331765973
POLE3	0.0493864271426857	DDB2	0.0197229079052022
ANKRD36BP2	0.0483248951400163	C1QBP	0.0197147028626663
FAM100B	0.0483248951400163	NACA	0.019300044395372
MRPS22	0.0481390340172488	GAPDH	0.0191457748670181
CACNA1A	0.0480332231648256	MT2A	0.018960957500115
GPS2	0.0480332231648256	RPS20	0.018960957500115
SLC25A5	0.0480332231648256	LRRC32	0.0187982660002832
SLC7A5P2	0.0480332231648256	TNRC6C	0.0186290558583279
TCL1A	0.0480332231648256	HIST1H2BI	0.018470751571979
TPM4	0.0480332231648256	RPL22	0.0180803761047385
CDKN2B	0.047842682071218	TMOD2	0.0176438826104996
FBXL20	0.047842682071218	HIST1H4C	0.0169800531944221
MARCKSL1	0.0462407346491044	FAM18B2	0.014424040526018
PGAM1	0.046185347179266	BCL11A	0.0137600910666385
MYD88	0.0453305392198682	HIST1H3H	0.0130640459490103

Continued on next page

Table 6.1 – continued from previous page

Gene	padj	Gene	padj
RAPGEF5	0.0453305392198682	CCL3	0.0126913996635382
SEMA4A	0.0453305392198682	CYP1B1	0.0126913996635382
BIRC5	0.0434579232466015	IRF8	0.0126913996635382
LMO2	0.0429064262148305	IRS2	0.0126913996635382
NLRP4	0.0429064262148305	RPL35	0.0126913996635382
RBM7	0.0429064262148305	TBCC	0.0126913996635382
KIF2C	0.0416305651785589	CCPG1	0.0124899488026773
SYTL1	0.041078218420487	CFL1	0.0124899488026773
RANBP1	0.0410228312489385	ELL3	0.0124703472322331
GOLGA8A	0.0392704675208476	HIST2H2AC	0.0124703472322331
NCF4	0.0392704675208476	HIST1H2BD	0.0124454815594565
RPL39	0.0392704675208476	RPL19	0.0113408091931427
NAB2	0.0386714438695081	UQCR10	0.0113408091931427
HIST1H2AM	0.0381753838397577	HIST1H2BJ	0.0111908502217577
HIST1H4B	0.0381753838397577	LY6E	0.0101240989421758
SNRPF	0.0381753838397577	SMN1	0.0101240989421758
ANTXR2	0.0378382503423391	HIST1H1E	0.0100107296285801
ATPIF1	0.0377662812363794	HIST1H2AL	0.0100107296285801
COX17	0.0374978448337278	RAC2	0.00985646928899781
LOC285758	0.0369456690557389	FLJ43663	0.00974323936413508
EID1	0.0367800094849309	BCL2A1	0.00937831974247774
INADL	0.0367800094849309	LSM6	0.00937831974247774
LCP1	0.0367800094849309	CD74	0.00590983018253672
SNX29	0.0356407389380155	PVT1	0.00590983018253672
CD72	0.0352698806508784	HIST1H2AJ	0.00567283270398546
N4BP2	0.0352698806508784	HIST1H2BF	0.00567283270398546
NUSAP1	0.0352698806508784	MRPS18B	0.00567283270398546
FBXO5	0.0352233609586013	VAV3	0.00562233294490733
TUBA1B	0.0352233609586013	PFN1	0.00539459191246031
IFITM2	0.0350946157929767	RPL23A	0.00511094895956291
MIF	0.0344988064043864	RASSF6	0.00500080480548445
TMCO7	0.0340602417566875	NFKBIE	0.00350045257636285

Continued on next page

Table 6.1 – continued from previous page

Gene	padj	Gene	padj
RPL14	0.0332747413675659	TREX1	0.00350045257636285
AAK1	0.0329404123308122	PDE4B	0.00343579054199575
HIST1H2BH	0.0328162212868041	PRDM8	0.00335984834029918
ING3	0.0320175269138185	CCNB1	0.00334160950091299
LOC100505812	0.0319385371903286	BACH2	0.00315723082229448
CBR1	0.0316305645183963	IFIT3	0.00284106233353294
CHI3L2	0.0295101636278342	COX6C	0.00282678622347304
LOC646329	0.0295101636278342	HIST1H2AE	0.00280890906530428
RPL8	0.0292436989028342	HIST1H2BK	0.00280890906530428
DCK	0.0291961519789457	TMSB4X	0.00280890906530428
MAD2L1	0.0291101012463462	CKAP2L	0.0025586265986473
HMGB2	0.0280460594795761	ASTN2	0.00195020467131566
SUMO3	0.0274356798140161	DUSP2	0.00195020467131566
C4orf46	0.0270576567173824	EGR3	0.00195020467131566
LYSMD2	0.0270576567173824	PNPLA7	0.00195020467131566
PSMA4	0.0270576567173824	SAT1	0.00195020467131566
SMS	0.0270576567173824	EID3	0.00188555341578105
SULF2	0.0270576567173824	PSME1	0.00188555341578105
TPI1	0.0270576567173824	ACTB	0.00139109987757177
HIST1H2BN	0.0256002811571811	IGLL5	0.00127388444193456
KIAA0040	0.0256002811571811	HIST1H2BB	0.00107127022610895
CAP1	0.024298401624602	PTMA	0.00107127022610895
MAP2K6	0.024298401624602	SSTR2	0.00107127022610895
HDAC5	0.0242919975648105	STARD9	0.00107127022610895
HIST1H2BL	0.0242919975648105	ZDHHC14	0.00104031773750262
HIST1H4D	0.0237866514479686	SBF2	0.000952973362878684
CCNB2	0.0228375384436799	TMEM163	0.000952973362878684
HIST2H3D	0.0223153810170486	COX7C	0.000945086067370795
ARPC5	0.0210455459049929	HIST1H4F	0.000945086067370795
C14orf2	0.0210455459049929	CCDC88B	0.000616176839499103
IDH3A	0.0210455459049929	IFI30	0.000616176839499103
HIST1H3G	0.0210362715710858	RPL36AL	0.000575857264211619

Continued on next page

Table 6.1 – continued from previous page

Gene	padj	Gene	padj
LSM5	0.0210362715710858	SERPINA9	0.000551511264784517
PSME2	0.0210362715710858	HIST2H2AB	0.000389510668245257
TCEAL8	0.0210362715710858	HIST1H2AG	4,44E+09
CD79A	0.0209769657049205	HIST1H2BC	4,27E+09
CCL4	0.02090268482058	MYL12A	6,07E+07
COX6A1	0.0205500444710553	LTA	5,64E+07
SNRPD1	0.0205500444710553	HIST2H2BF	3,37E+08
ACTG1	0.0205249820474698	DNAH7	2,63E+08
IFIT5	0.0205249820474698	LINC00152	3,86E+07
ZFYVE9	0.0205249820474698	PTPN6	3,62E+06

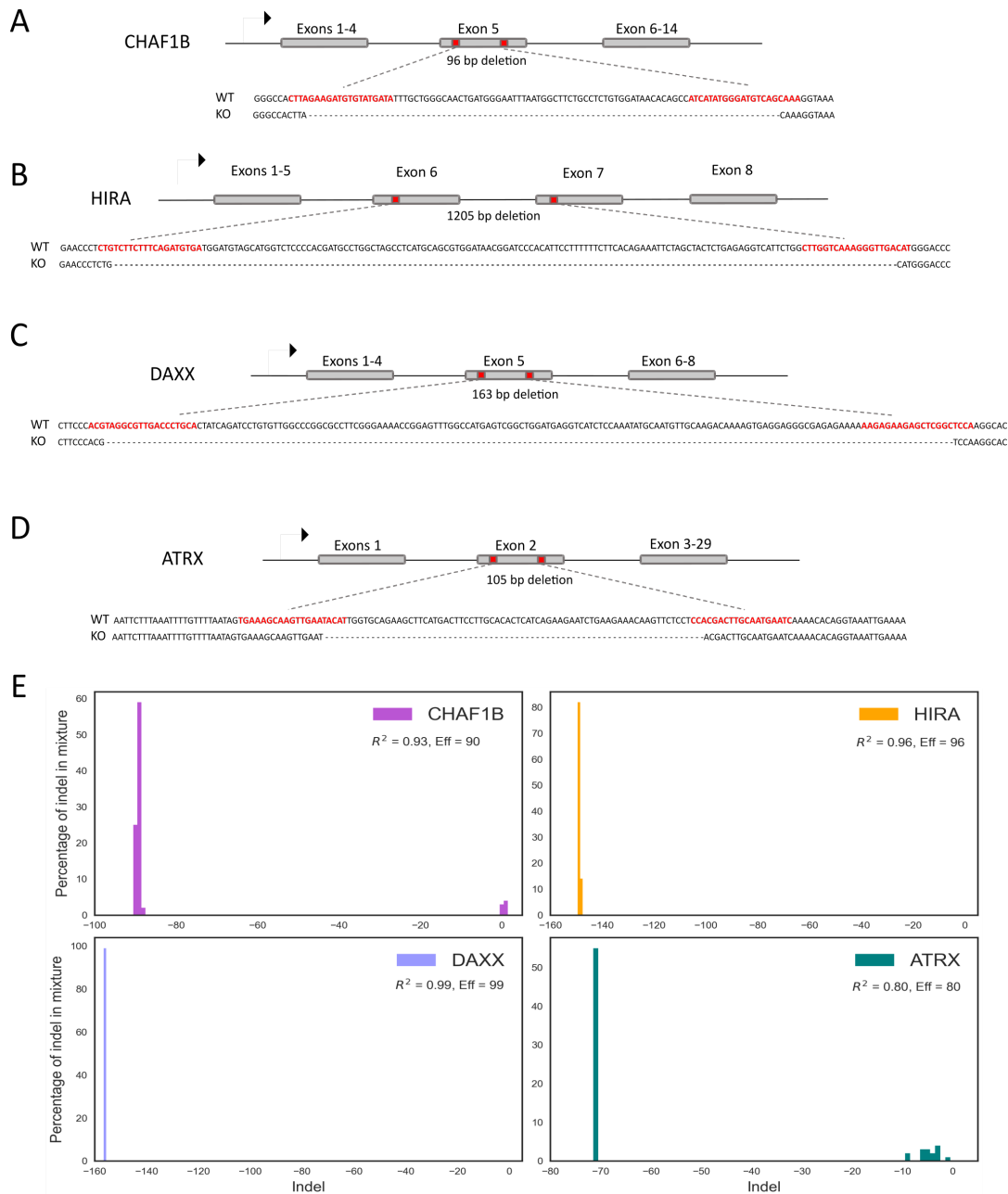


FIGURE 6.1: Target sites of gRNAs for four different cellular targets (*CHAF1B*, *HIRA*, *DAXX* and *ATRX*) with their corresponding knockout efficiencies. Blueprint of the cellular genes with the target sites of the RNP complexes and sequence alignment after CRISPR-Cas9 mediated deletion versus wildtype sequence including gRNA sequence information (red). **(A)** Blueprint of the *CHAF1B* gene with 14 exons and the target sites of the two RNP complexes within the 5th exon (chr21: 14,409-14,428; chr21:14,485-14,504) generating a 96 bp deletion between the target sites. **(B)** Blueprint of the *HIRA* gene with 8 exons and the target sites of the two RNP complexes within the 6th (chr22:33,633-33,652) and the 7th exons (chr22:34,818-34,837) generating a 1205 bp deletion between the target sites. **(C)** Blueprint of the *DAXX* gene with 8 exons and the two target sites of the two RNP complexes within the 5th exon (chr6:2,420-2,439; chr6:2,563-2,582) generating a 163 bp deletion between the target sites. **(D)** Blueprint of the *ATRX* gene with 29 exons and the two target site of the RNP complexes within the 2nd exon (chrX:68,993-69,012; chrX:69,078-69,097) generating a 105 bp deletion between the target sites. **(E)** B cells were treated with RNP complexes and infected with EBV to induce their activation and their proliferation. DNA samples were collected on the third day after nucleofection and next generation sequencing of samples via Sanger sequencing provided the analysis of the percentage of indels (%) with their corresponding indel length (bp) via Synthego webtool (<https://ice.synthego.com/#/>) as shown for each target.

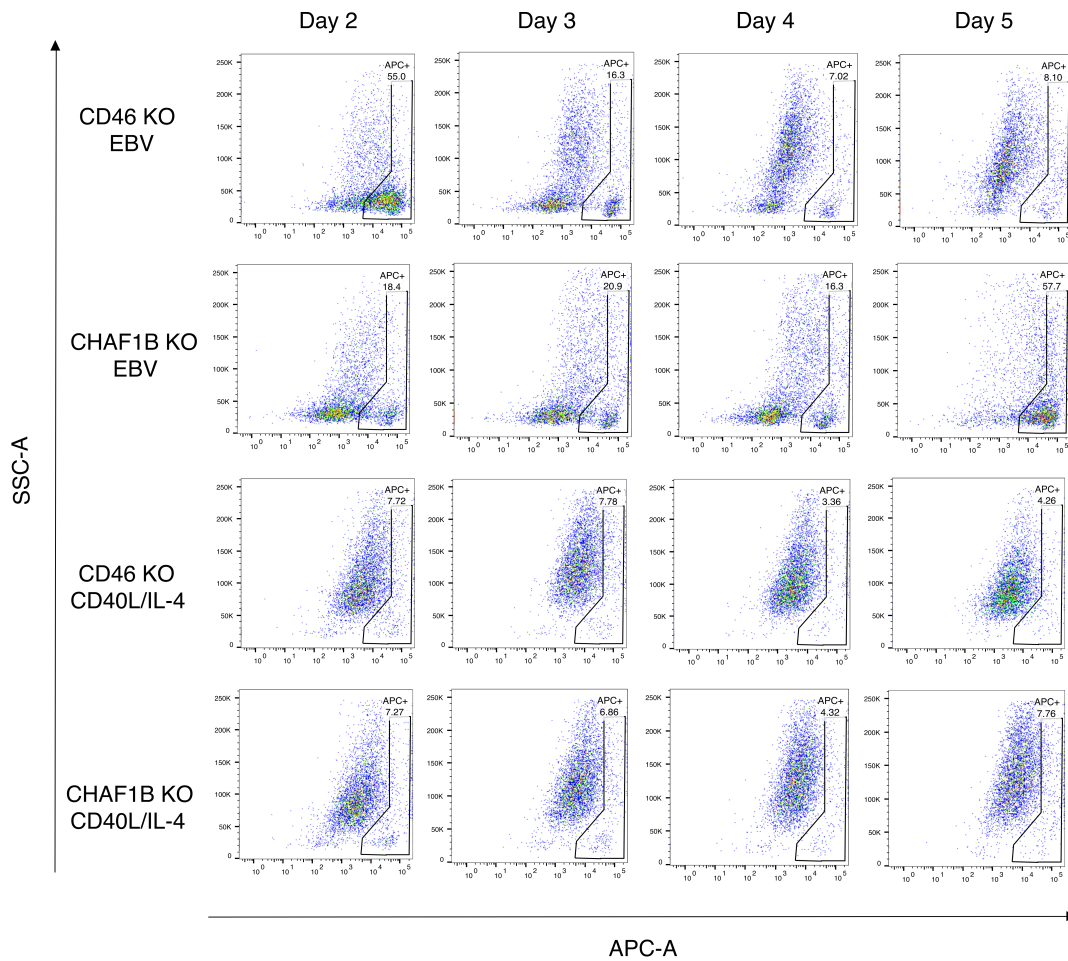


FIGURE 6.2: Tracking of apoptosis during the first days after CD46- and CHAF1B-RNP complexes nucleofection. The FACS plots show the apoptosis rate (Annexin V staining) of the CD46- and CHAF1B-RNP complexes nucleofected B cells at early time points following their infection with EBV or activation by CD40L/IL-4 stimulation. 2×10^5 cells were collected from each condition at different time points and incubated with APC-coupled Annexin V for 10 min prior to analysis by flow cytometry. The percentages of Annexin V positive cells are shown.

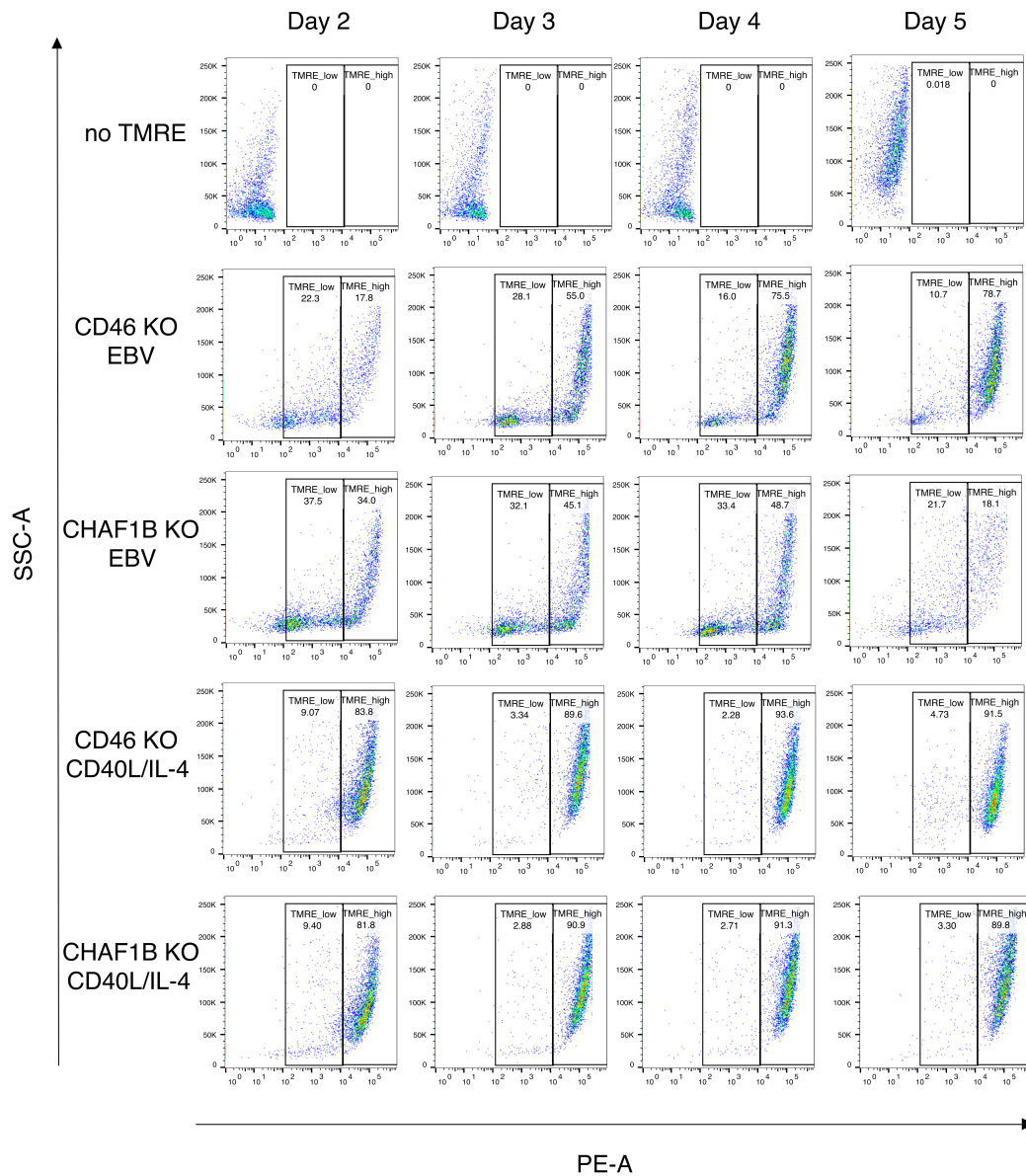


FIGURE 6.3: Tracking of mitochondrial activity in B cells nucleofected with CD46- and CHAF1B-RNP complexes and activated by CD40L/IL-4 or EBV during the first days. The FACS plots show the mitochondrial uptake of TMRE (coupled with PE-A) of the CD46- and CHAF1B-RNP complexes nucleofected B cells at early time points after their activation via EBV infection or CD40L/IL-4. 2×10^5 cells were incubated with 100 nM TMRE for 30 min prior to their collection. The percentages of positive cells as measured by flow cytometry are shown.

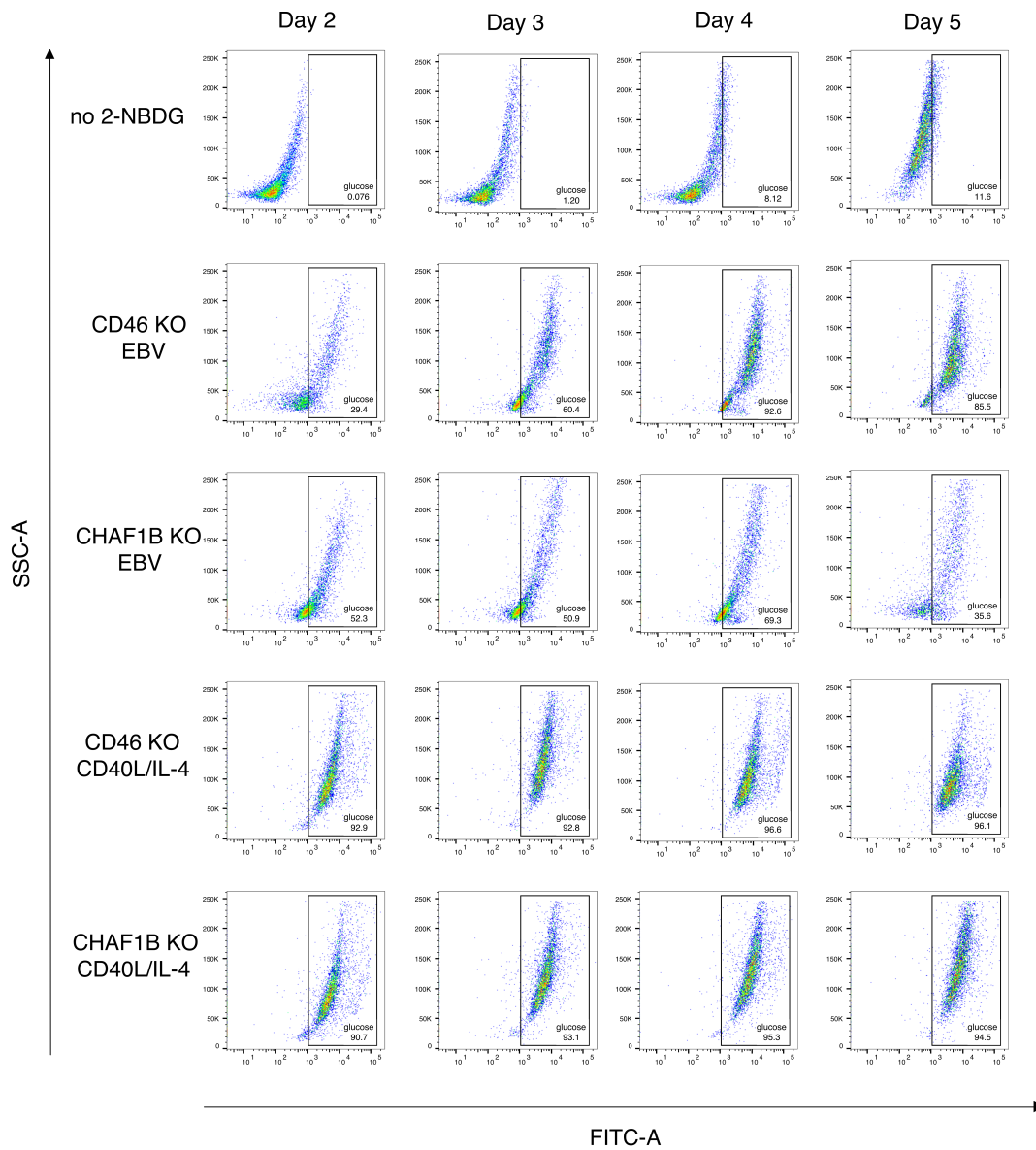


FIGURE 6.4: Uptake of the glucose analogue 2-NBDG (coupled with FITC-A) during the first days after CD46- and CHAF1B-RNP complexes nucleofection and activation by CD40L/IL-4 or EBV. The FACS plots show the glucose uptake of B cells nucleofected with CD46- or CHAF1B-RNP complexes at early time points following their culturing via EBV infection or CD40L/IL-4 activation. 2×10^5 cells were incubated with $100 \mu\text{M}$ 2-NBDG for an hour at 37°C prior to their analysis by flow cytometry. The percentages of positive cells measured are shown.

Bibliography

- Adam, Salomé, Sophie E. Polo, and Geneviève Almouzni (2013). “Transcription recovery after DNA damage requires chromatin priming by the H3.3 histone chaperone HIRA”. In: *Cell* 155.1, p. 94. ISSN: 10974172. DOI: 10.1016/j.cell.2013.08.029.
- Ahmad, Kami and Steven Henikoff (2002). “The histone variant H3.3 marks active chromatin by replication-independent nucleosome assembly”. In: *Molecular Cell* 9.6, pp. 1191–1200. ISSN: 10972765. DOI: 10.1016/S1097-2765(02)00542-7.
- Ahmad, Kami and Steven Henikoff (2021). “The H3.3K27M oncohistone antagonizes reprogramming in *Drosophila*”. In: *PLoS Genetics*. DOI: 10.1371/journal.pgen.1009225.
- Akidil, Ezgi et al. (2021). “Highly efficient CRISPR-Cas9-mediated gene knockout in primary human B cells for functional genetic studies of Epstein-Barr virus infection”. In: *PLoS Pathogens* 17.4. ISSN: 15537374. DOI: 10.1371/journal.ppat.1009117.
- Albanese, Manuel et al. (2022). “Rapid, efficient and activation-neutral gene editing of polyclonal primary human resting CD4+ T cells allows complex functional analyses”. In: *Nature Methods* 19.1, pp. 81–89. ISSN: 15487105. DOI: 10.1038/s41592-021-01328-8.
- Albright, Emily R. and Robert F. Kalejta (2016). “Canonical and variant forms of histone H3 are deposited onto the human cytomegalovirus genome during lytic and latent infections”. In: *Journal of Virology* 90.22, pp. 10309–10320. ISSN: 0022-538X. DOI: 10.1128/jvi.01220-16.
- Allday, Martin J. (2013). “EBV finds a polycomb-mediated, epigenetic solution to the problem of oncogenic stress responses triggered by infection”. In: *Frontiers in Genetics* 4.October, pp. 1–10. ISSN: 1664-8021. DOI: 10.3389/fgene.2013.00212.
- Allday, Martin J., Quentin Bazot, and Robert E. White (2015). “The EBNA3 family: Two oncoproteins and a tumour suppressor that are central to the biology of EBV in B cells”. In: *Springer* 391, pp. 61–117. ISSN: 21969965. DOI: 10.1007/978-3-319-22834-1_3.
- Allis, C. David and Thomas Jenuwein (2016). “The molecular hallmarks of epigenetic control”. In: *Nature Reviews Genetics* 17.8, pp. 487–500. ISSN: 14710064. DOI: 10.1038/nrg.2016.59. URL: <http://www.nature.com/doifinder/10.1038/nrg.2016.59>.
- Allshire, Robin C. and Gary H. Karpen (2008). “Epigenetic regulation of centromeric chromatin: old dogs, new tricks?” In: *Nature Reviews Genetics* 9.12, pp. 923–37. DOI: doi:10.1038/nrg2466.

- Altmann, Markus and Wolfgang Hammerschmidt (2005). "Epstein-Barr virus provides a new paradigm: A requirement for the immediate inhibition of apoptosis". In: *PLoS Biology* 3.12, pp. 1–10. ISSN: 15457885. DOI: 10.1371/journal.pbio.0030404.
- Argentaro, Anthony et al. (2007). "Structural consequences of disease-causing mutations in the ATRX-DNMT3-DNMT3L (ADD) domain of the chromatin-associated protein ATRX". In: *Proceedings of the National Academy of Sciences of the United States of America* 104.29, pp. 11939–11944. ISSN: 00278424. DOI: 10.1073/pnas.0704057104.
- Balakrishnan, Lata and Barry Milavetz (2017). *Epigenetic regulation of viral biological processes*. DOI: 10.3390/v9110346.
- Barrangou, Rodolphe et al. (2007). "CRISPR provides acquired resistance against viruses in prokaryotes". In: *Science* 315.5819, pp. 1709–1712. ISSN: 00368075. DOI: 10.1126/science.1138140.
- Baylin, Stephen B. and Peter A. Jones (2016). "Epigenetic determinants of cancer". In: *Cold Spring Harbor Laboratory Press*. DOI: 10.1101/cshperspect.a019505.
- Bi, Yanwei et al. (2014). "High-efficiency targeted editing of large viral genomes by RNA-guided nucleases". In: *PLoS Pathogens* 10.5. ISSN: 15537374. DOI: 10.1371/journal.ppat.1004090.
- Bjursell, Mikael et al. (2018). "Therapeutic genome editing with CRISPR/Cas9 in a humanized mouse model ameliorates α 1-antitrypsin deficiency phenotype". In: *EBioMedicine* 29, pp. 104–111. ISSN: 23523964. DOI: 10.1016/j.ebiom.2018.02.015.
- Blouin, Jean Louis et al. (1996). "Mapping of the gene for the p60 subunit of the human chromatin assembly factor (CAF1a) to the down syndrome region of chromosome 21". In: *Genomics* 33.2, pp. 309–312. ISSN: 08887543. DOI: 10.1006/geno.1996.0199.
- Bolger, Anthony M., Marc Lohse, and Bjoern Usadel (2014). "Trimmomatic: A flexible trimmer for Illumina sequence data". In: *Bioinformatics* 30.15, pp. 2114–2120. ISSN: 14602059. DOI: 10.1093/bioinformatics/btu170.
- Bolotin, Alexander et al. (2005). "Clustered regularly interspaced short palindrome repeats (CRISPRs) have spacers of extrachromosomal origin". In: *Microbiology* 151.8, pp. 2551–2561. ISSN: 13500872. DOI: 10.1099/mic.0.28048-0.
- Brinkman, Eva K. et al. (2018). "Kinetics and fidelity of the repair of Cas9-induced double-strand DNA breaks". In: *Molecular Cell* 70.5, 801–813.e6. ISSN: 10974164. DOI: 10.1016/j.molcel.2018.04.016.
- Brouns, Stan J.J. et al. (2008). "Small CRISPR RNAs guide antiviral defense in prokaryotes". In: *Science* 321.5891, pp. 960–964. ISSN: 00368075. DOI: 10.1126/science.1159689.
- Burgess, Rebecca J. and Zhiguo Zhang (2013). "Histone chaperones in nucleosome assembly and human disease". In: *Nature Structural and Molecular Biology* 20.1, pp. 14–22. ISSN: 15459993. DOI: 10.1038/nsmb.2461.

- Cabral, Joseph M., Hyung Suk Oh, and David M. Knipe (2018). "ATRX promotes maintenance of herpes simplex virus heterochromatin during chromatin stress". In: *eLife* 7, pp. 1–32. ISSN: 2050084X. DOI: 10.7554/eLife.40228.
- Caeser, Rebecca et al. (2019). "Genetic modification of primary human B cells to model high-grade lymphoma". In: *Nature Communications* 10.1, pp. 1–16. ISSN: 20411723. DOI: 10.1038/s41467-019-12494-x.
- Carl Costanzi & John R. Pehrson (1998). "Histone macroH2A1 is concentrated in the inactive X chromosome of female mammals". In: *Nature* 393.1997, pp. 1997–1999. DOI: 10.1038/31275.
- Carthew, Richard W. and Erik J. Sontheimer (2009). "Origins and mechanisms of miRNAs and siRNAs". In: *Cell* 136.4, pp. 642–655. DOI: 10.1016/j.cell.2009.01.035..
- Cattaneo, Roberto (2004). "Four viruses, two bacteria, and one receptor: membrane cofactor protein (CD46) as pathogens' magnet". In: *Journal of Virology* 78.9, pp. 4385–4388. ISSN: 0022-538X. DOI: 10.1128/jvi.78.9.4385-4388.2004.
- Chadwick, B P and H F Willard (2001). "Histone H2A variants and the inactive X chromosome: identification of a second macroH2A variant". In: *Human Molecular Genetics* 10.10, pp. 1101–1113.
- Chang, Howard Y. et al. (1998). "Activation of apoptosis signal-regulating kinase 1 (ASK1) by the adapter protein Daxx". In: *Science* 281.5384, pp. 1860–1863. ISSN: 00368075. DOI: 10.1126/science.281.5384.1860.
- Cheloufi, Sihem. et al. (2016). "The histone chaperone CAF-1 safeguards somatic cell identity". In: *Nature* 528.7581, pp. 218–224. DOI: 10.1038/nature15749.The.
- Cheong, Taek Chin, Mara Compagno, and Roberto Chiarle (2016). "Editing of mouse and human immunoglobulin genes by CRISPR-Cas9 system". In: *Nature Communications* 7, pp. 1–10. ISSN: 20411723. DOI: 10.1038/ncomms10934.
- Cheung, Ngai and Chi Wai Eric So (2011). "Transcriptional and epigenetic networks in haematological malignancy". In: *FEBS Letters* 585, pp. 2100–11. DOI: 10.1016/j.febslet.2011.03.068.
- Chicaybam, Leonardo et al. (2017). "An efficient electroporation protocol for the genetic modification of mammalian cells". In: *Frontiers in Bioengineering and Biotechnology* 4.January, pp. 1–13. ISSN: 22964185. DOI: 10.3389/fbioe.2016.00099.
- Chiu, Ya-Fang and Bill Sugden (2018). "Plasmid partitioning by human tumor viruses". In: *Journal of Virology* 92.9. DOI: 10.1128/JVI.02170-17.
- Cimprich, Karlene A. and David Cortez (2008). "ATR: an essential regulator of genome integrity". In: *Nature Reviews Molecular Cell Biology* 9. DOI: 10.1038/nrm2450.

- Clarke, Ryan et al. (2018). "Enhanced bacterial immunity and mammalian genome editing via RNA-polymerase-mediated dislodging of Cas9 from double-strand DNA breaks". In: *Molecular Cell* 71.1, 42–55.e8. ISSN: 10974164. DOI: 10.1016/j.molcel.2018.06.005.
- Cong, Le et al. (2013). "Multiplex genome engineering using CRISPR/Cas systems". In: *Science (New York, N.Y.)* 339.6121, pp. 819–823. ISSN: 15378276. DOI: 10.1126/science.1231143.Multiplex.
- Corpet, Armelle et al. (2014). "Dynamics of histone H3.3 deposition in proliferating and senescent cells reveals a DAXX-dependent targeting to PML-NBs important for pericentromeric heterochromatin organization". In: *Cell Cycle* 13, pp. 249–267. DOI: 10.4161/cc.26988.
- Crawford, Dorothy H. (2001). "Biology and disease associations of Epstein-Barr virus". In: *Philosophical Transactions of the Royal Society B: Biological Sciences* 356.1408, pp. 461–473. ISSN: 09628436. DOI: 10.1098/rstb.2000.0783.
- Crowley, Lisa C., Melinda E. Christensen, and Nigel J. Waterhouse (2016). "Measuring mitochondrial transmembrane potential by TMRE staining". In: *Cold Spring Harbor Protocols* 2016.12, pp. 1092–1096. ISSN: 15596095. DOI: 10.1101/pdb.prot087361.
- De Koning, Leanne et al. (2007). "Histone chaperones: An escort network regulating histone traffic". In: *Nature Structural and Molecular Biology* 14.11, pp. 997–1007. ISSN: 15459993. DOI: 10.1038/nsmb1318.
- Delbarre, Erwan. et al. (2013). "DAXX-dependent supply of soluble (H3.3-H4) dimers to PML bodies pending deposition into chromatin". In: *Genome Research* 23.3, pp. 440–451. ISSN: 10889051. DOI: 10.1101/gr.142703.112.
- Delecluse, Henri-Jacques et al. (1998). "Propagation and recovery of intact, infectious Epstein-Barr virus from prokaryotic to human cells." In: *Proceedings of the National Academy of Sciences of the United States of America* 95.14, pp. 8245–8250. ISSN: 0027-8424. DOI: 10.1073/pnas.95.14.8245.
- Deltcheva, Elitza et al. (2011). "CRISPR RNA maturation by trans-encoded small RNA and host factor RNase III". In: *Nature* 471, pp. 602–607. DOI: 10.1038/nature09886.
- Dent, Alexander L. et al. (1997). "Control of inflammation, cytokine expression, and germinal center formation by BCL-6". In: *Science* 276.5312, pp. 589–592. ISSN: 00368075. DOI: 10.1126/science.276.5312.589.
- Diemen, Ferdy R. van et al. (2015). "CRISPR/Cas9-mediated genome editing of herpesviruses limits productive and latent infections". In: *PLoS Pathogens* 12. DOI: 10.1371/journal.ppat.1005701.
- Drané, Pascal et al. (2010). "The death-associated protein DAXX is a novel histone chaperone involved in the replication-independent deposition of H3.3". In: *Genes and Development* 24.12, pp. 1253–1265. ISSN: 08909369. DOI: 10.1101/gad.566910.

- Duan, Yan et al. (2019). "CHAF1B promotes proliferation and reduces apoptosis in 95-D lung cancer cells and predicts a poor prognosis in non-small cell lung cancer". In: *Oncology Reports* 41.4, pp. 2518–2528. ISSN: 17912431. DOI: 10.3892/or.2019.6994.
- Ducker, Gregory S. and Joshua D. Rabinowitz (2017). "One-Carbon Metabolism in Health and Disease". In: *Cell Metabolism* 25.1, pp. 27–42. ISSN: 19327420. DOI: 10.1016/j.cmet.2016.08.009. URL: <http://dx.doi.org/10.1016/j.cmet.2016.08.009>.
- Dufort, Fay J. et al. (2007). "Cutting edge: IL-4-mediated protection of primary B lymphocytes from apoptosis via Stat6-dependent regulation of glycolytic metabolism". In: *The Journal of Immunology* 179.8, pp. 4953–4957. ISSN: 0022-1767. DOI: 10.4049/jimmunol.179.8.4953.
- Duncan J. Smith. and Iestyn Whitehouse. (2012). "Intrinsic coupling of lagging-strand synthesis to chromatin assembly". In: *Nature* 483, pp. 434–438. ISSN: 15378276. DOI: 10.1038/nature10895. Intrinsic.
- Dyson, P. J. and P. J. Farrell (1985). "Chromatin structure of Epstein-Barr virus". In: *Journal of General Virology* 66.9, pp. 1931–1940. ISSN: 00221317. DOI: 10.1099/0022-1317-66-9-1931.
- Elsässer, Simon J. et al. (2012). "DAXX envelops a histone H3.3–H4 dimer for H3.3-specific recognition". In: *Nature* 491, pp. 560–565. DOI: 10.1038/nature11608.
- Epstein, M.A., B.G. Achong, and Y.M. Barr (1964). "Virus particles in cultured lymphoblasts from Burkitt's lymphoma". In: *Preliminary Communications* 1, pp. 702–703. DOI: 10.1016/s0140-6736(64)91524-7.
- Escobar-Cabrera, Eric et al. (2010). "Structural characterization of the DAXX N-terminal helical bundle domain and its complex with Rassf1C". In: *Structure* 18.12, pp. 1642–1653. ISSN: 09692126. DOI: 10.1016/j.str.2010.09.016.
- Ewels, Philip et al. (2016). "MultiQC: Summarize analysis results for multiple tools and samples in a single report". In: *Bioinformatics* 32.19, pp. 3047–3048. ISSN: 14602059. DOI: 10.1093/bioinformatics/btw354.
- Eyquem, Justin et al. (2017). "Targeting a CAR to the TRAC locus with CRISPR/Cas9 enhances tumour rejection". In: *Nature* 543.7643, pp. 113–117. ISSN: 14764687. DOI: 10.1038/nature21405. URL: <http://dx.doi.org/10.1038/nature21405>.
- Feederle, Regina et al. (2004). "Efficient somatic gene targeting in the lymphoid human cell line DG75". In: *Gene* 343.1, pp. 91–97. ISSN: 03781119. DOI: 10.1016/j.gene.2004.08.005.
- Foltz, Daniel R et al. (2009). "Centromere-specific assembly of CENP-A nucleosomes is mediated by HJURP". In: *Cell* 137.3, pp. 472–84. DOI: 10.1016/j.cell.2009.02.039.
- Frappier, Lori (2015). "EBNA1". In: *Current Topics in Microbiology and Immunology* 391, pp. 3–34. ISSN: 21969965. DOI: 10.1007/978-3-319-22834-1_1.

- Friedel, Caroline C. et al. (2009). "Conserved principles of mammalian transcriptional regulation revealed by RNA half-life". In: *Nucleic Acids Research* 37. DOI: 10.1093/nar/gkp542.
- Fuchs, Anja et al. (2009). "CD46-induced human Treg enhance B-cell responses". In: *European Journal of Immunology* 39.11, pp. 3097–3109. ISSN: 00142980. DOI: 10.1002/eji.200939392.
- Funke, S et al. (2009). "Pseudotyping lentiviral vectors with the wild-type measles virus glycoproteins improves titer and selectivity". In: *Gene Therapy* 16, pp. 700–705. DOI: 10.1038/gt.2009.11.
- Funke, Sabrina et al. (2008). "Targeted cell entry of lentiviral vectors". In: *Mol Therapy* 16.8, pp. 1427–36. DOI: 10.1038/mt.2008.128.
- Gahn, Toni A. and Carl L. Schildkraut (1989). "The Epstein-Barr virus origin of plasmid replication, oriP, contains both the initiation and termination sites of DNA replication". In: *Cell* 58.3, pp. 527–535. ISSN: 00928674. DOI: 10.1016/0092-8674(89)90433-9.
- Gallastegui, Edurne et al. (2011). "Chromatin reassembly factors are involved in transcriptional interference promoting HIV latency". In: *Journal of Virology* 85.7, pp. 3187–3202. ISSN: 0022-538X. DOI: 10.1128/jvi.01920-10.
- Galvis, Alvaro E., Hugh Fisher, and David Camerini (2017). "NP-40 fractionation and nucleic acid extraction in mammalian cells". In: *Bio-Protocol* 7.20, pp. 1–8. ISSN: 2331-8325. DOI: 10.21769/bioprotoc.2584.
- Garibaldi, Angela, Francisco Carranza, and Klemens J. Hertel (2017). "Isolation of newly transcribed rna using the metabolic label 4-thiouridine". In: *Methods in Molecular Biology*. Vol. 1648, pp. 169–176. DOI: 10.1007/978-1-4939-7204-3_13.
- Geis, Franziska K. et al. (2022). "CHAF1A/B mediate silencing of unintegrated HIV-1 DNAs early in infection". In: *PNAS* 119.4. DOI: 10.1073/pnas.2116735119.
- Gibbons, R J. et al. (1995). "Mutations in a putative global transcriptional regulator cause X-linked mental retardation with alpha-thalassemia (ATR-X syndrome)". In: *Comparative Study* 80, pp. 837–45. DOI: 10.1016/0092-8674(95)90287-2.
- Gibbons, R J et al. (2000). "Mutations in ATRX, encoding a SWI/SNF-like protein, cause diverse changes in the pattern of DNA methylation". In: *Nature Genetics* 24, pp. 368–71. DOI: 10.1038/74191.
- Gil, Esús and Gordon Peters (2006). "Regulation of the INK4b-ARF-INK4a tumour suppressor locus: all for one or one for all". In: *Nature Reviews Molecular Cell Biology* 7. DOI: 10.1038/nrm1987.
- Gires, Olivier et al. (1997). "Latent membrane protein 1 of Epstein-Barr virus mimics a constitutively active receptor molecule". In: *EMBO Journal* 16.20, pp. 6131–6140. ISSN: 02614189. DOI: 10.1093/emboj/16.20.6131.
- Goldberg, Aaron D. et al. (2010). "Distinct Factors Control Histone Variant H3.3 Localization at Specific Genomic Regions". In: *Cell* 140.5, pp. 678–691. ISSN: 00928674. DOI: 10.1016/j.cell.2010.01.003.

- Goldman, Michael A. et al. (1984). "Replication timing of genes and middle repetitive sequences". In: *Science* 224.4650, pp. 686–692. ISSN: 00368075. DOI: 10.1126/science.6719109.
- Görisch, Sabine M. et al. (2005). "Histone acetylation increases chromatin accessibility". In: *Journal of Cell Science* 118.24, pp. 5825–5834. ISSN: 00219533. DOI: 10.1242/jcs.02689.
- Gottschalk, Stephen, Cliona M. Rooney, and Helen E. Heslop (2005). "Post-transplant lymphoproliferative disorders". In: *Annual Review of Medicine* 56, pp. 29–44. ISSN: 00664219. DOI: 10.1146/annurev.med.56.082103.104727.
- Graham, F. L. et al. (1977). "Characteristics of a human cell line transformed by DNA from human adenovirus type 5". In: *Journal of General Virology* 36.1, pp. 59–72. ISSN: 00221317. DOI: 10.1099/0022-1317-36-1-59.
- Greer, Eric L. and Yang Shi (2012). "Histone methylation: A dynamic mark in health, disease and inheritance". In: *Nature Reviews Genetics* 13.5, pp. 343–357. ISSN: 14710056. DOI: 10.1038/nrg3173. URL: <http://dx.doi.org/10.1038/nrg3173>.
- Hammerschmidt, Wolfgang and Bill Sugden (1988). "Identification and characterization of oriLyt, a lytic origin of DNA replication of Epstein-Barr virus". In: *Cell* 55.3, pp. 427–433. ISSN: 00928674. DOI: 10.1016/0092-8674(88)90028-1.
- Harada, S and E Kieff (1997). "Epstein-Barr virus nuclear protein LP stimulates EBNA-2 acidic domain-mediated transcriptional activation". In: *Journal of Virology* 71.9, pp. 6611–6618. ISSN: 0022-538X. DOI: 10.1128/jvi.71.9.6611-6618.1997.
- Harth-Hertle, Marie L. et al. (2013). "Inactivation of intergenic enhancers by EBNA3A initiates and maintains polycomb signatures across a chromatin domain encoding CXCL10 and CXCL9". In: *PLoS Pathogens* 9.9. ISSN: 15537366. DOI: 10.1371/journal.ppat.1003638.
- Hellebrand, E et al. (2006). "Epstein-Barr virus vector-mediated gene transfer into human B cells: potential for antitumor vaccination". In: *Gene Therapy*, pp. 150–62. DOI: 10.1038/sj.gt.3302602.
- Hendel, Ayal et al. (2015). "Chemically modified guide RNAs enhance CRISPR-Cas genome editing in human primary cells". In: *Nature Biotechnology* 33.9, pp. 985–989. ISSN: 15461696. DOI: 10.1038/nbt.3290.
- Heng Li, Bob Handsaker et al. (2009). "The sequence alignment/map format and SAMtools". In: *Bioinformatics Applications note* 25.16, pp. 2078–2079. DOI: 10.1093/bioinformatics/btp352.
- Henle, W. et al. (1967). "Herpes-type virus and chromosome marker in normal leukocytes after growth with irradiated burkitt cells". In: *Science* 157, pp. 1064–1065. DOI: 10.1126/science.157.3792.1064.
- Hoek, Maarten and Bruce Stillman (2003). "Chromatin assembly factor 1 is essential and couples chromatin assembly to DNA replication in vivo". In: *Proceedings of the National Academy of*

- Sciences of the United States of America* 100.21, pp. 12183–12188. ISSN: 00278424. DOI: 10.1073/pnas.1635158100.
- Hollenbach, Andrew D. et al. (2002). “Daxx and histone deacetylase II associate with chromatin through an interaction with core histones and the chromatin-associated protein Dek”. In: *Journal of Cell Science* 115.16, pp. 3319–3330. ISSN: 00219533. DOI: 10.1242/jcs.115.16.3319.
- Horlbeck, Max A. et al. (2016). “Nucleosomes impede cas9 access to DNA in vivo and in vitro”. In: *eLife* 5.MARCH2016, pp. 1–21. ISSN: 2050084X. DOI: 10.7554/eLife.12677.
- Huang, Hongda et al. (2016). “Structural basis underlying viral hijacking of a histone chaperone complex”. In: *Nature Communications* 7. ISSN: 20411723. DOI: 10.1038/ncomms12707.
- Hultquist, Judd F. et al. (2016). “A Cas9 ribonucleoprotein platform for functional genetic studies of HIV-host interactions in primary human T cells”. In: *Cell Reports* 17.5, pp. 1438–1452. ISSN: 22111247. DOI: 10.1016/j.celrep.2016.09.080.
- Hummeler, K., G. Henle, and W. Henle (1966). “Fine structure of a virus in cultured lymphoblasts from Burkitt lymphoma.” In: *Journal of bacteriology* 91.3, pp. 1366–1368. ISSN: 00219193. DOI: 10.1128/jb.91.3.1366-1368.1966.
- Hung, King L. et al. (2018). “Engineering protein-secreting plasma cells by homology-directed repair in primary human B cells”. In: *Molecular Therapy* 26.2, pp. 456–467. ISSN: 15250024. DOI: 10.1016/j.ymthe.2017.11.012.
- Jansen, Ruud. et al. (2002). “Identification of genes that are associated with DNA repeats in prokaryotes”. In: *Molecular Microbiology* 43.6, pp. 1565–1575. ISSN: 0950-382X. DOI: 10.1046/j.1365-2958.2002.02839.x. arXiv: 1305.4210.
- Jeltsch, A (2002). “Chemistry and biology of DNA methylation”. In: *ChemBioChem* 3, pp. 274–293.
- Jenuwein, T. and C. D. Allis (2001). “Translating the histone code”. In: *Science* 293.5532, pp. 1074–1080. ISSN: 00368075. DOI: 10.1126/science.1063127. arXiv: arXiv:1011.1669v3. URL: <http://www.sciencemag.org/cgi/doi/10.1126/science.1063127>.
- Jiang, Cizhong and B. Franklin Pugh (2009). “Nucleosome positioning and gene regulation: advances through genomics”. In: *Nature Reviews Genetics* 10.3, pp. 161–172. ISSN: 14710056. DOI: 10.1038/nrg2522.
- Jinek, Martin et al. (2012). “A programmable dual-RNA-guided DNA endonuclease in adaptive bacterial immunity”. In: *Science* 337.6096, pp. 816–821. ISSN: 10959203. DOI: 10.1126/science.1225829. arXiv: 38.
- Johnson, Matthew J. et al. (2018). “Engineering of primary human B cells with CRISPR/Cas9 targeted nuclease”. In: *Scientific Reports* 8.1, pp. 1–9. ISSN: 20452322. DOI: 10.1038/s41598-018-30358-0. URL: <http://dx.doi.org/10.1038/s41598-018-30358-0>.

- Kaiser, Carmen et al. (1999). "The Proto-Oncogene c- myc Is a Direct Target Gene of Epstein-Barr Virus Nuclear Antigen 2". In: *Journal of Virology* 73.5, pp. 4481–4484. ISSN: 0022-538X. DOI: 10.1128/jvi.73.5.4481-4484.1999.
- Kalla, M. et al. (2010). "AP-1 homolog BZLF1 of Epstein-Barr virus has two essential functions dependent on the epigenetic state of the viral genome". In: *Proceedings of the National Academy of Sciences of the United States of America* 107.2, pp. 850–855. DOI: 10.1073/pnas.0911948107.
- Katsanis, Nicholas and Elizabeth M.C. Fisher (1996). "The gene encoding the p60 subunit of chromatin assembly factor I (CAF1P60) maps to human chromosome 21q22.2, a region associated with some of the major features of Down syndrome". In: *Human Genetics* 98.4, pp. 497–499. ISSN: 03406717. DOI: 10.1007/s004390050246.
- Kaufman, Paul D. et al. (1995). "The p150 and p60 Subunits of Chromatin Assembly Factor I : A Molecular Link between Newly Synthesized Histones and DNA Replication". In: 81, pp. 1105–1114.
- Kempkes, B. et al. (1995). "B-cell proliferation and induction of early G1-regulating proteins by Epstein-Barr virus mutants conditional for EBNA2". In: *EMBO Journal* 14.1, pp. 88–96. ISSN: 02614189. DOI: 10.1002/j.1460-2075.1995.tb06978.x.
- Kempkes, Bettina and Paul D Ling (2015). "EBNA2 and Its Coactivator EBNA-LP". In: *Current topics in microbiology and immunology* 2. DOI: 10.1007/978-3-319-22834-1.
- Kennedy, Gregory and Bill Sugden (2003). "EBNA-1, a Bifunctional Transcriptional Activator". In: *Molecular and Cellular Biology* 23.19, pp. 6901–6908. ISSN: 0270-7306. DOI: 10.1128/mcb.23.19.6901-6908.2003.
- Khosravi, Mohammad Ali et al. (2019). "Targeted deletion of BCL11A gene by CRISPR-Cas9 system for fetal hemoglobin reactivation: A promising approach for gene therapy of beta thalassemia disease". In: *European Journal of Pharmacology* 854, pp. 398–405. ISSN: 18790712. DOI: 10.1016/j.ejphar.2019.04.042. URL: <https://doi.org/10.1016/j.ejphar.2019.04.042>.
- Kim, Daesik et al. (2015). "Digenome-seq: Genome-wide profiling of CRISPR-Cas9 off-target effects in human cells". In: *Nature Methods* 12.3, pp. 237–243. ISSN: 15487105. DOI: 10.1038/nmeth.3284.
- Kim, Sojung et al. (2014). "Highly efficient RNA-guide genome editing in human cells via delivery of purified Cas9 ribonucleoproteins". In: *Genome research* 24, pp. 1012–1019. ISSN: 15495469. DOI: 10.1101/gr.171322.113.Freely.
- Kim, William Y. and Norman E. Sharpless (2006). "The regulation of INK4/ARF in cancer and aging". In: *Cell* 127.2, pp. 265–275. ISSN: 00928674. DOI: 10.1016/j.cell.2006.10.003.
- Kimura, Hiroshi and Peter R. Cook (2001). "Kinetics of core histones in living human cells: Little exchange of H3 and H4 and some rapid exchange of H2B". In: *Journal of Cell Biology* 153.7, pp. 1341–1353. ISSN: 00219525. DOI: 10.1083/jcb.153.7.1341.

- Kinner, Andrea et al. (2008). "Gamma-H2AX in recognition and signaling of DNA double-strand breaks in the context of chromatin." In: *Nucleic acids research* 36.17, pp. 5678–5694. ISSN: 13624962. DOI: 10.1093/nar/gkn550.
- Kornberg, R. D. (1977). "Structure of chromatin." In: *Annual review of biochemistry* 46, pp. 931–954. ISSN: 00664154. DOI: 10.1146/annurev.bi.46.070177.004435.
- Kouzarides, Tony (2007). "Chromatin modifications and their function". In: *Cell* 128.4, pp. 693–705. ISSN: 00928674. DOI: 10.1016/j.cell.2007.02.005.
- Lakshmanan, Imayavaramban and Surinder Batra (2013). "Protocol for apoptosis assay by flow cytometry using Annexin V staining method". In: *Bio-Protocol* 3.6. ISSN: 2331-8325. DOI: 10.21769/bioprotoc.374.
- Lewis, Peter W. et al. (2010). "Daxx is an H3.3-specific histone chaperone and cooperates with ATRX in replication-independent chromatin assembly at telomeres". In: *PNAS* 107.32, pp. 14075–14080. DOI: 10.1073/pnas.1008850107.
- Li, E. and Y. Zhang (2014). "DNA methylation in mammals". In: *Published by Cold Spring Harbor Laboratory Press*. DOI: 10.1101/cshperspect.a019133.
- Li, Han et al. (2009). "The Ink4/Arf locus is a barrier for iPS cell reprogramming". In: *Nature* 460.7259, pp. 1136–1139. ISSN: 00280836. DOI: 10.1038/nature08290.
- Liang Wei Wang et al. (2019). "Epstein-barr-virus-induced one-carbon metabolism drives B cell transformation". In: *Cell Metabolism* 30, pp. 539–555.
- Lieber, Michael R. (2011). "The mechanism of DSB repair by the NHEJ". In: *Annual Review of Biochemistry* 79.3, pp. 181–211. DOI: 10.1146/annurev.biochem.052308.093131.The.
- Lin, Chih-Jen et al. (2014). "Hira-mediated H3.3 incorporation is required for DNA replication and ribosomal RNA transcription in the mouse zygote". In: *Developmental Cell*, pp. 268–279. DOI: 10.1016/j.devcel.2014.06.022.
- Little, Randall D. and Carl L. Schildkraut (1995). "Initiation of latent DNA replication in the Epstein-Barr virus genome can occur at sites other than the genetically defined origin". In: *Molecular and Cellular Biology* 15.5, pp. 2893–2903. ISSN: 0270-7306. DOI: 10.1128/mcb.15.5.2893.
- Liu, Dingsheng et al. (2012). "Immunophenotypic heterogeneity of normal plasma cells: Comparison with minimal residual plasma cell myeloma". In: *Journal of Clinical Pathology* 65.9, pp. 823–829. ISSN: 00219746. DOI: 10.1136/jclinpath-2012-200881.
- Liu, Xiaojuan et al. (2017). "CRISPR-Cas9-mediated multiplex gene editing in CAR-T cells". In: *Cell Research* 27.1, pp. 154–157. ISSN: 17487838. DOI: 10.1038/cr.2016.142.
- Lizasa, Hisashi et al. (2012). "Epstein-Barr Virus (EBV)-associated Gastric Carcinoma". In: *Viruses*.

- Love, Michael I., Wolfgang Huber, and Simon Anders (2014). “Moderated estimation of fold change and dispersion for RNA-seq data with DESeq2”. In: *Genome Biology* 15.12, pp. 1–21. ISSN: 1474760X. DOI: 10.1186/s13059-014-0550-8.
- Lovejoy, PathwayCourtney A. et al. (2012). “Loss of ATRX, genome instability, and an altered DNA damage response are hallmarks of the alternative lengthening of telomeres pathway”. In: *PLoS Genetics* 8.7. DOI: 0.1371/journal.pgen.1002772.
- Luger, Karolin et al. (1997). “Crystal structure of the nucleosome core particle at 2.8 Å resolution”. In: *Nature* 389.6648, pp. 251–260. ISSN: 00280836. DOI: 10.1038/38444.
- MacAlpine, David M. and Geneviève Almouzni (2013). “Chromatin and DNA replication”. In: *Cold Spring Harbor Perspectives in Biology* 5.8, pp. 1–22. ISSN: 19430264. DOI: 10.1101/cshperspect.a010207.
- Maier, Sabine et al. (2005). “A somatic knockout of CBF1 in a human b-cell line reveals that induction of CD21 and CCR7 by EBNA-2 is strictly CBF1 dependent and that downregulation of immunoglobulin M is partially CBF1 independent”. In: *Journal of virology* 79.14, pp. 8784–8792. DOI: 10.1128/JVI.79.14.8784-8792.2005.
- Maïga, Rayelle Itoua et al. (2014). “Flow cytometry assessment of in vitro generated CD138+ human plasma cells”. In: *BioMed Research International*, p. 8. DOI: 10.1155/2014/536482.
- Mali, Prashant et al. (2013). “RNA-guided human genome engineering via Cas9”. In: *Science* 339.6121, pp. 823–826. ISSN: 10959203. DOI: 10.1126/science.1232033. arXiv: arXiv:1011.1669v3.
- Mancao, Christoph and Wolfgang Hammerschmidt (2007). *Epstein-Barr virus latent membrane protein 2A is a B-cell receptor mimic and essential for B-cell survival*. DOI: 110:3715-21.
- Maruo, Seiji et al. (2006). “Epstein-Barr virus nuclear protein EBNA3C is required for cell cycle progression and growth maintenance of lymphoblastoid cells”. In: *Proceedings of the National Academy of Sciences of the United States of America* 103.51, pp. 19500–19505. ISSN: 00278424. DOI: 10.1073/pnas.0604919104.
- Mascolo, Massimo et al. (2010). “Overexpression of Chromatin Assembly Factor-1/p60 helps to predict the prognosis of melanoma patients”. In: *BMC Cancer* 10, pp. 1–14. ISSN: 14712407. DOI: 10.1186/1471-2407-10-63.
- Mathieson, Toby et al. (2018). “Systematic analysis of protein turnover in primary cells”. In: *Nature Communications* 9.1, pp. 1–10. ISSN: 20411723. DOI: 10.1038/s41467-018-03106-1. URL: <http://dx.doi.org/10.1038/s41467-018-03106-1>.
- McFadden, Karyn et al. (2016). “Metabolic stress is a barrier to Epstein-Barr virus-mediated B-cell immortalization”. In: *Proceedings of the National Academy of Sciences of the United States of America* 113.6, E782–E790. ISSN: 10916490. DOI: 10.1073/pnas.1517141113.

- McFarlane, Steven et al. (2019). "The histone chaperone HIRA promotes the induction of host innate immune defences in response to HSV-1 infection". In: *PLoS Pathogens* 15.3, pp. 1–36. ISSN: 15537374. DOI: 10.1371/journal.ppat.1007667.
- Mckenzie, Jessica and Ayman El-Guindy (2015). "Epstein-Barr virus lytic cycle reactivation". In: *Current Topics in Microbiology and Immunology* 391, pp. 237–261. ISSN: 21969965. DOI: 10.1007/978-3-319-22834-1_8.
- Middleton, T and B Sugden (1994). "Retention of plasmid DNA in mammalian cells is enhanced by binding of the Epstein-Barr virus replication protein EBNA1". In: *Journal of Virology* 68.6, pp. 4067–4071. ISSN: 0022-538X. DOI: 10.1128/jvi.68.6.4067-4071.1994.
- Min, Yi Li, Rhonda Bassel-Duby, and Eric N. Olson (2019). "CRISPR correction of duchenne muscular dystrophy". In: *Annual Review of Medicine* 70.October 2018, pp. 239–255. ISSN: 1545326X. DOI: 10.1146/annurev-med-081117-010451.
- Mojica., F J et al. (2000). "Biological significance of a family of regularly spaced repeats in the genomes of Archaea, Bacteria and mitochondria". In: *Mol Microbiology* 36.1, pp. 244–6. DOI: 10.1046/j.1365-2958.2000.01838.x.
- Mrozek-Gorska, Paulina et al. (2019). "Epstein–Barr virus reprograms human B lymphocytes immediately in the prelatent phase of infection". In: *Proceedings of the National Academy of Sciences* 116.32, pp. 16046–16055. ISSN: 0027-8424. DOI: 10.1073/pnas.1901314116.
- Nanbo, Asuka, Arthur Sugden, and Bill Sugden (2007). "The coupling of synthesis and partitioning of EBV's plasmid replicon is revealed in live cells". In: *EMBO Journal* 26.19, pp. 4252–4262. ISSN: 02614189. DOI: 10.1038/sj.emboj.7601853.
- Nashun, Buhe et al. (2015). "Continuous histone replacement by Hira is essential for normal transcriptional regulation and de novo DNA methylation during mouse oogenesis". In: *Molecular Cell* 60.4, pp. 611–625. ISSN: 10974164. DOI: 10.1016/j.molcel.2015.10.010. URL: <http://dx.doi.org/10.1016/j.molcel.2015.10.010>.
- Nathan, Dafna and Donald M. Crothers (2002). "Bending and flexibility of methylated and unmethylated EcoRI DNA". In: *Journal of Molecular Biology* 316.1, pp. 7–17. ISSN: 00222836. DOI: 10.1006/jmbi.2001.5247.
- Nemerow, G R et al. (1987). "Identification of gp350 as the viral glycoprotein mediating attachment of Epstein-Barr virus (EBV) to the EBV/C3d receptor of B cells: sequence homology of gp350 and C3 complement fragment C3d". In: *Journal of Virology* 61.5, pp. 1416–1420. ISSN: 0022-538X. DOI: 10.1128/jvi.61.5.1416-1420.1987.
- Neuhierl, B. et al. (2002). "Glycoprotein gp110 of Epstein–Barr virus determines viral tropism and efficiency of infection". In: *PNAS* 99.23, pp. 15036–15041. DOI: 10.1073.

- Norio, P, C L Schildkraut, and J L Yates (2000). "Initiation of DNA replication within oriP is dispensable for stable replication of the latent Epstein-Barr virus chromosome after infection of established cell lines". In: *Journal of Virology* 74.18, pp. 8563–74.
- Nutt, Stephen L. et al. (2015). "The generation of antibody-secreting plasma cells". In: *Nature Reviews Immunology* 15.3, pp. 160–171. ISSN: 14741741. DOI: 10.1038/nri3795. URL: <http://dx.doi.org/10.1038/nri3795>.
- Paíno, Teresa et al. (2014). "Phenotypic, genomic and functional characterization reveals no differences between CD138++ and CD138low subpopulations in multiple myeloma cell lines". In: *PLoS ONE* 9.3. ISSN: 19326203. DOI: 10.1371/journal.pone.0092378.
- Pan, Wei-Wei et al. (2013). "Death domain-associated protein DAXX promotes ovarian cancer development and chemoresistance". In: *The Journal of biological chemistry* 288.19, pp. 13620–13630. DOI: 10.1074/jbc.M112.446369.
- Paschos, Kostas et al. (2012). "BIM promoter directly targeted by EBNA3C in polycomb-mediated repression by EBV". In: *Nucleic Acids Research* 40.15, pp. 7233–7246. ISSN: 03051048. DOI: 10.1093/nar/gks391.
- Pchelintsev, Nikolay A. et al. (2013). "Placing the HIRA histone chaperone complex in the chromatin landscape". In: *Cell Reports* 3.4, pp. 1012–1019. ISSN: 22111247. DOI: 10.1016/j.celrep.2013.03.026.
- Pehrson, John R. and Victor A. Fried (1992). "MacroH2A, a core histone containing a large nonhistone region". In: *Science* 257.5075, pp. 1398–1400. ISSN: 00368075. DOI: 10.1126/science.1529340.
- Pennings, Sari, James Allan, and Colin S. Davey (2005). "DNA methylation, nucleosome formation and positioning". In: *Briefings in Functional Genomics and Proteomics* 3.4, pp. 351–361. ISSN: 14739550. DOI: 10.1093/bfpg/3.4.351.
- Pereira, Pedro D. et al. (2017). "Quantification of cell cycle kinetics by EdU (5-ethynyl-2-deoxyuridine)-coupled-fluorescence-intensity analysis". In: *Oncotarget* 8.25, pp. 40514–40532. DOI: 10.18632/oncotarget.17121.
- Pich, Dagmar et al. (2019). "First days in the life of naive human B lymphocytes infected with Epstein-Barr Virus". In: *mBio*. ISSN: 2150-7511. DOI: 10.1128/mbio.01723-19.
- Poleshko, Andrey et al. (2010). "Identification of a functional network of human epigenetic silencing factors". In: *Journal of Biological Chemistry* 285.1, pp. 422–433. ISSN: 00219258. DOI: 10.1074/jbc.M109.064667. URL: <http://dx.doi.org/10.1074/jbc.M109.064667>.
- Polo, Sophie E. et al. (2010). "Clinical significance and prognostic value of chromatin assembly factor-1 overexpression in human solid tumours". In: *Histopathology* 57.5, pp. 716–724. ISSN: 03090167. DOI: 10.1111/j.1365-2559.2010.03681.x.

- Pope, J. H., M. K. Horne, and W. Scott (1968). "Transformation of foetal human leukocytes in vitro by filtrates of a human leukaemic cell line containing herpes-like virus". In: *International Journal of Cancer* 3.6, pp. 857–866. ISSN: 10970215. DOI: 10.1002/ijc.2910030619.
- Probst, Aline V., Elaine Dunleavy, and Geneviève Almouzni (2009). "Epigenetic inheritance during the cell cycle". In: *Nature Reviews Molecular Cell Biology* 10.3, pp. 192–206. ISSN: 14710072. DOI: 10.1038/nrm2640.
- Pulvertaft, R.J.V. (1964). "Cytology of Burkitt's Tumour (African Lymphoma)". In: *The Lancet* 283.7327, pp. 238–240. ISSN: 01406736. DOI: 10.1016/S0140-6736(64)92345-1.
- Puto, Lorena A. and John C.Reed (2008). "Daxx represses RelB target promoters via DNA methyltransferase recruitment and DNA hypermethylation". In: *Genes & Development* 22(8), pp. 998–1010. DOI: 10.1101/gad.1632208.
- Qian, Yue-Wei et al. (1993). "A retinoblastoma-binding protein related to a negative regulator of Ras in yeast". In: *Letters to Nature* 364. DOI: 10.1038/364648a0..
- Quivy, Jean Pierre et al. (2004). "A CAF-1 dependent pool of HP1 during heterochromatin duplication". In: *EMBO Journal* 23.17, pp. 3516–3526. ISSN: 02614189. DOI: 10.1038/sj.emboj.7600362.
- Rabani, Michal et al. (2011). "Production and Degradation Dynamics in Mammalian Cells". In: *Nature Biotechnology* 29.5, pp. 436–442. DOI: 10.1038/nbt.1861..
- Rädle, Bernd et al. (2013). "Metabolic labeling of newly transcribed RNA for high resolution gene expression profiling of RNA synthesis, processing and decay in cell culture". In: *Journal of Visualized Experiments* 78, pp. 1–11. ISSN: 1940087X. DOI: 10.3791/50195.
- Radman-Livaja, Marta et al. (2010). "Replication and active demethylation represent partially overlapping mechanisms for erasure of H3K4me3 in budding yeast". In: *PLoS Genetics* 6.2. ISSN: 15537390. DOI: 10.1371/journal.pgen.1000837.
- Rai, Taranjit Singh et al. (2017). "Histone chaperone HIRA deposits histone H3.3 onto foreign viral DNA and contributes to anti-viral intrinsic immunity". In: *Nucleic Acids Research* 45.20, pp. 11673–11683. ISSN: 13624962. DOI: 10.1093/nar/gkx771.
- Raisner, Ryan M. and Hiten D. Madhani (2006). "Patterning chromatin: Form and function for H2A.Z variant nucleosomes". In: *Current Opinion in Genetics and Development* 16.2, pp. 119–124. ISSN: 0959437X. DOI: 10.1016/j.gde.2006.02.005.
- Ray-Gallet, Dominique et al. (2002). "HIRA is critical for a nucleosome assembly pathway independent of DNA synthesis". In: *Molecular Cell* 9.5, pp. 1091–1100. ISSN: 10972765. DOI: 10.1016/S1097-2765(02)00526-9.
- Ray-Gallet, Dominique et al. (2011). "Dynamics of histone H3 deposition in vivo reveal a nucleosome gap-filling mechanism for H3.3 to maintain chromatin integrity". In: *Molecular Cell*. ISSN: 10972765. DOI: 10.1016/j.molcel.2011.12.006.

- Richardson, C. D. et al. (2016). “Non-homologous DNA increases gene disruption efficiency by altering DNA repair outcomes”. In: *Nature Communications* 7, pp. 1–7. ISSN: 20411723. DOI: 10.1038/ncomms12463.
- Richmond, Timothy J. and Curt A. Davey (2003). “The structure of DNA in the nucleosome core”. In: *Nature* 423.6936, pp. 145–150. ISSN: 00280836. DOI: 10.1038/nature01595. URL: <http://www.nature.com/doi/10.1038/nature01595>.
- Rickinson, Alan B. et al. (2014). “Cellular immune controls over Epstein-Barr virus infection: New lessons from the clinic and the laboratory”. In: *Trends in Immunology* 35.4, pp. 159–169. ISSN: 14714981. DOI: 10.1016/j.it.2014.01.003.
- Ritchie, Kieran et al. (2008). “Loss of ATRX leads to chromosome cohesion and congression defects”. In: *Journal of Cell Biology* 180.2, pp. 315–324. ISSN: 00219525. DOI: 10.1083/jcb.200706083.
- Robillard, Nelly et al. (2014). “Immunophenotype of normal and myelomatous plasma-cell subsets”. In: *Frontiers in Immunology* 5, pp. 1–7. ISSN: 16643224. DOI: 10.3389/fimmu.2014.00137.
- Robinson, James T. et al. (2011). “Integrative genomics viewer”. In: *Nature Biotechnology* 29.1, pp. 24–26. ISSN: 10870156. DOI: 10.1038/nbt.1754.
- Robinson, William H. and Lawrence Steinman (2022). “Epstein-Barr virus and multiple sclerosis”. In: *Science* 375.6578, pp. 264–265. ISSN: 10959203. DOI: 10.1126/science.abm7930.
- Rogakou, Emmy P. et al. (1998). “DNA double-stranded breaks induce histone H2AX phosphorylation on serine 139”. In: *Journal of Biological Chemistry* 273.10, pp. 5858–5868. ISSN: 00219258. DOI: 10.1074/jbc.273.10.5858. URL: <http://dx.doi.org/10.1074/jbc.273.10.5858>.
- Rose, John C. et al. (2017). “Rapidly inducible Cas9 and DSB-ddPCR to probe editing kinetics”. In: *Nature Methods* 14.9, pp. 891–896. ISSN: 15487105. DOI: 10.1038/nmeth.4368. URL: <http://dx.doi.org/10.1038/nmeth.4368>.
- Rossetto, Dorine, Nikita Avvakumov, and Jacques Côté (2012). “Histone phosphorylation”. In: *Epigenetics* 7.10, pp. 1098–1108. ISSN: 1559-2294. DOI: 10.4161/epi.21975.
- Rowe, M. et al. (1985). “Distinctions between endemic and sporadic forms of epstein-barr virus-positive burkitt’s lymphoma”. In: *International Journal of Cancer* 35.4, pp. 435–441. ISSN: 10970215. DOI: 10.1002/ijc.2910350404.
- Saldivar, Joshua C., David Cortez, and Karlene A. Cimprich (2017). “The essential kinase ATR: Ensuring faithful duplication of a challenging genome”. In: *Nature Reviews Molecular Cell Biology* 18.10, pp. 622–636. ISSN: 14710080. DOI: 10.1038/nrm.2017.67.
- Sanchez, Erica L. and Michael Lagunoff (2015). “Viral activation of cellular metabolism”. In: *Virology* 479-480, pp. 609–618. ISSN: 10960341. DOI: 10.1016/j.virol.2015.02.038.

- Schaeffner, Marisa et al. (2019). "BZLF1 interacts with chromatin remodelers promoting escape from latent infections with EBV". In: *Life Science Alliance* 2.2, pp. 1–18. ISSN: 25751077. DOI: 10.26508/lsa.201800108.
- Schepers, Aloys et al. (2001). "Human origin recognition complex binds to the region of the latent origin of DNA replication of Epstein-Barr virus". In: *EMBO Journal* 20.16, pp. 4588–4602. ISSN: 02614189. DOI: 10.1093/emboj/20.16.4588.
- Schumann, Kathrin et al. (2015). "Generation of knock-in primary human T cells using Cas9 ribonucleoproteins". In: *Proceedings of the National Academy of Sciences of the United States of America* 112.33, pp. 10437–10442. ISSN: 10916490. DOI: 10.1073/pnas.1512503112.
- Schwartz, Brian E. and Kami Ahmad (2005). "Transcriptional activation triggers deposition and removal of the histone variant H3.3". In: *Genes and Development* 19.7, pp. 804–814. ISSN: 08909369. DOI: 10.1101/gad.1259805.
- Sears, John et al. (2003). "Metaphase chromosome tethering is necessary for the DNA synthesis and maintenance of oriP plasmids but is insufficient for transcription activation by Epstein-Barr nuclear antigen 1". In: *Journal of virology* 77.21, pp. 11767–80. DOI: 10.1128/jvi.77.21.11767-11780.2003.
- Seki, Akiko and Sascha Rutz (2018). "Optimized RNP transfection for highly efficient CRISPR/Cas9-mediated gene knockout in primary T cells". In: *Journal of Experimental Medicine* 215.3, pp. 985–997. ISSN: 15409538. DOI: 10.1084/jem.20171626.
- Seya, T. and J. P. Atkinson (1989). "Functional properties of membrane cofactor protein of complement". In: *Biochemical Journal* 264.2, pp. 581–588. ISSN: 02646021. DOI: 10.1042/bj2640581.
- Sharp, Judith A. et al. (2001). "Yeast histone deposition protein Asf1p requires Hir proteins and PCNA for heterochromatic silencing". In: *Current Biology* 11.7, pp. 463–473. ISSN: 09609822. DOI: 10.1016/S0960-9822(01)00140-3.
- Sharp, Judith A. et al. (2002). "Chromatin assembly factor I and Hir proteins contribute to building functional kinetochores in *S. cerevisiae*". In: *Genes and Development* 16.1, pp. 85–100. ISSN: 08909369. DOI: 10.1101/gad.925302.
- Shaw, J E, L F Levinger, and C W Carter (1979). "Nucleosomal structure of Epstein-Barr virus DNA in transformed cell lines". In: *Journal of Virology* 29.2, pp. 657–665. ISSN: 0022-538X. DOI: 10.1128/jvi.29.2.657-665.1979.
- Shibahara, Kei Ichi and Bruce Stillman (1999). "Replication-dependent marking of DNA by PCNA facilitates CAF-1-coupled inheritance of chromatin". In: *Cell* 96.4, pp. 575–585. ISSN: 00928674. DOI: 10.1016/S0092-8674(00)80661-3.

- Sinclair, Alison J. et al. (1994). "EBNA-2 and EBNA-LP cooperate to cause G0 to G1 transition during immortalization of resting human B lymphocytes by Epstein-Barr virus". In: *EMBO Journal* 13.14, pp. 3321–3328. ISSN: 02614189. DOI: 10.1002/j.1460-2075.1994.tb06634.x.
- Skalska, Lenka et al. (2013). "Induction of p16INK4a is the major barrier to proliferation when Epstein-Barr Virus (EBV) transforms primary b cells into lymphoblastoid cell lines". In: *PLoS Pathogens* 9.2. ISSN: 15537366. DOI: 10.1371/journal.ppat.1003187.
- Smith, Susan and Bruce Stillman (1989). "Purification and characterization of CAF-I, a human cell factor required for chromatin assembly during DNA replication in vitro". In: *Cell* 58.1, pp. 15–25. ISSN: 00928674. DOI: 10.1016/0092-8674(89)90398-X.
- Speck, P., K. M. Haan, and R. Longnecker (2000). *Epstein-Barr virus entry into cells*. DOI: 10.1006/viro.2000.0624.
- Staibano, S. et al. (2007). "Chromatin assembly factor-1 (CAF-1)-mediated regulation of cell proliferation and DNA repair: A link with the biological behaviour of squamous cell carcinoma of the tongue?" In: *Histopathology* 50.7, pp. 911–919. ISSN: 03090167. DOI: 10.1111/j.1365-2559.2007.02698.x.
- Steinbrück, Lisa et al. (2015). "K1 and K15 of Kaposi's Sarcoma-Associated Herpesvirus Are Partial Functional Homologues of Latent Membrane Protein 2A of Epstein-Barr Virus." In: *Journal of virology* 89.14, pp. 7248–61. ISSN: 1098-5514. DOI: 10.1128/JVI.00839-15.
- Sternberg, Samuel H. et al. (2014). "DNA interrogation by the CRISPR RNA-guided endonuclease Cas9". In: *Nature* 507.7490, pp. 62–67. ISSN: 14764687. DOI: 10.1038/nature13011.
- Steven Henikoff and M. Mitchell Smith (2015). "Histone variants and epigenetics". In: *Cold Spring Harbor Laboratory Press* 7. DOI: 10.1101/cshperspect.a019364.
- Styles, Christine T. et al. (2017). "EBV epigenetically suppresses the B cell-to-plasma cell differentiation pathway while establishing long-term latency". In: *PLoS Biology* 15.8, pp. 1–30. ISSN: 15457885. DOI: 10.1371/journal.pbio.2001992.
- Sun, Wei and Wei Chen (2018). "Metabolic labeling of newly synthesized RNA with 4sU to in parallel assess RNA transcription and decay". In: *Methods in Molecular Biology* 1720, pp. 25–34. ISSN: 10643745. DOI: 10.1007/978-1-4939-7540-2_3.
- Tagami, Hideaki et al. (2004). "Histone H3.1 and H3.3 complexes mediate nucleosome assembly pathways dependent or independent of DNA synthesis". In: *Cell* 116.1, pp. 51–61. ISSN: 00928674. DOI: 10.1016/S0092-8674(03)01064-X.
- Takami, Yasunari et al. (2007). "Essential role of chromatin assembly factor-1-mediated rapid nucleosome assembly for DNA replication and cell division in vertebrate cells". In: *Molecular biology of the cell* 18, pp. 129–141. ISSN: 1059-1524. DOI: 10.1091/mbc.E06.

- Tanner, Jerome et al. (1987). "Epstein-barr virus gp350/220 binding to the B lymphocyte C3d receptor mediates adsorption, capping, and endocytosis". In: *Cell* 50.2, pp. 203–213. ISSN: 00928674. DOI: 10.1016/0092-8674(87)90216-9.
- Taranjit Singh, Rai. et al. (2011). "Human CABIN1 is a functional member of the human HIRA/UBN1/ASF1a histone H3.3 chaperone complex". In: *Molecular and Cellular Biology* 31.19, pp. 4107–4118. DOI: 10.1128/MCB.05546-11.
- Taylor, Graham S. et al. (2015). "The immunology of Epstein-Barr virus-induced disease". In: *Annual Review of Immunology* 33, pp. 787–821. ISSN: 15453278. DOI: 10.1146/annurev-immunol-032414-112326.
- Tayrac, Marie de et al. (2013). "Prognostic significance of EDN/RB, HJURP, p60/CAF-1 and PDL14, four new markers in high-grade gliomas." In: *PloS one* 8.9, pp. 1–10. ISSN: 19326203. DOI: 10.1371/journal.pone.0073332.
- Thorley-Lawson, David A. (2015). "EBV persistence—introducing the virus". In: *Epstein Barr Virus* 1.Pt 1, pp. 151–209. DOI: 10.1007/978-3-319-22822-8_8..
- Tierney, R. J. et al. (2000). "Methylation of transcription factor binding sites in the Epstein-Barr virus latent cycle promoter coincides with promoter down-regulation during virus-induced B-cell transformation". In: *Journal of Virology* 74.22, pp. 10468–10479. DOI: 10.1128/jvi.74.22.10468-10479.2000.
- Tomari, Yukihide and Phillip D. Zamore (2005). "Perspective: machines for RNAi". In: *Genes and Development* 19.5, pp. 517–529. ISSN: 08909369. DOI: 10.1101/gad.1284105.
- Toth, Zsolt., Kevin. Brulois, and Jae U. Jung (2013). "The chromatin landscape of Kaposi's Sarcoma-Associated Herpesvirus". In: *Viruses* 5.5, pp. 1346–1373. DOI: 10.3390/v5051346.
- Tsai, K. et al. (2014). "Viral reprogramming of the Daxx histone H3.3 chaperone during early Epstein-Barr virus infection". In: *Journal of Virology* 88.24, pp. 14350–14363. ISSN: 0022-538X. DOI: 10.1128/jvi.01895-14.
- Tsai, Kevin et al. (2011). "EBV tegument protein BNRF1 disrupts DAXX-ATRAX to activate viral early gene transcription". In: *PLoS Pathogens* 7.11. ISSN: 15537366. DOI: 10.1371/journal.ppat.1002376.
- Tsourlakis, Maria Christina et al. (2013). "Overexpression of the chromatin remodeler death-domain-associated protein in prostate cancer is an independent predictor of early prostate-specific antigen recurrence". In: *Human Pathology* 44.9, pp. 1789–1796. ISSN: 00468177. DOI: 10.1016/j.humpath.2013.01.022. URL: <http://dx.doi.org/10.1016/j.humpath.2013.01.022>.
- Tyagi, Monica et al. (2016). "Chromatin remodelers: We are the drivers!!" In: *Nucleus* 7.4, pp. 388–404. DOI: 10.1080/19491034.2016.1211217.

- Tyler, Jessica K. et al. (2001). "Interaction between the Drosophila CAF-1 and ASF1 Chromatin Assembly Factors". In: *Molecular and Cellular Biology* 21.19, pp. 6574–6584. ISSN: 0270-7306. DOI: 10.1128/mcb.21.19.6574-6584.2001.
- Valouev, Anton et al. (2008). "Genome-wide analysis of transcription factor binding sites based on ChIP-Seq data". In: *Nature Methods* 5.9, pp. 829–834. ISSN: 15487091. DOI: 10.1038/nmeth.1246.
- Verreault, Alain (2003). "Histone deposition at the replication fork: A matter of urgency". In: *Molecular Cell* 11.2, pp. 283–284. ISSN: 10972765. DOI: 10.1016/S1097-2765(03)00052-2.
- Volk, Andrew and John D. Crispino (2015). "The role of the chromatin assembly complex (CAF-1) and its p60 subunit (CHAF1b) in homeostasis and disease". In: *Biochimica et Biophysica Acta - Gene Regulatory Mechanisms* 1849.8, pp. 979–986. ISSN: 18764320. DOI: 10.1016/j.bbagr.2015.05.009.
- Volk, Andrew et al. (2018). "A CHAF1B-dependent molecular switch in hematopoiesis and leukemia pathogenesis". In: *Cancer Cell* 34.5, 707–723.e7. ISSN: 18783686. DOI: 10.1016/j.ccell.2018.10.004. URL: <https://doi.org/10.1016/j.ccell.2018.10.004>.
- Wang, Chen-Yu and Sugden Bill (2008). "Identifying a property of origins of DNA synthesis required to support plasmids stably in human cells". In: *PNAS* 105, pp. 9639–9644. DOI: 10.1073/pnas.0801378105.
- Wang, Dong et al. (2018). "CRISPR/Cas9 genome editing technology significantly accelerated herpes simplex virus research". In: *Cancer Gene Therapy* 25.5-6, pp. 93–105. ISSN: 14765500. DOI: 10.1038/s41417-018-0016-3. URL: <http://dx.doi.org/10.1038/s41417-018-0016-3>.
- Wang, Hailong et al. (2013). "The interaction of CtIP and Nbs1 connects CDK and ATM to regulate HR-mediated double-strand break repair". In: *PLoS Genetics* 9.2. DOI: 10.1371/journal.pgen.1003277.
- Ward, Irene M. and Junjie Chen (2001). "Histone H2AX is phosphorylated in an ATR-dependent manner in response to replicational stress". In: *Journal of Biological Chemistry* 276.51, pp. 47759–47762. ISSN: 00219258. DOI: 10.1074/jbc.C100569200. URL: <http://dx.doi.org/10.1074/jbc.C100569200>.
- Weinhold, B (2006). "Epigenetics: The Science of Change." In: *Environmental health perspectives*. 114.3. DOI: 10.1289/ehp.114-a160.
- Wen, Wangrong et al. (2007). "Epstein-Barr virus BZLF1 gene, a switch from latency to lytic infection, is expressed as an immediate-early gene after primary infection of b lymphocytes". In: *Journal of virology* 81, pp. 1037–1042. DOI: 10.1128/JVI.01416-06.
- White, Robert E. et al. (2012). "EBNA3B-deficient EBV promotes B cell lymphomagenesis in humanized mice and is found in human tumors". In: *Journal of Clinical Investigation* 122.4, pp. 1487–1502. ISSN: 00219738. DOI: 10.1172/JCI58092.

- Wiesner, Martina et al. (2008). "Conditional immortalization of human B cells by CD40 ligation". In: *PLoS ONE* 3.1. ISSN: 19326203. DOI: 10.1371/journal.pone.0001464.
- Windhager, Lukas et al. (2012). "Ultrashort and progressive 4sU-tagging reveals key characteristics of RNA processing at nucleotide resolution". In: *Genome Research* 22.10, pp. 2031–2042. DOI: 10.1101/gr.131847.111.22.
- Woellmer, Anne, Jose M. Arteaga-Salas, and Wolfgang Hammerschmidt (2012). "BZLF1 Governs CpG-Methylated Chromatin of Epstein-Barr Virus Reversing Epigenetic Repression". In: *PLoS Pathogens* 8.9. ISSN: 15537366. DOI: 10.1371/journal.ppat.1002902.
- Woellmer, Anne and Wolfgang Hammerschmidt (2013). "Epstein-Barr virus and host cell methylation: regulation of latency, replication and virus reactivation". In: *Current Opinion in Virology* 3.3, pp. 260–265. ISSN: 18796257. DOI: 10.1016/j.coviro.2013.03.005.
- Wong, Lee H. et al. (2010). "ATRX interacts with H3.3 in maintaining telomere structural integrity in pluripotent embryonic stem cells". In: *Letter* 20.3, pp. 351–60. DOI: 10.1101/gr.101477.109.
- Wu, Chung An M. et al. (2018). "Genetic engineering in primary human B cells with CRISPR-Cas9 ribonucleoproteins". In: *Journal of Immunological Methods* 457, pp. 33–40. ISSN: 18727905. DOI: 10.1016/j.jim.2018.03.009.
- Wysokenski, D A and J L Yates (1989). "Multiple EBNA1-binding sites are required to form an EBNA1-dependent enhancer and to activate a minimal replicative origin within oriP of Epstein-Barr virus". In: *Journal of Virology* 63.6, pp. 2657–2666. ISSN: 0022-538X. DOI: 10.1128/jvi.63.6.2657-2666.1989.
- Xiao, L. et al. (2014). "Targeting Epstein-Barr virus oncoprotein LMP1-mediated glycolysis sensitizes nasopharyngeal carcinoma to radiation therapy". In: *Oncogene* 33.37, pp. 4568–4578. ISSN: 14765594. DOI: 10.1038/onc.2014.32.
- Xu, Mo et al. (2010). "Partitioning of histone H3-H4 tetramers during DNA replication-dependent chromatin assembly". In: *Science* 94. DOI: 10.1126/science.1178994.
- Yang, Bin Xia et al. (2015). "Systematic identification of factors for provirus silencing in embryonic stem cells". In: *Cell* 163.1, pp. 230–245. ISSN: 10974172. DOI: 10.1016/j.cell.2015.08.037.
- Young, Lawrence S. and Alan B. Rickinson (2004). "Epstein-Barr virus: 40 years on". In: *Nature Reviews Cancer* 4, pp. 757–768. DOI: doi:10.1038/nrc1452..
- Zhang, Wei et al. (2013). "Structural plasticity of histones H3-H4 facilitates their allosteric exchange between RbAp48 and ASF1". In: *Nature Structural and Molecular Biology* 20.1, pp. 29–35. ISSN: 15459993. DOI: 10.1038/nsmb.2446.
- Zhang, Yuchen et al. (2020). "Histone loaders CAF-1 and HIRA restrict Epstein-Barr virus b-cell lytic reactivation". In: *mBio* 11.5, pp. 1–24. ISSN: 21507511. DOI: 10.1128/mBio.01063-20.

-
- Zhu, Qianzheng et al. (2009). "Chromatin restoration following nucleotide excision repair involves the incorporation of ubiquitinated H2A at damaged genomic sites". In: *DNA Repair* 8.2, pp. 262–273. ISSN: 15687864. DOI: 10.1016/j.dnarep.2008.11.007.
- Zou, Chenhui, Yajie Wang, and Zhufang Shen (2005). "2-NBDG as a fluorescent indicator for direct glucose uptake measurement". In: *Journal of Biochemical and Biophysical Methods* 64.3, pp. 207–215. ISSN: 0165022X. DOI: 10.1016/j.jbbm.2005.08.001.

Acknowledgement

First of all, I would like to express my gratitude to Wolfgang who provided me with the opportunity to join his group and supported me to grow personally and professionally. I appreciate your patience, encouragement and guidance through this journey whenever I had any doubt in myself and my abilities! Thank you very much for being always approachable and providing valuable advice on my project, personal relations and scientific questions.

I would like to thank Bettina Kempkes, Maria Elena Torres-Padilla and Gunnar Schotta for participating as advisors in my thesis advisory committee and for the valuable suggestions as well as nice atmosphere during these meetings.

Members of the Hammerschmidt group, I would like to thank all of you for the family-like environment and inspiring working atmosphere! Roswitha- Thank you for taking such good care of me beyond my research work. Dagi- Thank you for your patience and help with my cell culture and FACS questions! Christine- Thank you for being a role model with your precise pipetting skills and constant help for ordering my valuable reagents! Manuel- It was great to be around you both professionally and personally. You taught me how to make the best out of what I have and celebrate my small successes along the way with your positive attitude. Adam- Thank you for the occasional chats along with the sweets which provided me an extra boost of energy. It was relaxing to talk and work with you! Paulina- Thank you for introducing me to the lab, your guidance through this journey and sharing your experience in the lab! Bianca- Thank you for putting me out of my comfort zone. Alex- Thank you for the great collaboration and help with data analysis.

Special thanks go to people from the group of AG Zeidler, AG Moosmann, AG Mautner and AG Strobl for nice conversations about life and sharing your experiences. Especially, my dear Sophie, thank you very much for being there for me in good and not so good times!

Bugüne kadar tüm seçimlerimde yanımda olup beni her anlamda destekleyen aileme ne kadar teşekkür etsem az, iyi ki varsınız! Last but not least, my Kevin'cim, this journey would not be same without your constant love, support and understanding. Thank you for easing this journey and looking out for me all along the way!

Curriculum Vitae

Ezgi Akidil

✉ akidil.ezgi@gmail.com

Education

- **Technical University of Munich** **Munich, Germany**
PostDoc, The Rechts der Isar Hospital 2022 – present
- **Ludwig Maximilian University of Munich** **Munich, Germany**
PhD, Faculty of Biology 2018 – 2022
- **University of Göttingen** **Göttingen, Germany**
M.Sc. Microbiology and Biochemistry, Faculty of Biology and Psychology 2015 – 2018
- **Koç University** **Istanbul, Turkey**
B.Sc. Molecular Biology and Genetics, College of Sciences 2010 – 2015
 - Accepted to Koç University with half scholarship due to high ranking score on the nationwide University Entrance Examination
- **Maastricht University** **Maastricht, Netherlands**
Erasmus Exchange Program, September – December 2014
 - Successfully completed one semester in the Human Movement Sciences track within the Biomedical Sciences Program as a part of 4th year of B.Sc.

Publications

- **Akidil E**, Albanese M, Buschle A, Ruhle A, Pich D, Keppler OT, Hammerschmidt W (2021). Highly efficient CRISPR-Cas9-mediated gene knockout in primary human B cells for functional genetic studies of Epstein-Barr virus infection. *PLoS Pathog*, 17(4), e1009117.
- Chen, Yen-Fu Adam, Mocanu B, **Akidil E**, Pich D, Mautner J, Hammerschmidt W (2021). Systematic analysis of Epstein-Barr virus genes and their individual contribution to virus production and composition. *BioRxiv*.
- Pich D, Mrozek-Gorska P, Bouvet M, Sugimoto A, **Akidil E**, Grundhoff A, Hamperl S, Hammerschmidt W (2019). First days in the life of naive human B lymphocytes infected with Epstein-Barr virus. *mBio*, 10, e01723–19.